Hochschule für Angewandte Wissenschaften Hamburg
Hamburg University of Applied Sciences

Diplomarbeit

Department Fahrzeugtechnik und Flugzeugbau

Performance assessment of part-electric General Aviation aircraft

Kolja Seeckt

27. Februar 2006

Hochschule für Angewandte Wissenschaften Hamburg
Department Fahrzeugtechnik + Flugzeugbau
Berliner Tor 9
20099 Hamburg

in Zusammenarbeit mit:

University of Limerick
Department of Mechanical & Aeronautical Engineering
Limerick
Ireland

Verfasser: Kolja Seeckt
Abgabedatum: 27. Februar 2006

1. Prüfer: Prof. Dr.-Ing. Dieter Scholz, MSME
2. Prüfer: Prof. Dr.-Ing. Hartmut Zingel

Betreuer: Dr. Trevor Young

Abstract

A study was undertaken that investigates analytically a change of a General Aviation aircraft's powerplant from an internal combustion (IC) engine to a hybrid engine consisting of an IC engine plus an electric motor. For this purpose, the motor glider *Aeromot AMT 200 Super Ximango* was chosen as reference aircraft, and its drag polar and primary performance characteristics (e.g. drag and drag power versus speed, range, endurance) were determined. Afterwards, equations were determined to estimate the masses of the new IC engine and electric motor depending on their type of construction and power output. Furthermore, a tool in form of a *Microsoft Excel* spreadsheet was created to determine and compare aircraft mass, power demand, energy consumption, energy costs and carbon dioxide (CO_2) -emissions of the reference and the hybrid aircraft. This tool can be adapted to different reference aircraft, reference missions, battery types, fuel and electricity costs and power splits between IC engine and electric motor. A first attempt to describe the *AMT 200* by means of an idealised parabolic drag polar showed that this leads to very poor results during cruise flight for this type of aircraft. In a second step, another drag polar equation was used, which led to realistic results compared to real aircraft data taken from the *AMT 200*'s flight manual. Large fractions of electrically produced shaft power lead to large mass penalties of the hybrid aircraft – especially due to a large battery mass. Nevertheless, this thesis' reference cruise flight mission of 2.5 h flight in 2,500 ft at a speed of 50 m/s (180 km/h, 97 kn), shows a reduction in energy costs and CO_2-emissions of an order of magnitude of 50 percent at a 50:50 power split between IC engine and electric motor.

Hochschule für Angewandte Wissenschaften Hamburg
Hamburg University of Applied Sciences

DEPARTMENT OF AUTOMOTIVE AND AERONAUTICAL ENGINEERING

Performance assessment of part-electric General Aviation aircraft

Task definition of *Diplomarbeit* at HAW Hamburg

Background

The power of an internal combustion (IC) engine, being approximately proportional to the mass flow of air into the engine, reduces with an increase in altitude as the air density drops. At an altitude of 8000ft (2440m), which is typical for a long distance cruise of a light aircraft, the power output is reduced by approximately 21% (the air density is about 0.79 of that at sea level). The power output of an electric motor is independent from this density change, so that a hybrid engine, consisting of an internal combustion engine and an electric motor, would suffer a smaller reduction in power output. Currently this power loss is prevented by engine mounted turbo- or superchargers. Solar cells, attached to the aircraft's upper surfaces, are a possibility to partly recharge the energy storage during flight..

Objective

The objective is to assess if a hybrid engine, is, or under what circumstances could be, a competitive alternative to the currently used IC aero-engines. The investigation shall consider aspects of technical feasibility, operating costs, and environmental pollution. Furthermore, it is required that the investigation considers a practical and useful design, rather than an experimental, technology demonstrator. Task breakdown:

- The candidate shall perform a literature review of (1) existing applications of hybrid and electric propulsion systems in General Aviation (GA) aircraft, (2) automotive hybrid engines, and (3) electric motors, energy storage devices and solar cells.
- The candidate shall select an aerodynamically efficient GA aircraft (or number of aircraft) as a reference aircraft and shall determine its primary aerodynamic and performance characteristics (e.g. drag polar, propeller efficiencies, power, range, climb performance and endurance).
- The candidate shall complete a short concept design study, which will replace the existing IC engine with a hypothetical hybrid engine. Considering a reference mission, the required fuel volume and battery capacity will be determined. The primary output of the study will be the change in aircraft weight.

- The candidate shall investigate the maturity of the technologies used (e.g. the battery weight and storage capacity, fuel cost, electric motor power to weight ratio, solar panel efficiency) and explore the future viability of the concept.

The results have to be documented in a report. The report has to be written in a form up to internationally excepted scientific standards. The application of the German DIN standards is one excepted method to achieve the required scientific format.

The thesis is prepared at the University of Limerick, Department of Mechanical & Aeronautical Engineering. Supervisor is Dr. Trevor Young.

Declaration

This diplom thesis is entirely my own work. Where use has been made of the work of others, it has been fully acknowledged and referenced.

February 27, 2006

Date Signature

Contents

List of Figures

List of Tables

Nomenclature

a	Speed of Sound
A	Aspect Ratio
A_P	Propeller Area (Disc described by the spinning Propeller)
b	Wing Span
c_R	Wing Root Chord
c_T	Wing Tip Chord
c'	Specific Fuel Consumption (SFC) (of Piston or Turboprop Aircraft)
C	Costs
C_D	Drag Coefficient
$C_{D,0}$	Lift-independent Drag Coefficient (Zero-Lift Drag Coefficient)
$C_{D,i}$	Lift-dependent Drag Coefficient
C_L	Lift Coefficient
d_P	Propeller Diameter
D	Drag Force
e	Oswald Efficiency Factor
e	Specific CO_2-Emission
E	Energy Consumption
E	Lift-to-Drag Ratio
E	Glide Ratio
f	Fraction of electrically produced Shaft Power of the total Shaft Power
g	Acceleration due to Gravity
h	Height, Altitude
h_{abs}	Absolute Ceiling
k	Correlation Factor
L	Lift Force
m	Aircraft Mass
m_{AF}	Airframe Mass
m_B	Battery Mass
$m_{B,inst}$	Battery Installation Mass
m_{Bat}	Overall Battery Mass ($= m_B + m_{B,inst}$)
m_e	Mass of Electric Motor incl. Control Device
m_{em}	Mass of Electric Motor
m_{emc}	Mass of Electric Motor Control Device
m_{empty}	Aircraft Empty Mass
m_F	Fuel Mass

m_{ic}	Mass of Internal Combustion (IC) Engine
m_{MTO}	Maximum Take-Off Mass
m_{PL}	Payload
m_{ZF}	Maximum Zero-Fuel Mass
M	Mach Number
p_e	Electricity Tariff
p_F	Fuel Price
P	Power
P_D	Drag Power (required Power)
P_S	Shaft Power
$P_{S,cont}$	Maximum Continuous Shaft Power
$P_{S,e}$	Electrically generated Shaft Power
$P_{S,ic}$	Shaft Power produced by the Internal Combustion Engine
P_T	Thrust Power
q	Dynamic Pressure
Q	Fuel burned per Unit Time
R	Range
s	Distance
S	Wing Reference Area
S_{wet}	Aircraft Wetted Area
t	Airfoil Thickness
t	Endurance
T	Thrust
V	Velocity, True Airspeed (TAS)
V_{cr}	Cruise Speed
V_E	Equivalent Airspeed (EAS)
V_y	Best Climb Speed
V_z	Vertical Speed (z-Axis)
W	Weight
W_{TO}	Take-Off Weight

Greek

γ	Flight Path Angle
η_P	Propeller Efficiency
λ	Wing Taper Ratio
ρ	Density
σ	Relative Density
φ_{25}	Wing Sweep Angle of 25 Percent-Line

Subscript

0	Value at Mean Sea Level (except for $C_{D,0}$)
1, 2, 3, ...	Counter
cr	Cruise
e	Electricity
E	Energy
F	Fuel
max	Maximum Value
min	Minimum Value
ref	Reference (Aircraft) Value

List of Abbreviations

AC	Alternating Current
CO_2	Carbon Dioxide
DC	Direct Current
DLR	Deutsches Zentrum für Luft- und Raumfahrt (German Aerospace Center)
EAS	Equivalent Airspeed
ERAST	Environmental Research Aircraft and Sensor Technology (project)
IC	Internal Combustion (Engine)
ISA	International Standard Atmosphere
MSL	Mean Sea Level
NACA	National Advisory Committee for Aeronautics
NASA	National Aeronautics and Space Administration
ROC	Rate of Climb
ROS	Rate of Sink
SFC	Specific Fuel Consumption
SI	Système International d'Unités (International System of Units)
TAS	True Airspeed
UL	Ultralight
URL	Universal Resource Locator
VDI	Verein Deutscher Ingenieure (Association of German engineers)

Terms and Definitions

Air Density Drop with increasing Altitude

In the International Standard Atmosphere (ISA), the development of the air density with increasing altitude is defined as

$$\rho = \rho_0 \left(1 - k_a \cdot h\right)^{4.25588} \quad ,$$

where:

- $\rho_0 = 1.225 \frac{\text{kg}}{\text{m}^3}$,
- $k_a = 6.8756 \cdot 10^{-6} \frac{1}{\text{ft}}$ and
- h in ft.

Breguet Range Equation

For piston-propeller aircraft, the Breguet range equation is

$$R = \frac{\eta_P E}{c' g} \ln\left(\frac{m_1}{m_2}\right) \quad .$$

It is applicable for flight schedules (i.e. reference cruise flights) of constant lift coefficient C_L (flight schedules one and two).

Drag, D

An aircraft's drag D is defined as

$$D = \frac{1}{2} \rho V^2 C_D S \quad .$$

In unaccelerated level-flight, the drag is equal to the engines' thrust T.

Drag Polar

The drag polar describes the relationship between the drag coefficient C_D and the lift coefficient C_L. The overall drag coefficient C_D consists of at least two components: one constant (parasite) and one lift-dependent (induced).

$$C_D = C_{D,0} + C_{D,i}$$

The idealised parabolic drag polar has the form:

$$C_D = C_{D,0} + \frac{C_L^2}{\pi A e}.$$

Besides the parabolic drag polar, other, more accurate, models of an aircraft's drag polar are in use. E.g.:

$$C_D = C_{D,\min} + k_1\left(C_L - C_L\left(C_{D,\min}\right)\right)^2 + k_2\left(C_L - C_L\left(C_{D,\min}\right)\right)^4 \quad \text{and}$$

$$C_D = C_{D_0} + C_{D_1} C_L + C_{D_2} C_L^2 \quad (\textbf{Bert 1999}).$$

Engine Power Loss with increasing Altitude

Two equations to estimate the aircraft's piston-engine's power-loss with increasing altitude were found during the literature review. The first one, e.g. given in **Raymer 1999**, is as follows.

$$\frac{P_S}{P_{S,0}} = \sigma - \frac{1-\sigma}{7.55}$$

The second one, e.g. given in **Young 2005**, is

$$\frac{P_S}{P_{S,0}} = \sigma\left(1 + c_h\right) - c_h \quad ,$$

in which

$$c_h = 0.132 \quad .$$

A comparison of these equations shows the following:

$$\sigma - \frac{1-\sigma}{7.55} = \sigma - \frac{1}{7.55} + \frac{\sigma}{7.55} = \sigma - 0.13245 + 0.13245\sigma$$

$$\sigma\left(1+c_h\right) - c_h = \sigma(1+0.132) - 0.132 = \sigma - 0.132 + 0.132\sigma$$

.

$$\sigma - \frac{1-\sigma}{7.55} \approx \sigma\left(1+c_h\right) - c_h$$

These two equations deliver practically the same results, as both are based on the method developed by Gagg and Farrar (**Gagg 1934**).

Equivalent Airspeed, V_E

This speed takes into consideration that the air density drops with increasing altitude. It is defined as the speed that has to be flown at Sea level to produce the same aerodynamic pressure.

$$q = \frac{1}{2}\rho V^2 = \frac{1}{2}\rho_0 V_E^2$$

$$V_E = \sqrt{\sigma}\, V = \sqrt{\frac{\rho}{\rho_0}}\, V$$

Flight Polar

An aircraft's flight polar describes the aircraft's gliding/soaring performance. The flight polar shows the aircraft's rate of sink (ROS, V_z) versus airspeed (V).

Flight Schedule

For cruise flight, there are three flight schedules that are of practical interest:

- Flight Schedule 1: Cruise flight at constant altitude and constant lift coefficient
- Flight Schedule 2: Cruise flight at constant airspeed and constant lift coefficient
- Flight Schedule 3: Cruise flight at constant altitude and constant airspeed.

Glide Ratio
See Lift-to-Drag Ratio

Lift
The lift of an aircraft is defined as

$$L = \frac{1}{2}\rho V^2 C_L S \quad .$$

In unaccelerated level-flight, the lift equals the weight of the aircraft.

$$L = W = mg$$

This leads to

$$C_L = \frac{2mg}{\rho V^2 S} \quad .$$

Lift Coefficient for minimum Drag and maximum Lift-to-Drag Ratio
The lift-to-drag ratio is defined as

$$E = \frac{L}{D} = \frac{C_L}{C_D} = \frac{C_L}{C_{D,0} + \frac{C_L^2}{\pi A e}} \quad .$$

$$\frac{1}{E} = \frac{C_{D,0}}{C_L} + \frac{C_L}{\pi A e}$$

The needed value of C_L for this equation's minimum value can be found by differentiating 1/E with respect to C_L:

$$\frac{d\left(\frac{1}{E}\right)}{dC_L} = \frac{d\left(\frac{C_{D,0}}{C_L} + \frac{C_L}{\pi A e}\right)}{dC_L} = 0 \quad .$$

$$\Rightarrow \quad C_{L,D_{\min}} = \sqrt{\pi A e C_{D,0}}$$

Note: the gained value is only applicable when using the idealised parabolic drag polar ($C_D = C_{D,0} + C_L^2/(\pi Ae)$).

Lift-to-Drag Ratio

The lift-to-drag ratio E is an aircraft's most important parameter for its aerodynamic efficiency. It is defined as

$$E = \frac{L}{D} = \frac{C_L}{C_D} \quad .$$

For small aircraft, especially sailplanes, the *glide ratio* is used. The glide ratio is defined as

$$E = \frac{\text{horizontal distance flown}}{\text{vertical distance flown}} = \frac{V \cdot \cos\gamma}{V_z} \quad .$$

At a small flight path angle γ, the difference between the indicated airspeed and the horizontal speed is very small (e.g. $\gamma = 10° \Rightarrow \cos\gamma = 0.985$). That is why, in practice, both speeds and both ratios are often treated as the same.

Maximum Lift-to-Drag Ratio

Using the lift-coefficient for minimum Drag $C_{L,D_{\min}}$ to determine the lift-to-drag ratio E, delivers the maximum lift-to-drag ratio $E_{\max}$.

$$E_{\max} = \frac{C_{L,D_{\min}}}{C_D} = \frac{\sqrt{\pi Ae C_{D,0}}}{C_{D,0} + \frac{\sqrt{\pi Ae C_{D,0}}^2}{\pi Ae}}$$

$$= \frac{1}{2}\sqrt{\frac{\pi Ae}{C_{D,0}}}$$

Note: the gained value is only applicable when using the idealised parabolic drag polar ($C_D = C_{D,0} + C_L^2/(\pi Ae)$).

Minimum Drag

Using the minimum drag speed $V_{D_{\min}}$ to determine D, the result is $D_{\min}$.

$$D_{\min} = 2mg\sqrt{\frac{C_{D,0}}{\pi Ae}}$$

Note: the gained value is only applicable when using the idealised parabolic drag polar ($C_D = C_{D,0} + C_L^2/(\pi Ae)$).

Minimum Drag Speed

The drag of an aircraft is defined as

$$D = \frac{1}{2}\rho V^2 C_D S \quad ,$$

and C_L may be expressed in unaccelerated level-flight as

$$C_L = \frac{2mg}{\rho V^2 S} \quad .$$

This delivers, using the parabolic drag polar,

$$D = \frac{1}{2}\rho V^2 \left(C_{D,0} + \frac{1}{\pi Ae} \cdot \left(\frac{2mg}{\rho V^2 S} \right)^2 \right) S \quad .$$

Differentiating this equation with respect to V leads to the minimum drag speed $V_{D_{\min}}$:

$$\frac{dD}{dV} = 0$$

.

$$\Rightarrow \quad V_{D_{\min}} = \left(\frac{2mg}{\rho S} \sqrt{\frac{1}{\pi Ae C_{D,0}}} \right)^{1/2}$$

Note: the gained value is only applicable when using the idealised parabolic drag polar ($C_D = C_{D,0} + C_L^2/(\pi Ae)$).

Minimum (Drag) Power

This value is achieved by using $V_{P_{D,\min}}$ in the equation $P_D = DV$.

$$P_{D,\min} = \frac{1}{2}\rho V_{P_{D,\min}}^3 S\left(C_{D,0} + \frac{\left(\frac{2mg}{\rho V_{P_{D,\min}}^2 S}\right)^2}{\pi Ae}\right)$$

Note: the gained value is only applicable when using the idealised parabolic drag polar ($C_D = C_{D,0} + C_L^2/(\pi Ae)$).

Minimum Power Speed

An aircraft's drag power is defined as its drag D times its speed V.

$$P_D = DV = \frac{1}{2}\rho V^3 S\left(C_{D,0} + \frac{\left(\frac{2mg}{\rho V^2 S}\right)^2}{\pi Ae}\right)$$

To find the minimum power speed $V_{P_{D,\min}}$, one differentiates this equation with respect to V.

$$\frac{dP_D}{dV} = 0$$

$$\Rightarrow \quad V_{P_{D,\min}} = \frac{1}{\sqrt[4]{3}}\left(\frac{2mg}{\rho S}\sqrt{\frac{1}{\pi Ae C_{D,0}}}\right)^{1/2}$$

$$= \frac{1}{\sqrt[4]{3}} V_{D_{\min}}$$

Note: the gained value is only applicable when using the idealised parabolic drag polar ($C_D = C_{D,0} + C_L^2/(\pi Ae)$).

Oswald Efficiency Factor

The Oswald efficiency factor *e* is named after the American NACA-scientist W. B. Oswald, who first used this correlation factor in 1933 to integrate an aircraft's finite wing planform into affected calculations (**Oswald 1933**).

Specific Fuel Consumption

The specific fuel consumption (SFC) of piston-propeller and turboprop aircraft is given the symbol *c*' ; (the symbol *c* is used for turbojet/turbofan aircraft). It describes the mass of fuel needed to produce one unit of power for one unit of time.

$$\mathrm{SFC} = c' = \frac{Q}{P_S} \quad \left[\frac{\mathrm{kg}}{\mathrm{Ws}}\right]$$

1 Introduction

1.1 Motivation

Today, most powered General Aviation aircraft use an internal combustion engine as their power source. These engines burn fossil fuel – often, the very expensive aviation gasoline, Avgas. This makes engine powered flight an expensive way of travelling or hobby. In recent years, the expenses for fuel have been increasing rapidly, as fuel prices have been growing faster than they had always been. Reasons for this accelerated increase are, amongst others, the fast growing worldwide energy demands and the uncertain political situation in the Middle East.

Despite the financial efforts, there are two more main aspects of the consumption of fossil fuels that support the demand for a change in energy supply:

- The world's resources of fossil oil are limited and going to be depleted in a few decades.

- Burning fossil fuels produces carbon dioxide (CO_2) which is known to be one of the most important greenhouse gases (**Bundesumweltministerium 2005**).

All these facts led to a start in rethinking the power supply of all types of vehicles. Due to the by far biggest market, the largest efforts to reduce fuel consumption and environmental pollution have been undertaken in automotive industry. Parts of these efforts are cars that are powered by a hybrid engine consisting of a combination of an internal combustion engine and an electric motor. These cars show large achievements regarding their fuel consumption, which makes hybrid engine technology an interesting field to investigate regarding its abilities in the different operational circumstances of General Aviation aircraft. In addition, new battery types of a high electricity storage capacity and very high efficiencies of modern electric motors make electric energy appear to be an attractive future energy supply for General Aviation aircraft.

1.2 Objectives

Changing a General Aviation aircraft's engine from a single internal combustion (IC) engine to a combination of an IC engine and an electric motor is a very extensive and complex project.

This thesis sets a starting point for a complete analytical process of investigating and assessing this change. It shows the reader which and how data of a reference aircraft can be used to setup a flight mechanical model of the reference aircraft and how to proceed with the gained model. Furthermore, methods of mass estimation of particular components of the new hybrid aircraft are presented, which can be improved by future users.

As the main performance indicators of a hypothetical hybrid aircraft are costs and carbon dioxide emissions, values for these parameters are already calculated at the end of this flight mechanical investigation step. This gives the user the opportunity to have, as early as possible in the process, a view on these important parameters.

1.3 Report Structure

Chapter 2 includes results of the literature review. The main aspects of the literature review are previous projects on hybrid and electrically powered General Aviation aircraft, automotive hybrid engines and descriptions of electric components, such as electric motors, electric energy storage devices, fuel cells and solar cells.

Chapter 3 deals with the selection of a reference aircraft for the concept design study. Here, the criteria for a reference aircraft are named and potential reference aircraft are described. Afterwards, a reference aircraft is selected.

Chapter 4 describes the first attempt to determine the main performance characteristics of the reference aircraft. In this chapter, the calculations are based on the idealised parabolic drag polar and general literature data. This chapter shows the resulting inaccuracies and problems coming from the improper input data and drag polar.

Chapter 5 contains the second step to determine the main performance characteristics of the reference aircraft. The calculations in this chapter are based on more sophisticated input data and a more accurate drag polar equation.

Chapter 6 describes the working steps and results of the concept design study to determine aircraft and engine component masses, energy costs and carbon dioxide-emissions.

Chapter 7 describes shortly the created tool in form of a *Microsoft Excel* spreadsheet. This tool can be used to automate, simplify and accelerate future investigations on other reference aircraft and reference missions.

Appendix A contains copies of the cited pages of the reference aircraft's flight manual. These copies show the reader the input data gained from this thesis' most important reference.

Appendix B includes print-outs of the created *Microsoft Excel* spreadsheet-tool in addition to the descriptions given in chapter seven.

Appendix C lists up the input data on reference internal combustion engines (power output and mass). This data is used in chapter six to estimate an internal combustion engine mass.

Appendix D is a CD-ROM, which contains this report in PDF-format and the created *Microsoft Excel* spreadsheet.

2 Literature Review

2.1 Hybrid and Electric Propulsion Systems in General Aviation Aircraft

No existing aircraft using a hybrid propulsion system consisting of an IC engine and an electric motor was found during this thesis' literature review. The most important aircraft using electric propulsion systems are described below. All of these, except for the *AE-1 Silent* and the *Antares*, may be called technology demonstrators or at least aircraft developed for very special tasks.

2.1.1 *Pathfinder, Pathfinder-Plus, Centurion, Helios*

The *Pathfinder* is an unmanned flying wing aircraft which was used for the technology demonstration of applying solar power for long duration, high altitude flight. It was developed, built and operated by *AeroVironment Inc*., Monrovia, California, USA. Most of its upper wing surface is covered with solar arrays which provide the power for the aircraft's electric motors and systems. A backup battery system allows for two to five hours flight after dark. The aircraft flies at a speed of 15 to 25 mile/h (24 to 40 km/h, 13 to 22 kn). (**NASA 2005a**)

The aircraft was first developed in the early 1980's for a classified US government program as the HALSOL (High-ALtitude SOLar) aircraft. After several modifications, ten years in storage and some low-altitude checkout flights in 1993 and 1994, the aircraft was adopted into NASA's Environmental Research Aircraft and Sensor Technology (ERAST) project in late 1994. It set new world altitude records for solar-powered aircraft of 50,500 feet (15,400 m) and later of 71,530 feet (21,800 m) which was as well a record for propeller-driven aircraft. (**NASA 2005a**)

Figure 2.1 Photograph of the *Pathfinder-Plus* (**NASA 2005a**)

In 1998, the aircraft reached an unofficial record altitude for propeller-driven aircraft of 80,201 feet (24,445 m) after it was modified into the longer-winged *Pathfinder-Plus* configuration, which is shown in figure 2.1. The most important changes during this modification were:

- Using a centre wing section twice as long as the original (44 feet, 13.4 m)
- More efficient solar cells (19 percent vs. 14 percent) on the new centre section, which resulted in a power boost from about 7.5 kW to about 12.5 kW
- Eight instead of six electric motors (**NASA 2005a**).

The *Centurion*, which flew for the first time in 1998, has a wingspan of 206 feet (62.8 m). This is more than twice as large as the span of the original *Pathfinder*. Furthermore, the extreme-altitude airfoil used for the *Pathfinder-Plus* wing centre-section is used for the whole wing. Four instead of two underwing pods house the landing gear and electronic systems, and the aircraft is fitted with 14 electric motors. 80 percent of the enlarged upper wing surface is covered with solar arrays which produce up to 31,000 Watt of electric power. The aircraft's backup battery system was changed to Lithium-Ions. (**NASA 2005b**)

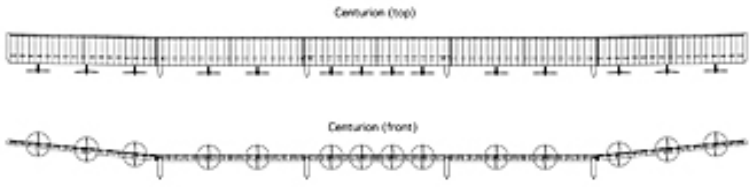

Figure 2.2 Drawing of the *Centurion* (**NASA 2005b**)

The *Centurion* (see figure 2.2) is a further development of the *Pathfinder/Pathfinder-Plus* for the attempts of the ERAST program to achieve "semi-perpetual flight for extended-duration science studies" (**NASA 2005b**). This goal was intended to be achieved by the final aircraft, the *Helios*.

"The two primary goals of the Helios Prototype development are to demonstrate sustained flight at an altitude near 100,000 feet and flying non-stop for at least 24 hours, including at least 14 hours above 50,000 feet." (**NASA 2005c**). The aircraft has a wingspan of 247 feet (75.3 m), a wing chord of 8 feet (2.4 m), five underwing pods and is powered by 14 brushless, direct-current electric motors of 1.5 kW each. The electrical power is gained by 62,120 silicon-based solar cells of 19 percent efficiency. In 2001, the aircraft set a new unofficial world altitude record for sustained horizontal flight of a winged aircraft of 96,863 feet (29,524 m). To achieve ultra-long durations of several weeks or months, the *Helios* is fitted with an

onboard fuel cell based energy system to sustain flight after dark. On June 26, 2004, after nine successful flights, the aircraft crashed into the Pacific Ocean after it experienced control difficulties and became unstable (**NASA 2005d**). Figure 2.3 shows the aircraft during take-off.

Figure 2.3 Photograph of the *Helios* (**NASA 2005c**)

2.1.2 *Icaré II, Solair II*

The *Icaré II* was developed by the University of Stuttgart, Germany, to participate in the Berblinger prize of the City of Ulm, Germany, in 1996. This prize was awarded for a self-launching, solar-electric motor glider capable to sustain horizontal flight using only solar energy at solar radiation conditions of 500 W/m². (**Universität Stuttgart 2005a**; **Voit-Nitschmann 2001**)

The *Icaré II* is powered by a specially developed 12,000 Watt electric motor (mass: 11.7 kg), located in the top of the vertical stabilizer. 20.7 m² of the upper wing and horizontal stabilizer surfaces are covered with solar-arrays of 17 percent efficiency. On June 17, 2003, the *Icaré II* set an unofficial world record for solar-powered aircraft flying more than 350 km. (**Voit-Nitschmann 2001**)

The aircraft has an airframe mass of 168 kg, a maximum take-off mass of 374 kg, and its propulsion system (batteries, motor, control units, propeller, solar generator) weights 79 kg (**Voit-Nitschmann 2005**). The aircraft is shown in figures 2.4 and 2.5.

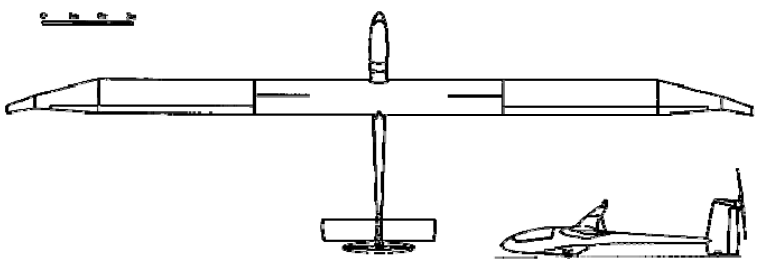

Figure 2.4 Drawing of the *Icaré 2* (**Universität Stuttgart 2005b**)

Figure 2.5 Photograph of the *Icaré 2* (**Universität Stuttgart 2005c**)

The *Solair II* (see figure 2.6) was developed by the University of Visual Arts, Hamburg. Initially, *Solair II* was also meant to participate in the Berblinger prize, but was not ready to fly in time. It took off for the first time in 1998 and is currently equipped with a new propulsion system after it experienced some technical problems. The new concept still uses the initial 17.3 percent efficient solar cells but also two new permanent magnet three-phase electric motors with a power output of 4.8 kW each. (**Solair 2005**)

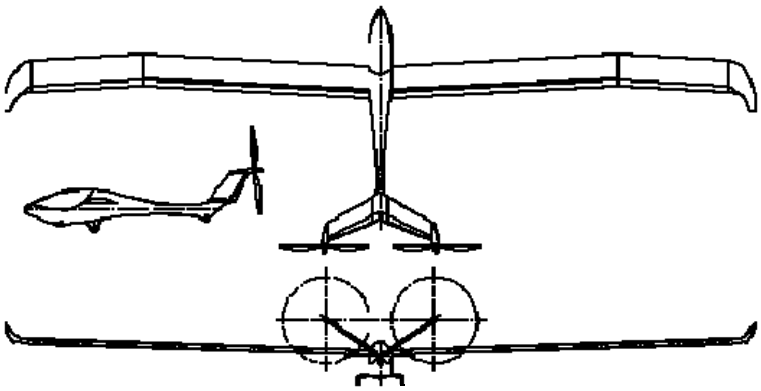

Figure 2.6 Drawing of the *Solair II* (**Solair 2005**)

2.1.3 *AE-1 Silent, Antares*

Neither the *AE-1 Silent* nor the *Antares* was developed as a technology demonstrator or for scientific competition; they both are 'real' General Aviation aircraft, designed for the real aircraft market. Another commonality is that both only use battery packs as power sources and no additional solar cells.

The *AE-1 Silent* (see figure 2.7) is a self-launching sailplane that was developed by the German firm *Air Energy* and type-certified in Germany in May 1998 as Ultralight (UL) aircraft. It uses a 13 kW electric motor (mass: 8.5 kg) that drives a retractable propeller located on the boom behind the cockpit. The aircraft's batteries provide 1.4 kWh of electric energy and have a mass of 40 kg. The whole drive-unit has a mass 65 kg. (**Air Energy 2005**)

Figure 2.7 Photograph of the *AE-1 Silent* (**Air Energy 2005**)

The *Antares* was developed by *Lange Flugzeugbau* in Germany. This "Electric Motorglider" uses a 42 kW brushless DC electric motor that is directly connected to the propeller (**Lange Flugzeugbau 2005**). Similar to the *AE-1 Silent,* the propeller is also located on the boom behind the cockpit (see figure 2.8). Its Lithium-Ion battery system allows for climbing altitudes of more than 3,000 m.

Figure 2.8 Photograph of the *Antares* (**Lange Flugzeugbau 2005**)

2.1.4 Fuel Cell Technology in General Aviation Aircraft

The *Global Observer* was developed by *AeroVironment Inc*., Monrovia, California, USA. This aircraft is powered by a fuel cell using liquid hydrogen and had its first flight on May 26, 2005. It has a wingspan of fifty foot (15.2 m) and is the prototype aircraft of the *Global Observer* HALE (High-Altitude Long-Endurance) platform. This aircraft is intended to be capable of carrying a payload of 1,000 lb (454 kg) for over one week and operate at altitudes of 65,000 ft (19,800 m). (**AeroVironment 2005)**

Figure 2.9 Photograph of the *Global Observer* (**AeroVironment 2005**)

Boeing 2003 gives information about the plans of the *Boeing* Research and Technology Center in Madrid to develop and flight-test a *Fuel Cell Demonstrator airplane* based on the *Diamond Aircraft HK36 Super Dimona* (in North America known as *Katana Xtreme*). A principal drawing of this demonstrator aircraft is shown in figure 2.10. This aircraft was intended to make its first flights in late 2004 or early 2005, but no newer information on the progress of this program have been published since then. At the beginning of this thesis, the related *Boeing* website was completely blank and is now no longer available at all (http://www.boeing.com/phantom/advsystems/fuelcell.html). A query posted to *Boeing* on the topic *Fuel Cell Demonstrator airplane* was not answered.

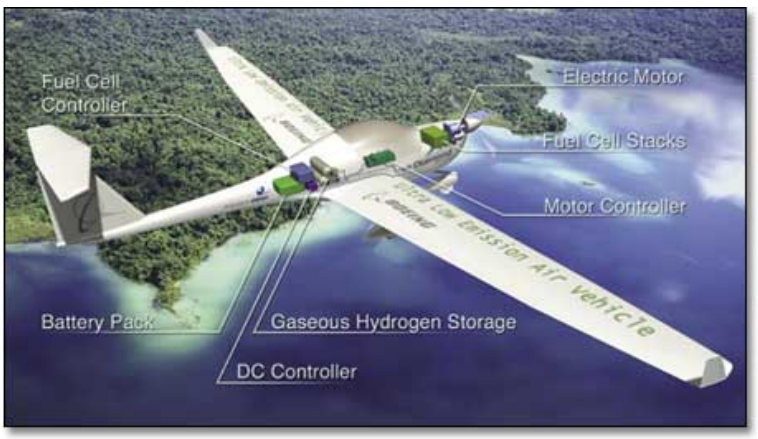

Figure 2.10 Principal Drawing of *Boeing*'s *Fuel Cell Demonstrator airplane* (**Boeing 2003**)

As a part of NASA's attempts to "Revolutionize Aviation; Enable the safe, environmentally friendly expansion of aviation" (**Wickenheiser 2003**, p.1), NASA Glenn Research Center has analytically evaluated electric propulsion systems for their performance impacts on two General Aviation aircraft: the home-built two-seater *Dyn Aero MCR 01* and the four-seater *Cirrus SR-20*. Both investigations led to one final result: "… demonstrations on general aviation aircraft using electric drive propulsion are possible with current off-the-shelf technology. In addition, general aviation aircraft with reasonable payload and range capability may be possible with technology currently in development." (**Wickenheiser 2003**, p.10). This work is partly based on **Berton 2003**.

2.2 Electric Motors

An electric motor is a machine to convert electric energy into mechanical motion. Depending on their application, many different types of electric motors exist. In the electric aircraft of the literature review, mostly brushless permanent-magnet direct-current (DC) motors are used.

Farschtschi 2001 gives helpful information on electric motors for non-specialists in electrical engineering. According to **Farschtschi 2001**, DC motors' most important advantages are:

- simple and cost-effective adjustment of engine speed,
- large range of possible engine speeds,
- applicable, where no alternating current (AC) is available (e.g. in vehicles), and
- direct current electric energy is easy to store (e.g. batteries).

For this thesis, the most interesting data on an electric motor is its power density (i.e. its power output versus mass). Especially gaining information on motor masses turned out to be more complicated than it was expected. The most valuable reference for motor masses and the development of motor mass with increasing power output is **PML Flightlink 2005**. Here, a motor series of a favourable construction type is presented, and the masses of different motor sizes are given.

2.3 Automotive Hybrid Engines

Generally one can differentiate between two types of hybrid propulsion systems: serial and parallel. In addition, most vehicles that have any kind of electric drive use "regenerative braking", which means using the electric motor as a generator to recharge the batteries (and/or super-capacitors).

A serial hybrid propulsion system uses an IC engine to drive a generator, which produces electric energy for an electric motor to propel the car. Regenerated brake energy and excessively produced electric energy can be used to recharge the energy storage devices. This stored energy is used in times of large energy demands – especially during acceleration. The big advantage of this type of hybrid propulsion system, against the sole use of an IC engine, is that an electric motor works much more efficiently over a wide range of speeds than an IC engine. This means that the IC engine may run at its most efficient operating point and a transmission becomes redundant. The serial hybrid system is practically applied in vehicles whose driving cycles incorporate many accelerations and decelerations, especially buses. A serial hybrid propulsion system is not useful for the investigation in this thesis, as the IC engine in an aircraft is already operated in its almost best operating point and the benefits of using the electric motor as a generator during deceleration phases do not occur in flight.

Today, in passenger cars, parallel hybrid systems are mostly used. In this type of hybrid engine, both the IC engine and the electric motor are mechanically connected to the transmission and drive train. This fact leads to various possible power splits between the electric motor and the IC engine. One possibility, which for example is used in the *Honda Insight* (**Honda 2005**), is an IC engine used as the main power source and an electric motor/generator used to support it during acceleration and to regain brake power. Another possibility (e.g. used in the *Toyota Prius* (**Toyota 2005**)) is an IC engine and an electric motor, which both are able to propel the car alone or in combination.

Good general information on hybrid engines is given in the online encyclopaedia **www.wikipedia.org 2006a**. More detailed information can be found on car manufacturer's websites, especially Toyota's **www.hybridsynergydrive.com 2006**. (Note: When visiting this website, use the given link in the section "References" or make sure in another way to be linked to the English version of this site (e.g. click "ENGLISH" in the upper right corner); the German and French versions are less extensive.)

2.4 Electric Energy Storage Devices

2.4.1 Batteries

Batteries are the most common known devices to store electric energy. Rechargeable batteries are also called secondary batteries or accumulators. The energy is not directly stored as electric energy, but as chemical energy in galvanic elements/cells and is converted into electric energy by means of a chemical reaction.

Several different types of batteries exist, which also have large differences in storage capacity and handling characteristics (recharging procedure, auto-ignition, memory-effect, etc.). Today, the most often used types are: lead acid, nickel cadmium (NiCd), nickel metal hydride (NiMH) and lithium ion (Li-Ion). More modern types are e.g. lithium polymer (LiPoly, LiPo) and reusable alkaline batteries.

An extensive and generally understandable reference on battery technology is **www.batteryuniversity.com 2005**. On this website, many aspects of battery technology and applications are presented. For this study, especially the battery type's energy densities are of importance. Modern Li-Ion and LiPoly batteries, here, show values of up to 100-160 Wh/kg. For comparison: less modern lead acid batteries show values of only 30-50 Wh/kg.

Table 2.1, taken from **www.batteryuniversity.com 2005**, lists up the most important data on the named battery types.

During this literature review, another type of battery was found, that appears to be interesting for future projects. This type is currently developed by the German firm *fortu PowerCell GmbH* and uses a system based on inorganic components. A corporate presentation (**solarmobil.net 2005)** quotes practical energy densities of up to 200 Wh/kg and easy handling qualities.

Table 2.1 Characteristics of common Battery Types (**www.batteryuniversity.com 2005**)

	Nickel-cadmium	Nickel-metal-hydride	Lead-acid	Lithium-ion	Lithium-ion-polymer	Reusable alkaline
Gravimetric Energy Density (Wh/kg)	45-80	60-120	30-50	110-160	100-130	80 (initial)
Internal Resistance (includes peripheral circuits) in mΩ	100 to 200[1] 6V pack	200 to 300[1] 6V pack	<100[1] 12V pack	150 to 250[1] 7.2V pack	200 to 300[1] 7.2V pack	200 to 2000[1] 6V pack
Cycle Life (to 80% of initial capacity)	1500[2]	300 to 500[2,3]	200 to 300[2]	300 to 500[3]	300 to 500	50[3] (to 50% capacity)
Fast Charge Time	1h typical	2 to 4h	8 to 16h	2 to 4h	2 to 4h	2 to 3h
Overcharge Tolerance	moderate	low	high	very low	low	moderate
Self-discharge / Month (room temperature)	20%[4]	30%[4]	5%	10%[5]	~10%[5]	0.3%
Cell Voltage (nominal)	1.25V[6]	1.25V[6]	2V	3.6V	3.6V	1.5V
Load Current peak best result	20C 1C	5C 0.5C or lower	5C[7] 0.2C	>2C 1C or lower	>2C 1C or lower	0.5C 0.2C or lower
Operating Temperature[8] (discharge only)	-40 to 60°C	-20 to 60°C	-20 to 60°C	-20 to 60°C	0 to 60°C	0 to 65°C
Maintenance Requirement	30 to 60 days	60 to 90 days	3 to 6 months[9]	not required	not required.	not required
Typical Battery Cost[10] (US$, reference only)	$50 (7.2V)	$60 (7.2V)	$25 (6V)	$100 (7.2V)	$100 (7.2V)	$5 (9V)
Cost per Cycle (US$)[11]	$0.04	$0.12	$0.10	$0.14	$0.29	$0.10-0.50
Commercial use since	1950	1990	1970	1991	1999	1992
Toxicity	Highly toxic, harmful to environment	Relatively low toxicity, should be recycled	Toxic lead and acids, harmful to environment	Low toxicity, can be disposed in small quantities	Low toxicity can be disposed in small quantities	Low toxicity, may contain mercury

2.4.2 Super-Capacitors

Super Capacitors, also called Ultra-capacitors, "… store electricity by physically separating positive and negative charges—unlike batteries which do so chemically. … With no moving parts, they also have a very long lifespan—probably longer than any car." (**RMI 2006**). In automotive industry, super-capacitors are used for storing occurring high power levels during regenerative braking (e.g. in the *Honda FCX*, (**Honda 2006a**)).

Compared to many battery types, super-capacitors have a greater **power** density. This makes them interesting for applications in hybrid cars, where very high power levels can be provided during acceleration (**Honda 2006a**) and absorbed during regenerative braking.

Today, super-capacitors' biggest disadvantage is their very low energy density of only 1-5 Wh/kg (**Skeleton Technologies 2003**, p.A4); *Skeleton Technologies*' efforts aim for an energy density of 11 Wh/kg, which still is very low compared to modern batteries.

2.5 Fuel Cells

Today, many different types of fuel cells exist, but they all have in common that they produce electricity by means of a chemical reaction, just like batteries. Typically, in fuel cells, hydrogen and oxygen are used as reactants. The difference to batteries lays in that they are "… designed for continuous replenishment of the reactants consumed; i.e. it produces electricity from an external fuel supply of hydrogen and oxygen as opposed to the limited internal energy storage capacity of a battery." (**www.wikipedia.org 2005**). Using pure hydrogen (and oxygen of the surrounding air) for the chemical reaction, fuel cells ideally produce only water as reaction product.

In automotive technology, especially proton exchange membrane fuel cells (PEMFC) are of interest. On **Honda 2006b**, the principal function is described as follows.

- *When hydrogen is delivered to the hydrogen electrode it is ionized by a catalytic reaction with the platinum electrode, emitting electrons.*
- *After emitting electrons, the hydrogen ions pass through an electrolytic membrane (ion exchange membrane), where they bond with oxygen ions from oxygen delivered to the oxygen electrode (+) and the previously emitted electrons arriving via an external circuit.*
- *This reaction creates a DC electrical current, generating electricity. Water is generated at the oxygen electrode as a byproduct, and some of this water is used for humidification.*

A schematic drawing of the electricity generation process inside a proton exchange membrane fuel cell is shown in figure 2.11.

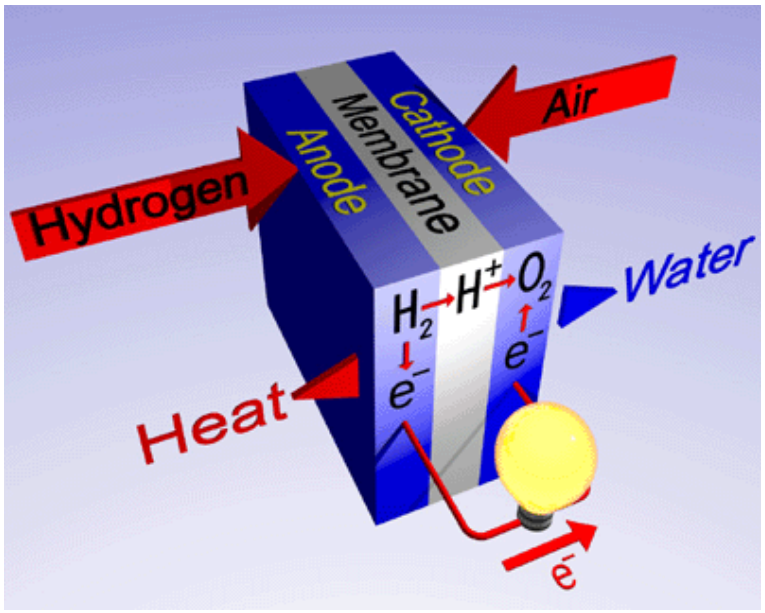

Figure 2.11 Schematic Drawing of Electricity Generation inside a Proton Exchange Membrane Fuel Cell (PEMFC) (**www.fuelcelltoday.com 2005b)**

On the internet, an extensive amount of information on fuel cells can be found. Good basic information on this technology is given on **www.wikipedia.org 2005**. More detailed information, especially on applications, manufacturers, and environmental issues can be found on websites such as **www.fuelcells.org 2005**, **www.fuelcellworld.org 2005** and (in partly German language) **www.fuelcelltoday.com 2005a**.

Further special information (in German language) on fuel cells in automotive applications was found in the VDI-report 1565 (**VDI 2000**). Even though this report's date of issue is 2000 and it does not represent the latest state of the art, parts of this report present valuable, general aspects of fuel cell technology and its practical application. These aspects are for example earlier developments, different possible fuels and distribution of new types of fuel for fuel cell driven cars.

One more very helpful document on future developments in fuel cell applications and attendant circumstances is **Pehnt 2001** of the DLR (German Aerospace Center). In this article, many issues concerning fuel cells in view of transport sector development, environmental aspects, competing technologies, etc. are presented and assessed. This assessment, for example, goes down to global resources and potential annual output of platinum, which is essential in fuel cell technology. Although this is much deeper than needed for a technical assessment of a fuel cell powered General Aviation aircraft, this document shows the reader in a plain manner the circumstances and new, more broadly problems of an application of fuel cell technology.

2.6 Solar Cells

Solar cells are made of semiconductor materials (e.g. silicon) that convert solar radiation energy into electric energy by means of the photovoltaic effect. Today, several types of solar cells are used, which differ significantly in efficiency and costs. Especially a solar cell's microstructure has a major effect on its efficiency. Amorphous solar cells have worst efficiencies, followed by polycrystalline and modern mono-crystalline solar cells, which have efficiencies of up to more than twenty percent. (**www.wikipedia.org 2006b**)

Currently new types of solar cells are being developed. Some cells have efficiencies (under laboratory conditions) of more than thirty percent (**Fraunhofer ISE 2002**). Furthermore, so called thin-film solar cells are being developed and improved, which are of significantly less mass but still very expensive.

Figure 2.12 shows the developments in efficiency of different types of solar cells since 1976.

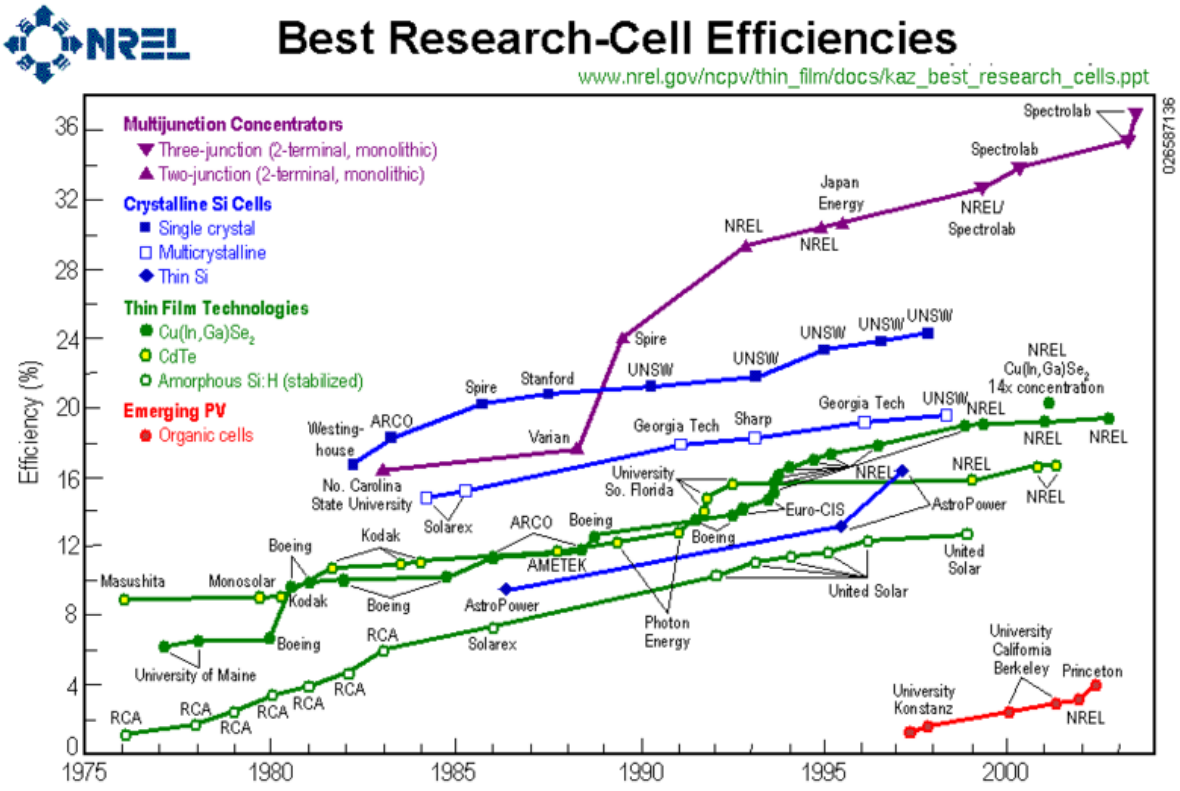

Figure 2.12 Developments of Research-Solar Cell Efficiencies (**NREL 2006**)

3 Selection of a Reference Aircraft

3.1 Criteria for and Pre-Selection of a Reference Aircraft

The task of this thesis demands an *aerodynamically efficient*, General Aviation reference aircraft. The most important indicator for the aerodynamic efficiency of an aircraft is its maximum lift-to-drag ratio E_{max}. In general: the higher an aircraft's lift-to-drag ratio, the better its aerodynamic performance.

While studying **Jackson 2005**, it becomes apparent that motor gliders, along with some others, have the highest lift-to-drag ratios of all powered General Aviation aircraft. This reduces the number of potential reference aircraft to only a few. Although there are some other General Aviation aircraft with excellent aerodynamic efficiency, the reference aircraft was chosen to be a motor glider for the following general reason. Motor gliders are relatively cheap and produced in series. This supports the demand for a *practical and useful design*, as it significantly reduces the price and simplifies the procuring of a real aircraft for modification.

3.2 Descriptions of potential Reference Aircraft

Jackson 2005 (p.[19]) lists six entries in the category "motor gliders":

- *AMS Carat*
- *Aeromot Ximango*
- *Diamond HK36*
- *Scheibe SF 25C Falke*
- *Stemme S10* and *S15*
- *Stemme S6, S8* and *S15-8*

AMS Carat
This Slovenian aircraft had its first flight in 1997. At that time it still had the name *Technoflug TFK-2 Carat*, before its promotion and marketing was transferred to *AMS-Flight*. The aircraft is shown in figure 3.1.

The *AMS Carat* is a single-seated low wing aircraft, which uses the wings and the horizontal tail of the *Schempp-Hirth Discus* sailplane. Winglets are optional, and the landing gear is retractable. The aircraft's structure is mostly made of glass fibre and carbon fibre composites. It is powered by a *Sauer E1S* internal combustion engine, which is a conversion of a

Volkswagen automotive engine and produces 40 kW of maximum continuous power. The fixed-pitch propeller folds forward when the engine is not running. The *AMS Carat* has a maximum take-off mass of 470 kg and a maximum glide ratio of 35. (**Jackson 2005**, p.468-469)

Figure: 3.1 Photograph of the *AMS Carat* (**AMS 2006**)

Aeromot Ximango

The *Aeromot Ximango* (see figure 3.2) was designed by *French Aérostructure* (*Fournier*) under the name *RF-10*. It had its first flight in 1981, before all production rights were sold to the Brazilian *Aeromot Indústria Mecânico-Metalúrgica* in 1985. Since then, several versions were derived from this initial design, now called *AMT 100 Ximango*. (**Jackson 2005**, p.18)

Figure 3.2 Photograph of the *AMT 200* (**Aeromot 2006**)

The *AMT 200 Super Ximango* is generally similar to the *100*-series except for its engine. The *Super Ximango* has been produced since 1995; in 1997 several improvements on the design were implemented. The *AMT 200* is a low wing motor glider with retractable gear and T tail. It uses a NACA 64_3-618 wing section and a *Rotax 912A* powerplant, which produces a

maximum power of 59.6 kW. The *Super Ximango*'s two-blade three-position variable-pitch propeller is a *Hoffmann HO-V62R/170FA*. Most of the structure is made of glass fibre composites. The *AMT 200* has a maximum take-off mass of 850 kg, a maximum glide ratio of 31.1 and offers a two-pilot, side by side accommodation. (**Jackson 2005**, p.18-19)

Diamond HK36

In Europe, the *Diamond HK36* is known under the marketing name *Super Dimona*, while in North America it is known as the *Katana Xtreme*. It had its first flight in 1980 as the *Hoffmann H-36 Dimona* (*Diamond*); today it is manufactured by the Austrian firm *Diamond Aircraft Industries*. (**Jackson 2005**, p.12)

It is a typical motor glider with a two-pilot, side by side accommodation, low/mid wing, T tail and a non-retractable landing gear. Its structure mostly consists of glass fibre composites; the wing spar is made of carbon fibre composites. The *HK36* uses a 59.6 kW maximum power *Rotax* engine type *912A*, that drives a three-position constant-speed and feathering propeller. The *Diamond HK36* has a maximum take-off mass of 770 kg and a maximum glide ratio of 27. (**Jackson 2005**, p.12-13)

> *Diamond Aircraft was selected in July 2003 to supply a Katana Xtreme airframe for the Boeing Fuel Cell Demonstrator project led by Boeing's Madrid-based Technology Center. Work to integrate Proton Exchange Membrane fuel cells supplied by Intelligent Energy (UK) was scheduled to begin in the summer of 2003, with first flight expected in late 2004 or early 2005.*
> (**Jackson 2005**, p.12)

The aircraft is shown in figure 3.3.

Figure 3.3 Photograph of the *Diamond HK36* (**Diamond 2006**)

Scheibe SF 25C Falke

This motor glider is manufactured by the German firm *Scheibe Flugzeugbau*. The first motorised aircraft of this original sailplane had its first flight in 1963 (see figure 3.4). It can be powered by a number of different powerplants and propellers. The *Falke*'s structure is made of the materials and construction methods steel-fabric and wood. It has a maximum take-off mass of 650 kg and a maximum glide ratio of 24. (**Jackson 2005**, p.186-187)

Figure 3.4 Photograph of the *SF 25C Falke* (**airliners.net 2006a**)

Stemme S10* and *S15

The *Stemme S10* prototype was first flown in 1986, from which the *S15* was derived as one of several manned and unmanned versions with for example underwing hardpoints for sensor pods in law-enforcement or scientific missions. These motor gliders are manufactured by the German *Stemme AG* and known in the US under the marketing name *Chrysalis*. The *S10* is also operated by the US Air Force under the designation *TC-11A*. (**Jackson 2005**, p.188-189)

The aircraft is equipped with retractable landing gear, shoulder wing and T tail (see figure 3.5). Its *Rotax 914F2 / S1* powerplant (84.6 kW) is located behind the two-pilot, side by side cockpit and drives a retractable variable-pitch propeller, which is located behind a moveable nosecone. The structure is mostly made of carbon fibre composites. The maximum glide ratio is 50; the maximum take-off mass is 850 kg. (**Jackson 2005**, p.188-189)

Figure 3.5 Photograph of the *Stemme S10* (**airliners.net 2006b**)

Stemme S6, S8* and *S15-8

These motor gliders are developed as part of a platform strategy. The design concept of a mid-mounted motor and driveshaft was adopted from the *S10/S15* as the general construction. Several versions are planned: two *S2* glider versions, five *S6* versions, six *S8* versions (see figure 3.6) and the *S15-8* version. Some versions include special features for reconnaissance and surveillance missions. Several powerplants of various maximum power levels are planned to be available. The maximum take-off mass of most versions is 850 kg, and the maximum glide ratios lie between 32 and 39. (**Jackson 2005**, p.189-190)

Figure 3.6 Drawing of the *Stemme S8* (**Stemme 2006**)

3.3 Selection of the *AMT 200 Super Ximango* as Reference Aircraft

The *AMT 200 Super Ximango* was chosen as the reference aircraft for all further work in this thesis due to the greatest availability of information on this aircraft. The Department of Mechanical and Aeronautical Engineering at the University of Limerick already possessed extensive data on this aircraft, including a complete flight manual, so that no further time had to be spent on detailed information retrieval.

Table 3.1 contains the collection of the input data to determine the *AMT 200*'s performance characteristics; figure 3.7 shows a three-view drawing of the aircraft.

Table 3.1 Input Data to determine the *AMT 200*'s Performance Characteristics

Item	Symbol	Value	Unit	Reference
Wing Area	S	18.7	m²	**Aeromot 2002**, p.7.1
Wind Span	b	17.47	m	**Aeromot 2002**, p.7.1
Wing Tip Chord	c_T	1.46	m	**Aeromot 2002**, p.1.4[a]
Wing Root Chord	c_R	0.49	m	**Aeromot 2002**, p.1.4[a]
Propeller Diameter	d_P	1.7	m	**Aeromot 2002**, p.2.2[b]
Maximum Take-off Mass	m_{MTO}	850	kg	**Aeromot 2002**, p.2.3
Cruise Speed	V_{cr}	50	m/s	**Aeromot 2002**, p.5.3
Maximum Engine Shaft Power	$P_{S,\max}$	59.6	kW	**Aeromot 2002**, p.2.2
Maximum continuous Engine Shaft Power	$P_{S,cont}$	58	kW	**Aeromot 2002**, p.2.2
Cruise Fuel Flow (at V_{cr} = 97 kts)	Q_{cr}	17	l/h	**Aeromot 2002**, p.5.3
Usable Fuel Capacity	-	88	l	**Aeromot 2002**, p.2.2

[a] Measured from three-view drawing

[b] Interpretation in accordance with **Jackson 2005** (p.857)

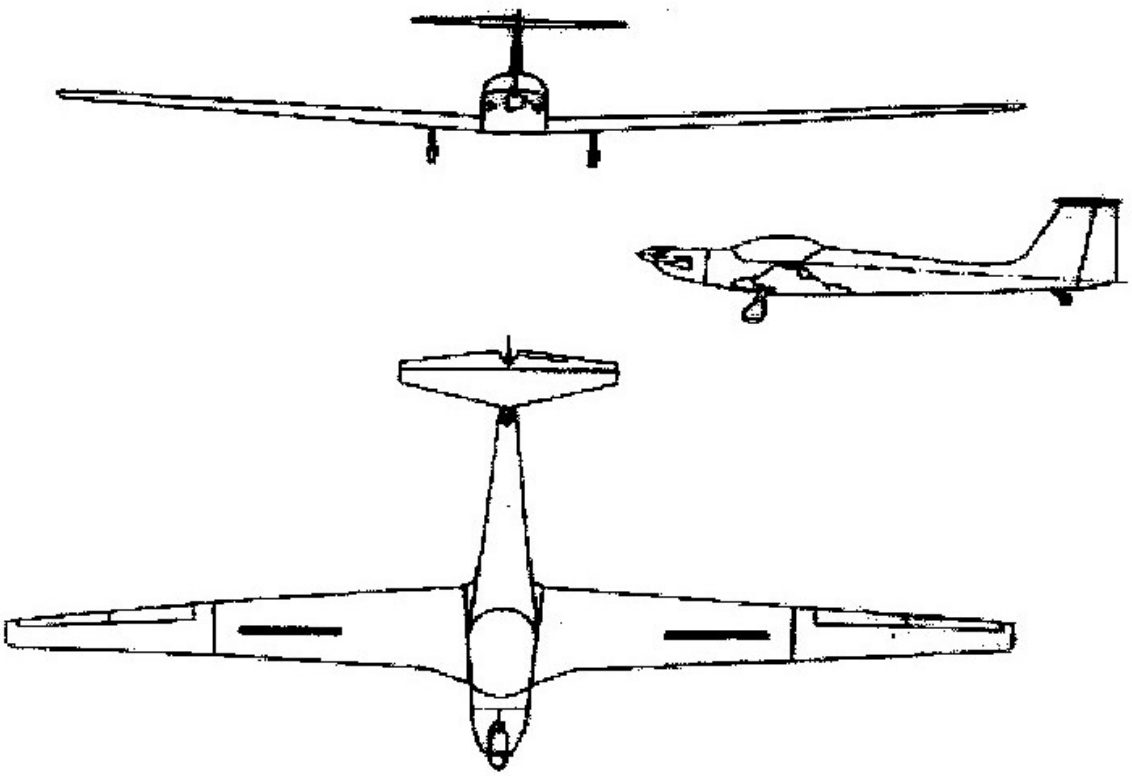

Figure 3.7 Three-View Drawing of the *AMT 200* (**Aeromot 2002**, p.1.4)

4 Determination of Performance Characteristics – Iteration Step I

In this chapter, a determination of the *AMT 200*'s performance characteristics based on the idealised parabolic drag polar is started. Using the idealised parabolic drag polar is the common first attempt to analyze an aircraft's performance characteristics because of the relatively convenient procedure and equations. It is shown that using the idealised parabolic drag polar is not suitable for this type of reference aircraft. That is why this chapter is the first of two iteration steps. The second one, using a different drag polar equation, is described in chapter five.

4.1 Determination of the Parabolic Drag Polar

As defined above, the idealised parabolic drag polar is given by the equation

$$C_D = C_{D,0} + \frac{C_L^2}{\pi A e} \quad , \tag{4.1}$$

in which the zero-lift drag coefficient $C_{D,0}$, and the Oswald efficiency factor e are not yet given. The aspect ratio A is found using the following equation.

$$\begin{aligned} A &= \frac{b^2}{S} \\ &= 16.32 \end{aligned} \tag{4.2}$$

4.1.1 Estimation of the Oswald Efficiency Factor, *e*

An equation to estimate the Oswald efficiency factor for flight Mach numbers $M < 0.95$ and aspect ratios $A > 5$ is given in **Howe 2000** (p.146).

$$e = \frac{1}{\left(1 + 0.12\, M^6\right)\left(1 + \dfrac{0.142 + f(\lambda)\, A \left(10\, t/c\right)^{0.33}}{\cos\left(\varphi_{25}\right)^2}\right) + \dfrac{0.1\left(3\, N_e + 1\right)}{\left(4 + A\right)^{0.8}}} \tag{4.3}$$

$$f\left(\lambda\right) = 0,005\left(1 + 1,5\left(\lambda - 0,6\right)^2\right) \tag{4.4}$$

The variables used in these equations are:

- M: Flight Mach number
  The Mach number is the relation of true airspeed to the speed of sound.

$$M = \frac{V}{a} \tag{4.5}$$

  The *AMT* 200's flight manual gives a typical cruise speed value of V = 180 km/h = 50 m/s (**Aeromot 2002**, p.5.3) at Sea level. The speed of sound at Sea level is a_0 = 340.3 m/s; so $\boldsymbol{M = 0.147}$.

- A: (Effective) aspect ratio
  "Effective" means that the area of an aircraft's winglets has to be added to the wing area. As the *AMT 200* has no winglets, the effective aspect ratio is the determined aspect ratio of $\boldsymbol{A = 16.32}$.

- t/c: Relative airfoil thickness
  The airfoil used for the *AMT 200* is a NACA 64_3-618 (**Aeromot 2002**, p.7.1). The last two numbers represent the airfoil thickness in percent; so $\boldsymbol{t/c = 0.18}$.

- φ_{25}: Wing sweep-angle of the 25 percent-chord line
  Measuring from the three-view drawing given in the *AMT 200*'s flight manual (**Aeromot 2002**, p.1.4) gives a wing sweep-angle of the 25 percent-chord line of $\boldsymbol{\varphi_{25} = 2°}$.

- N_e: Number of engines *on top of* the wing
  There are no engines on top of the wing; so $\boldsymbol{N_e = 0}$.

- λ: Wing taper ratio
  The taper ratio is the relation of wing tip chord to wing root chord.

$$\lambda = \frac{c_T}{c_R} \tag{4.6}$$

  So, $\boldsymbol{\lambda = 0.34}$. Using $\lambda = 0.34$ leads to a $f(\lambda) = 0.005524$.

These variables give a value of

$$\boldsymbol{e = 0.793} \quad .$$

This value lies in a realistic order of magnitude and will be used in this **first** iteration step to investigate the *AMT 200*'s performance characteristics.

4.1.2 Estimation of the Zero-Lift Drag Coefficient, $C_{D,0}$

This estimation is performed according to a method given in **Roskam 1997** (p.118-127), in which the zero-lift drag coefficient is expressed as the relation of the *equivalent parasite area f* to the wing area *S*.

$$C_{D,0} = \frac{f}{S} \tag{4.7}$$

f is obtained using the following equation:

$$\log_{10} f = a + b \log_{10} S_{wet} \quad . \tag{4.8}$$

Herein, S_{wet} is the aircraft's wetted area in ft², and *a* and *b* are correlation coefficients that are functions of the *equivalent skin friction coefficient* c_f, which "… is determined by the smoothness and streamlining designed into the airplane." (**Roskam 1997**, p.121).

As there is no information given about the aircraft's wetted area yet, figure 3.21a "Effect of Equivalent Skin Friction and Wetted Area on Equivalent Parasite Area for Single Engine Propeller Driven Airplanes", (**Roskam 1997**, p.119) is used to assume the applicable equivalent skin friction coefficient. The typical sailplane is located on the c_f = 0.0030-line, and other, *less smooth and streamlined* General Aviation aircraft, are mostly found between c_f = 0.0040 and c_f = 0.0100 . E.g. the *Cessna 180* has a c_f of 0.0063 . For the following step, a value of c_f = 0.0040 is used.

Table 3.4 in **Roskam 1997** (p.122) "Correlation Coefficients for Parasite Area Versus Wetted Area (Eqn. (3.21))" shows for c_f = 0.0040 values of the correlation coefficients *a* and *b* of *a* = -2.3979 and *b* = 1.0000 .

To use equation (4.8), a value for the aircraft's wetted area has to be determined, which correlates to the aircraft's take-off weight given by equation (4.9):

$$\log_{10} S_{wet} = c + d \log_{10} W_{TO} \quad , \tag{4.9}$$

where S is in ft², and W_{TO} is in lb.

The correlation coefficients c and d are given in **Roskam 1997** (table 3.5) "Regression Line Coefficients for Take-off Weight Versus Wetted Area (Eqn. (3.22))" for *Single Engine Propeller Driven* as $c = 1.0892$ and $d = 0.5147$. Including the *AMT 200*'s take-off mass of $m_{MTO} = 850$ kg, which is a take-off weight of $W_{TO} = 1{,}874$ lb, equations (4.9) and (4.8) deliver $\log_{10} S_{wet} = 2.7737$ and $f = 2.3757$.

As $S = 18.7$ m² = 201.3 ft², equation (4.7) leads to a value of

$$\boldsymbol{C_{D,0} = 0.0118} \quad .$$

Compared to other aircraft's zero-lift drag coefficient (**Loftin 1980**, table 5.1), the achieved value of $C_{D,0}$ appears to be **too small** for the reference aircraft *AMT 200 Super Ximango* but will be used in this **first** iteration step.

4.1.3 Plot of the Parabolic Drag Polar

The following table 4.1 contains the gained input data for the plot of the drag polar in figure 4.1.

Table 4.1 Calculated Input Data for the Plot of the Parabolic Drag Polar

Item	Symbol	Value
Aspect Ratio	A	16.32
Oswald Efficiency Factor	e	0.793
Zero-Lift Drag Coefficient	$C_{D,0}$	0.0118

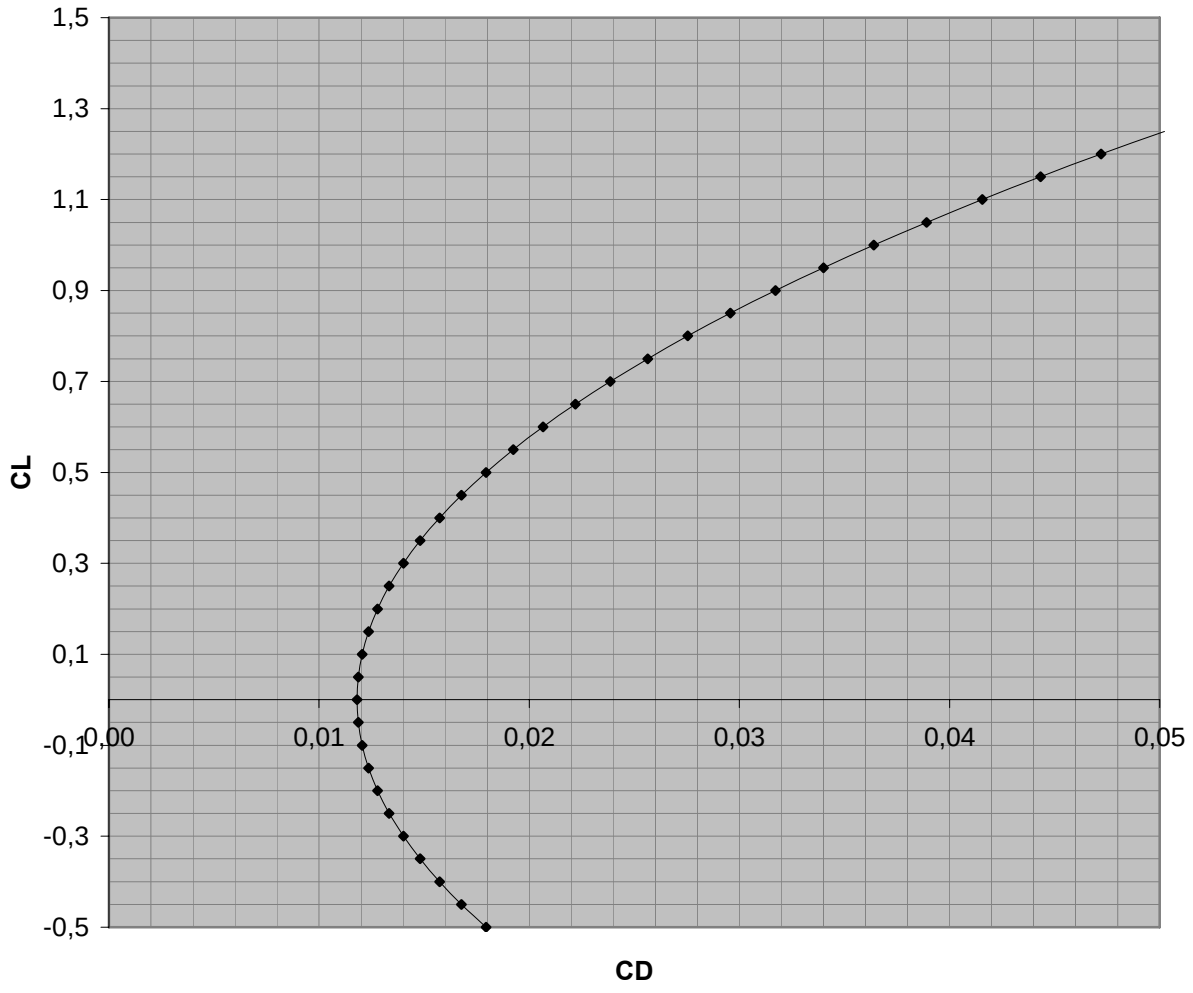

Figure 4.1 Parabolic Drag Polar

4.1.4 Performance Characteristics based on the Parabolic Drag Polar

In the following table, the resulting values of minimum drag, maximum lift-to-drag ratio, minimum power and the correlating speeds are listed. The derivations of the equations used are shown in the section "Terms and Definitions".

Table 4.2 Performance Characteristics based on the Parabolic Drag Polar[a]

Item	Equation	Result
Minimum Drag Speed	$V_{D_{\min}} = \left(\frac{2mg}{\rho S} \sqrt{\frac{1}{\pi A e C_{D,0}}} \right)^{1/2}$	**32.4 m/s** = 63 kn
Minimum Drag	$D_{\min} = 2mg\sqrt{\frac{C_{D,0}}{\pi A e}}$	**284 N**
Maximum Lift-to-Drag Ratio	$E_{\max} = \left(\frac{L}{D} \right)_{\max} = \frac{1}{2}\sqrt{\frac{\pi A e}{C_{D,0}}}$	**29.4**
Minimum Power Speed	$V_{P_{D,\min}} = \frac{1}{\sqrt[4]{3}} \cdot V_{D_{\min}} = 0.760 \cdot V_{D_{\min}}$	**24.6 m/s** = 48 kn
Minimum Power	$P_{D,\min} = \frac{1}{2}\rho V_{P_{D,\min}}^3 S \left(C_{D,0} + \frac{\left(\frac{2mg}{\rho V_{P_{D,\min}}^2 S} \right)^2}{\pi A e} \right)$	**8.1 kW**

[a] Explanations of the equations used can be found in section "Terms and Definitions"

The values listed in table 4.2 are direct results of the idealised parabolic drag polar. They are of a realistic order of magnitude. Even though the parabolic drag polar is quite well applicable for the determination of these special values, it must be pointed out that a determination of these and additional values is performed in chapter five based on more sophisticated input data.

4.2 Powerplant Performance

In this section, the determined idealised drag polar is used for a start of the calculation of performance characteristics like range and endurance. But as section 4.2.2 already shows the poor quality of the determined drag polar, the determination process is stopped there. Chapter 5 includes the calculations and results based on more sophisticated input data.

4.2.1 Estimation of the Propeller Efficiency

The shaft power P_S produced by the aircraft's piston engine cannot be totally converted into thrust power P_T, as there are always losses suffered. These losses occur due to skin friction, compressibility effects on the fast moving propeller blades and the fact that the so called *slipstream* of accelerated air contains translational and rotational motions (**Anderson 2005**, p.646), which are of no use to move the aircraft forward. The reducing factor is given the name *propeller efficiency* η_P.

$$\eta_P = \frac{P_T}{P_S} < 1 \tag{4.10}$$

Determination or estimation of η_P is a very complex procedure in which many influencing variables have to be accounted for. A quick (but rough) way to achieve a value of η_P is given in **Stinton 1983** (p.302). This method will be used in this **first** iteration step to determine the *AMT 200*'s specific fuel consumption.

$$\eta_P = \frac{1.6}{1 + \sqrt{1 + \frac{C_D S}{A_P}}} \tag{4.11}$$

Herein, A_P is the *propeller area*: the area of the disc described by the spinning propeller.

$$A_P = \frac{d_P^2 \pi}{4} = \frac{(1.7\text{m})^2 \pi}{4} = 2.27\text{m}^2 \tag{4.12}$$

The propeller efficiency and the needed value of C_D are determined in the following for cruise flight.

$$C_{L,cr} = \frac{2mg}{\rho V_{cr}^2 S} = 0.291 \tag{4.13}$$

$$C_{D,cr} = C_{D,0} + \frac{C_{L,cr}^2}{\pi A e} = 0.0139 \tag{4.14}$$

$$\eta_{P,cr} = \frac{1.6}{1 + \sqrt{1 + \frac{0.0139 \cdot 18.7\ \mathrm{m}^2}{2.27\ \mathrm{m}^2}}} \tag{4.15}$$

$$\boldsymbol{\eta_{P,cr} = 0.78}$$

This value lies in a realistic order of magnitude, but appears to be too small. As no better data on the propeller efficiency is available yet, it will be used for this **first** iteration step.

4.2.2 Determination of the Specific Fuel Consumption

The specific fuel consumption (SFC) of a piston-propeller aircraft is given the symbol *c'* ; (the symbol *c* is used for turbojet/turbofan aircraft). It describes the mass of fuel needed to produce one unit of power for one unit of time.

$$\mathrm{SFC} = c' = \frac{Q}{P_S} \quad \left[\frac{\mathrm{kg}}{\mathrm{Ws}}\right] \tag{4.16}$$

Typical values of the specific fuel consumption for a piston-propeller aircraft are shown in table 4.3.

Table 4.3 Typical Values of the Specific Fuel Consumption for Piston-Propeller Aircraft (based on **Raymer 1999**, p.23)

Propeller Type	**Cruise** $\left[\frac{\mathrm{kg}}{\mathrm{Ws}}\right]$	**Loiter** $\left[\frac{\mathrm{kg}}{\mathrm{Ws}}\right]$
Fixed-Pitch	$6.8 \cdot 10^{-8}$	$8.5 \cdot 10^{-8}$
Variable-Pitch	$6.8 \cdot 10^{-8}$	$8.5 \cdot 10^{-8}$

During unaccelerated level flight, such as cruise flight, the thrust (power) equals the drag (power). Using equation (4.10), it is

$$P_{S,cr} = \frac{D_{cr} V_{cr}}{\eta_{P,cr}} = \frac{\rho V_{cr}^3 C_{D,cr} S}{2\eta_{P,cr}} = 25.5\text{kW} \quad . \tag{4.17}$$

"At the maximum cruise power, the SFC is nearly independent of altitude and forward speed." (**Young 2005**, p.109). So that, using a fuel density of ρ_F = 0.72 kg/l (Avgas (**Raymer 1999**, p.268)),

$$c' = \frac{Q_{cr}}{P_{S,cr}} = \frac{17\,\frac{\text{l}}{\text{h}} \cdot 0.72\,\frac{\text{kg}}{\text{l}}}{25.5\,\text{kW}} \quad . \tag{4.18}$$

$$\boldsymbol{c' = 13.3 \cdot 10^{-8}\ \frac{\text{kg}}{\text{Ws}}}$$

This value of SFC is far from an acceptable order of magnitude. As the values of SFC given in table 4.3 represent an average of many aircraft, there are a lot of aircraft included that are older and less efficient than the *AMT 200*. This leads to the fact that the *AMT 200*'s specific fuel consumption is expected to be less than the given average values. The gained value of SFC is too large by about a factor of two.

4.3 Cessation of Iteration Step I

The too large value of the specific fuel consumption results from the idealised parabolic drag polar equation. The drag polar equation delivers too small values of the drag coefficient at cruise flight condition, where relatively high speeds and resulting low values of the lift coefficient are existent. A comparison of the parabolic drag polar and real aircraft data is given in section 5.1.3.

Too small values of C_D lead to too small values of drag and drag power. As in the flight manual of the *AMT 200* the fuel flow is given (**Aeromot 2002**, p.5.3), the resulting **specific** fuel consumption in equation (4.18) must be very high to fit into this equation, where the real fuel flow is used.

All following calculations would suffer from this unrealistic value. That is why a new iteration step to determine the *AMT 200*'s performance characteristics is started in chapter 5.

5 Determination of Performance Characteristics – Iteration Step II

This chapter includes the second iteration step to determine the *AMT 200*'s performance characteristics. It is based on a new drag polar, which is derived from flight polar data given in the aircraft's flight manual.

5.1 Determination of the Drag Polar

5.1.1 Conversion of Flight Polar Data into Drag Polar-Reference Points

In the flight manual, the flight polar of the *AMT 200* is given (**Aeromot 2002**, p.5.4); see figure 5.1 and Appendix A.

This polar is used to quantify the *AMT 200*'s soaring performance. In table 5.1 the measured values of V_z (Rate of Sink, ROS) versus the airspeed V are displayed. The highlighted values are the ones, which are directly given as numbers; all other values are either calculated or measured out of the flight polar. It must be pointed out that the given values **do not** correspond exactly to the grid. So, only the highlighted numbers can be accurately regarded as numbers given by the manufacturer.

For **gliding flight**, the lift coefficient is calculated using

$$C_L = \frac{2mg\cos\gamma}{\rho V^2 S} \quad , \tag{5.1}$$

where the flight path angle γ is

$$\gamma = \arcsin\left(\frac{V_z}{V}\right) \quad . \tag{5.2}$$

By means of this angle, the glide ratio can be determined. This is almost the lift-to-drag ratio (see section "Terms and Definitions").

$$E = \frac{1}{\tan\gamma} \tag{5.3}$$

Here, for m the aircraft's maximum take-off mass m_{MTO} is used, and as the flight polar is given for Sea level, the air density of $\rho_0 = 1.225$ kg/m³ has to be applied.

The drag coefficient is calculated

$$C_D = \frac{C_L}{E} \quad . \tag{5.4}$$

In this manner the given flight polar is converted into the aircraft's drag polar (see figure 5.2).

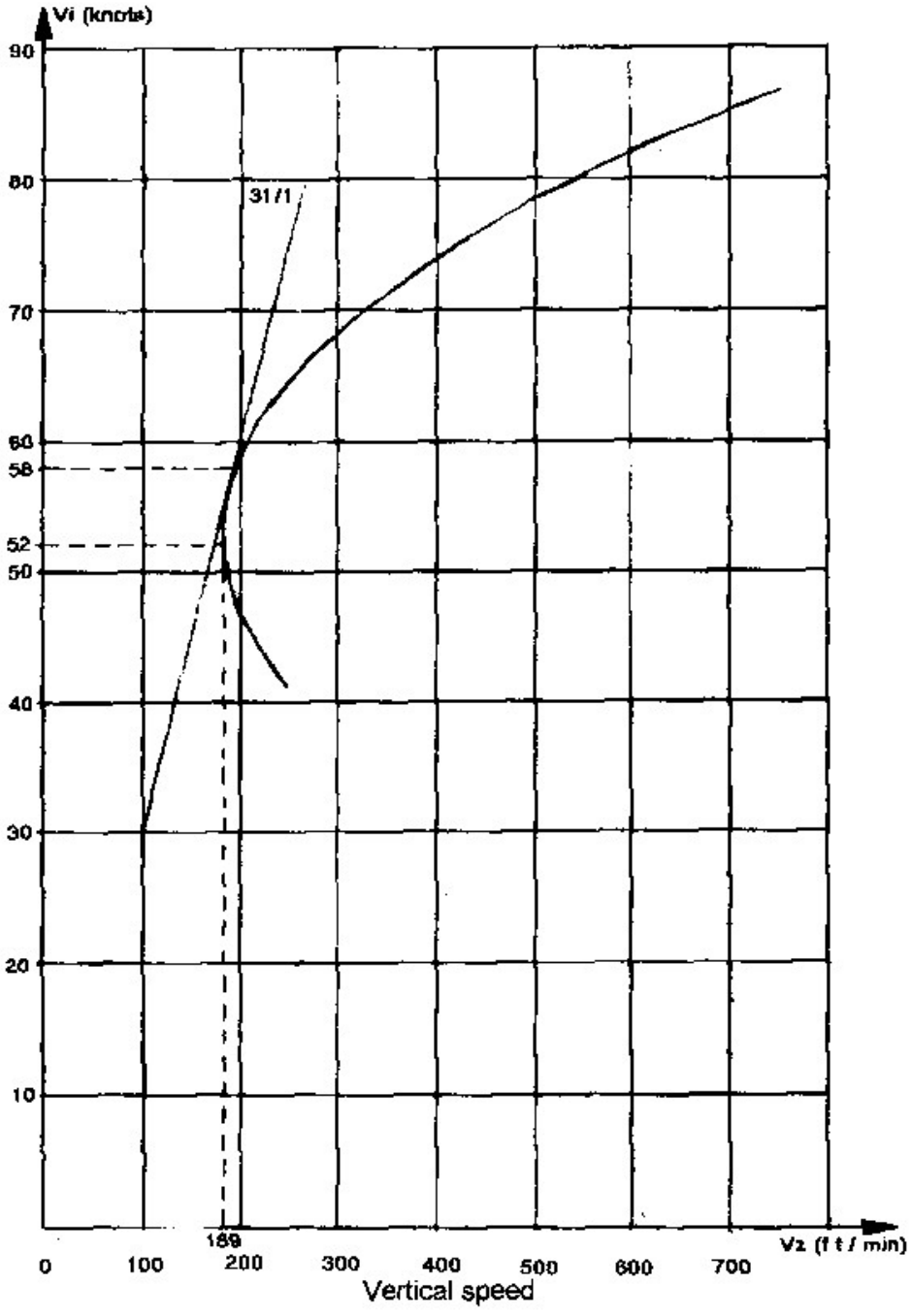

Figure 5.1 Flight Polar given in the Flight Manual (**Aeromot 2002**, p.5.4)

Table 5.1 Data based on the *AMT 200*'s Flight Polar[a]

Airspeed V		**Vertical Speed** V_z		**Lift-to-Drag Ratio = Glide Ratio**[b] E	**Lift Coefficient** C_L	**Drag Coefficient** C_D
kn	m/s	ft/min	m/s			
41	21.1	-250	-1.27	16.6	1.636	0.0985
46.8	24.1	-200	-1.02	23.7	1.256	0.0532
50	25.7	-191	-0.97	26.5	1.1	0.0415
52	26.8	**-189**	-0.96	27.8	1.017	0.0365
58	29.8	-189.5	-0.96	**31**	0.817	0.0264
59.7	30.7	-200	-1.02	30.2	0.771	0.0255
68.5	35.2	-300	-1.52	23.1	0.586	0.0254
73.8	38	-400	-2.03	18.6	0.505	0.0271
78.5	40.4	-500	-2.54	15.9	0.446	0.0281
82	42.2	-600	-3.05	13.8	0.408	0.0296
85	43.7	-700	-3.56	12.3	0.379	0.0310

[a] Bold Numbers indicate concrete Manufacturer's Data

[b] See section "Terms and Definitions" for further details on Lift-to-Drag and Glide Ratio

5.1.2 Lift and Drag Coefficients for Cruise Flight

In addition to the points mentioned in the flight manual, one more very important point has to be determined: the cruise flight, as this point is not yet represented by the data taken from the flight polar.

For cruise flight the following data was gained from the flight manual (**Aeromot 2002**) and the Propeller manufacturer, *Hoffmann Propeller GmbH & Co KG* (**Bichlmeyr 2006**):

- V_{cr} = 50 m/s (**Aeromot 2002**, p.5.3)
- $P_{S,cr}$ = 55 kW (**Bichlmeyr 2006**)
- $\eta_{P,cr}$ = 0.826 (**Bichlmeyr 2006**).

As the propeller efficiency is given by

$$\eta_P = \frac{P_T}{P_S} = \frac{P_D}{P_S} \quad , \tag{5.5}$$

and the drag power is given by

$$P_D = \frac{1}{2}\rho V^3 C_D S \quad , \tag{5.6}$$

the drag coefficient for cruise flight results as

$$C_{D,cr} = \frac{2\eta_{P,cr} P_{S,cr}}{\rho V_{cr}^3 S} = \frac{2 \cdot 0.826 \cdot 55{,}000\ \text{W}}{1.225 \frac{\text{kg}}{\text{m}^3} \cdot \left(50 \frac{\text{m}}{\text{s}}\right)^3 \cdot 18.7\ \text{m}^2} \quad . \tag{5.7}$$

$$\boldsymbol{C_{D,cr}} = \mathbf{0.0317}$$

The related Lift coefficient $C_{L,cr}$ is

$$C_{L,cr} = \frac{2mg}{\rho V_{cr}^2 S} = \frac{2 \cdot 850\ \text{kg} \cdot 9.81 \frac{\text{m}}{\text{s}^2}}{1.225 \frac{\text{kg}}{\text{m}^3} \cdot \left(50 \frac{\text{m}}{\text{s}}\right)^2 \cdot 18.7\ \text{m}^2} \quad . \tag{5.8}$$

$$\boldsymbol{C_{L,cr}} = \mathbf{0.291}$$

5.1.3 Determination of the Drag Polar-Equation

To best match with the determined reference points in table 5.1 and with the cruise flight, a new drag polar-equation will be applied, having the form

$$C_D = C_{D,\min} + k\left(C_L - C_L\left(C_{D,\min}\right)\right)^2 \quad . \tag{5.9}$$

The values of $C_{D,\min}$, k and $C_L(C_{D,\min})$ are **numerically** found using the *Microsoft Excel* Ad-In *Solver* to minimise the sum of the squares of the differences between flight manual and drag polar reference points. The principal use of *Solver* is shown in appendix B, p.113.

The resulting values of $C_{D,\min}$, k and $C_L(C_{D,\min})$ are:

- $C_{D,\min}$ = **0.0251**
- k = **0.0733** and
- $C_L(C_{D,\min})$ = **0.633** .

Hence, the resulting drag polar-equation is

$$C_D = \mathbf{0.0251} + \mathbf{0.0733}\left(C_L - \mathbf{0.633}\right)^2 \quad . \tag{5.10}$$

Figure 5.2 shows the results of the determined drag polar-equation, the cruise flight reference point, the converted data from the flight manual and the idealised parabolic drag polar of chapter four.

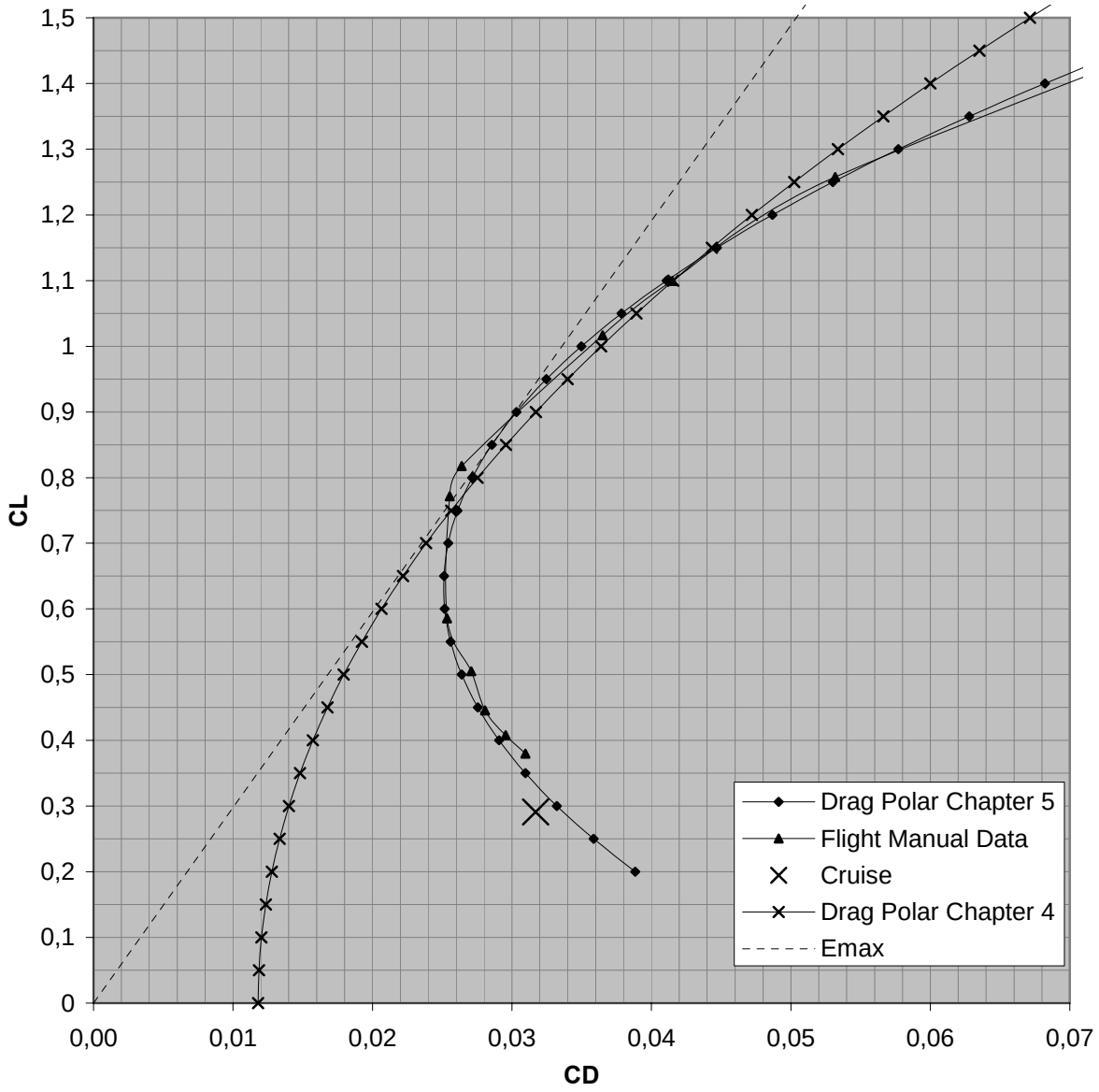

Figure 5.2 Comparison of Drag Polar Data derived from Flight Manual and Drag Polar-Equations

In figure 5.2, it is apparent why the parabolic drag polar is not applicable for a complete determination of the *AMT 200*'s performance characteristics, but for the determination of the maximum lift-to-drag ratio etc. In the region of the maximum lift-to-drag ratio, the flight manual data and both drag polar equations correspond quite well. But especially in regions of lower lift coefficient (higher speeds, e.g. cruise flight) the parabolic drag polar's values of the related drag coefficient are far too low. The reason for this is the *AMT 200*'s relatively thick and highly cambered airfoil (NACA 64_3-618, **Aeromot 2002**, p.7.1), which is optimised for low to moderate airspeeds.

5.1.4 Performance Characteristics based on the Drag Polar

The developments of drag and drag power versus speed are shown in figure 5.3. The used equations are

$$\begin{aligned} D &= \frac{1}{2}\rho V^2 C_D(V) S \\ &= \frac{1}{2}\rho V^2 S\left(0.0251 + 0.0733\left(\frac{2mg}{\rho V^2 S} - 0.633\right)^2\right) \end{aligned} \tag{5.11}$$

and

$$P_D = DV = \frac{1}{2}\rho V^3 C_D(V) S \quad . \tag{5.12}$$

A **numerical** search for minimum drag and minimum drag power (using *Solver*) leads to the values displayed in table 5.2. The detailed work steps are shown in appendix B, p.115.

Table 5.2 Values of Performance Characteristics

Item	Symbol	Value	Value given in Flight Manual
Minimum Drag Speed	$V_{D_{\min}} = V_{E_{\max}}$	**29.06 m/s** = 56.5 kn	29.8 m/s = 58 kn
Minimum Drag	$D_{\min}$	**280 N**	-
Maximum Lift-to-Drag Ratio	$E_{\max}$	**29.8**	31
Minimum Power Speed	$V_{P_{D,\min}}$	**27.13 m/s** = 52.7 kn	26.75 m/s = 52 kn
Minimum Drag Power	$P_{D,\min}$	**7.9 kW**	-

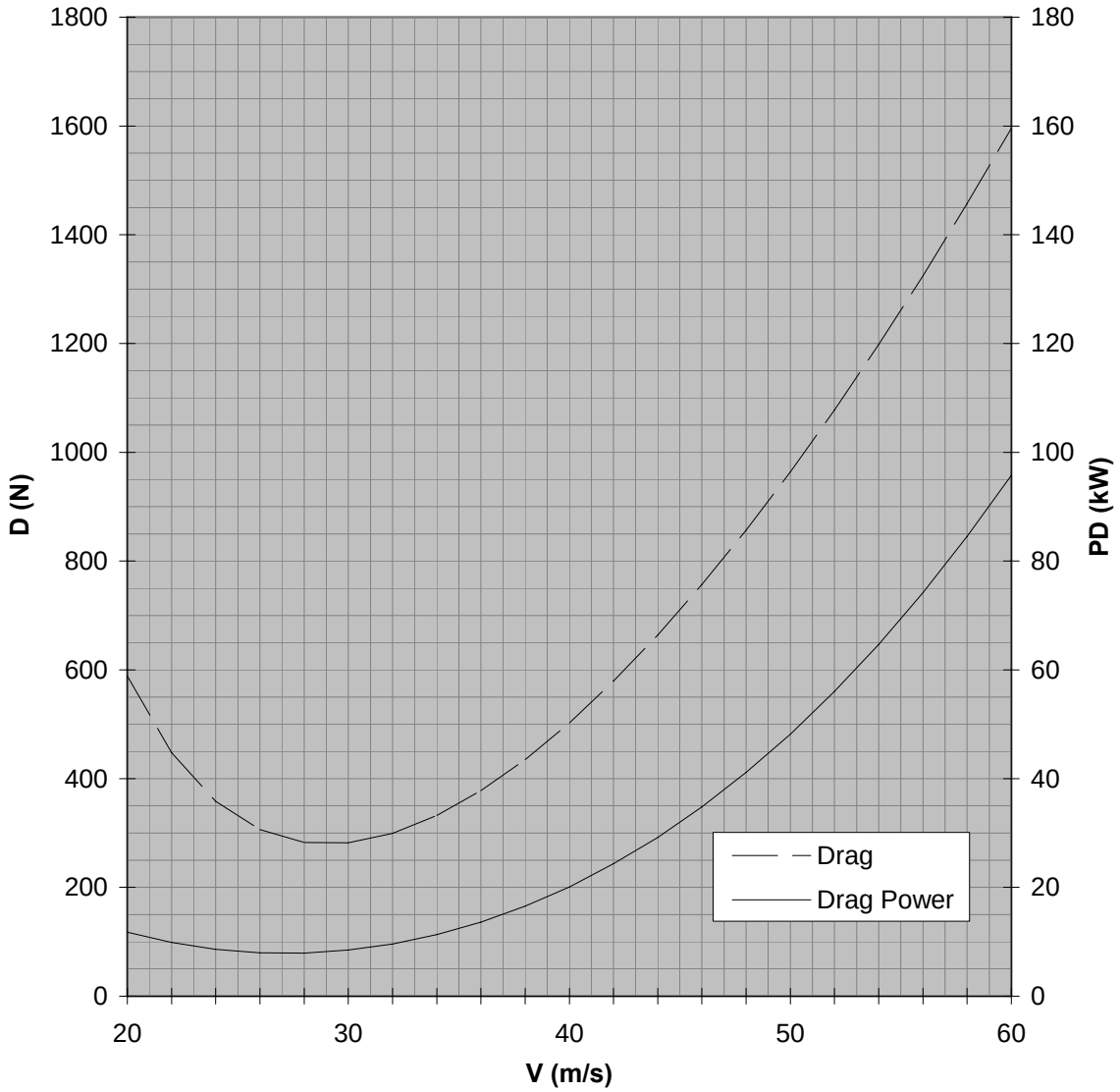

Figure 5.3 Drag and Drag Power versus Speed

5.2 Powerplant Performance

In this section, the *AMT 200*'s range and endurances of the flight schedules one and two (both with constant lift coefficient) are determined. Flight schedules one and two are chosen, because they deliver the maximum range and endurances. The needed values of specific fuel consumption and propeller efficiency are determined using propeller and aircraft manufacturers' data.

5.2.1 Determination of the Specific Fuel Consumption

Using the given value of P_S = 55 kW for cruise flight (**Bichlmeyr 2006**), the specific fuel consumption results as:

$$c' = \frac{Q_{cr}}{P_{S,cr}} = \frac{17\,\frac{\mathrm{l}}{\mathrm{h}} \cdot 0.72\,\frac{\mathrm{kg}}{\mathrm{l}}}{55\,\mathrm{kW}} \quad . \tag{5.13}$$

$$\boldsymbol{c' = 6.18 \cdot 10^{-8}\ \frac{kg}{Ws}}$$

Compared to the data taken from **Raymer 1999** and shown in table 4.3, this value appears to be very realistic and will be used in the following sections.

5.2.2 Propeller efficiency

Due to the rough estimations for the propeller efficiency in the first iteration step, a query was posted to the propeller manufacturer *Hoffmann Propeller*. Part of the answer (**Bichlmeyr 2006)** is the diagram shown in figure 5.4, in which the propeller efficiency is given for different airspeeds and different propeller speeds.

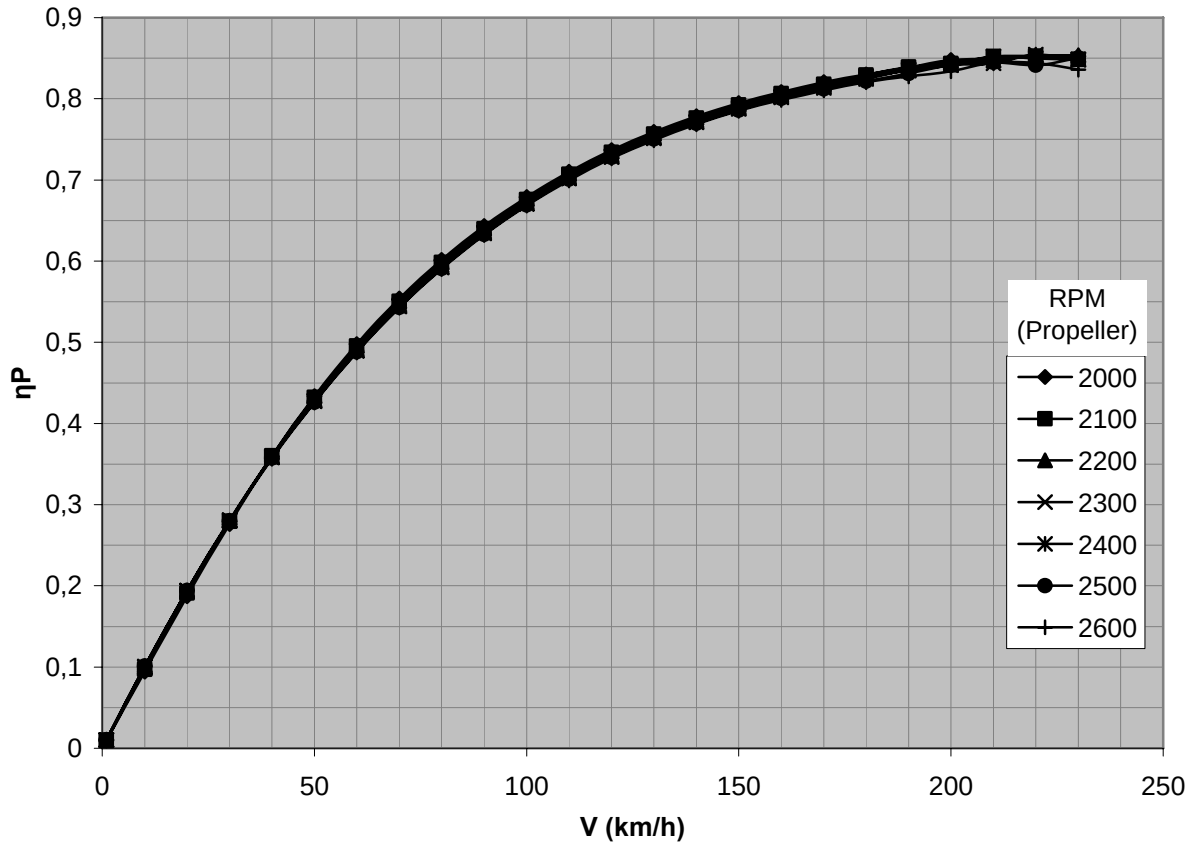

Figure 5.4 Propeller efficiency versus speed (based on **Bichlmeyr 2006**)

An average of these curves is represented by the following equation; ***V* is in m/s.**

$$\eta_P = 3.48 \cdot 10^{-6} V^3 - 6.19 \cdot 10^{-4} V^2 + 3.88 \cdot 10^{-2} V - 7.12 \cdot 10^{-4} \quad (5.14)$$

5.2.3 Range

To determine the maximum cruise flight range and endurance of the *AMT 200*, the *Breguet Range Equation* is used. This equation is applicable to flight schedules, in which the lift coefficient is kept constant during flight. This leads to the fact that with decreasing aircraft mass, the pilot either has to reduce speed to keep up level flight (flight schedule one) or fly a cruise climb (flight schedule two). There are other flight schedules possible, but these two lead to the greatest range *R*.

The Breguet range equation is given as

$$R = \frac{\eta_P E}{c'g} \ln\left(\frac{m_1}{m_2}\right) \quad , \tag{5.15}$$

in which m_1 is the aircraft mass at the beginning and m_2 at the end of the cruise flight. The results of this equation are plotted against the speed in figure 5.5.

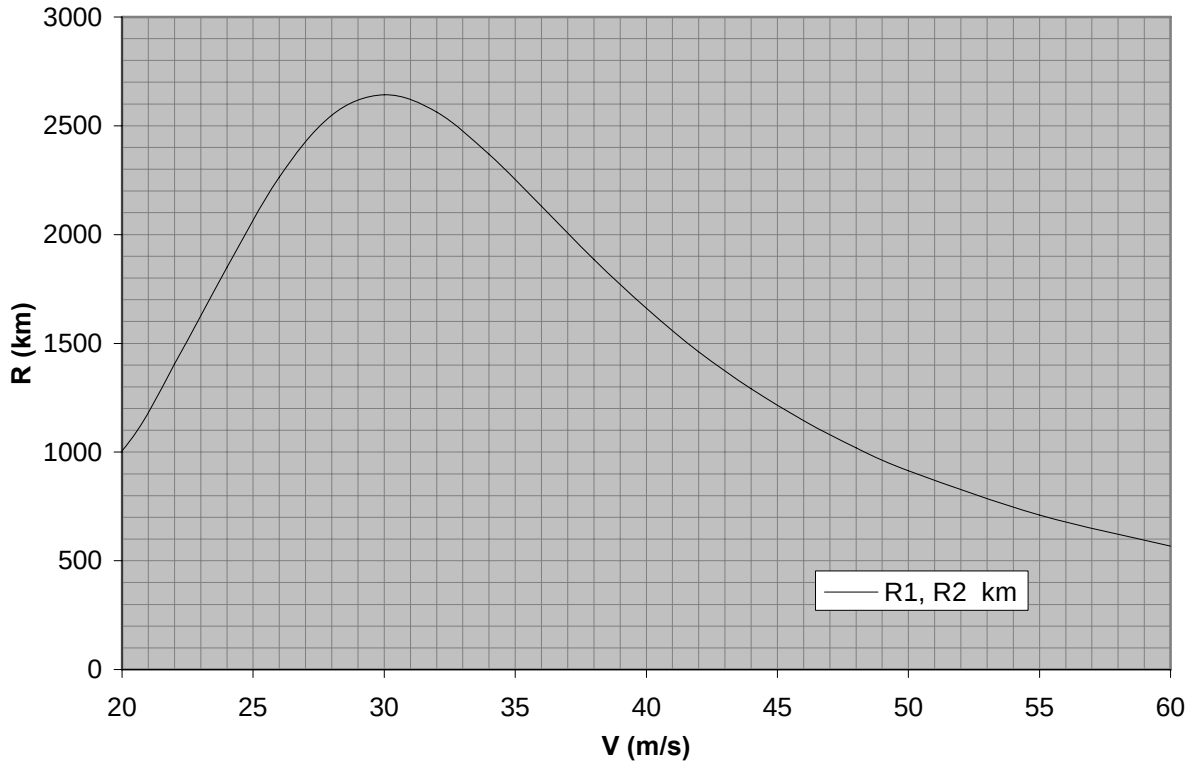

Figure 5.5 Range versus Speed

It can be seen that the greatest range is achieved when flying with a speed of slightly more than $V = V_{D_{\min}} = V_{E_{\max}}$. Higher speeds are of less bad influence on the range than lower ones, as with increasing airspeed propeller efficiency rises.

A numerical search for the maximum range value (using *Solver*, see appendix B) leads to

***R* = 2643 km at a speed of *V* = 30 m/s** (58.3 kn).

For cruise flight, a range of

***R* = 913 km at a speed of V_{cr} = 50 m/s** (97.2 kn)

is determined.

The value of R = 913 km at a speed of 50 m/s is of a very realistic order of magnitude, but **Jackson 2005** gives maximum range values of R = 1100 km for "best power" setting and R = 1400 km for "best efficiency". Hence, the determined maximum range value is about a factor of two larger.

In **Jackson 2005** no reference for the range values is given, and my query posted to the aircraft manufacturer on this topic was not answered. One first attempt to explain the difference between the determined and the literature data is that possibly different flight schedules and an idealised parabolic drag polar were used for the literature value. (Using the idealised parabolic drag polar of chapter four leads to the same values of 1100 km and 1400 km.)

5.2.4 Endurance

For flight schedule one (constant altitude and constant lift coefficient) the endurance is calculated using

$$t_1 = \frac{2\eta_P E}{c' g V_1}\left(\sqrt{\frac{m_1}{m_2}} - 1\right) \quad . \tag{5.16}$$

Here, V_1 is the speed at the beginning of the endurance.

The endurance for flight schedule two (constant speed and constant lift coefficient) is given as

$$t_2 = \frac{\eta_P E}{c' g V} \ln\left(\frac{m_1}{m_2}\right) \quad . \tag{5.17}$$

Figure 5.6 shows that both flight schedules have their maximum endurance at the same speed: a speed slightly higher than minimum power speed $V_{P_{D,\min}}$. The reason for this again lies in better propeller efficiency at higher speeds.

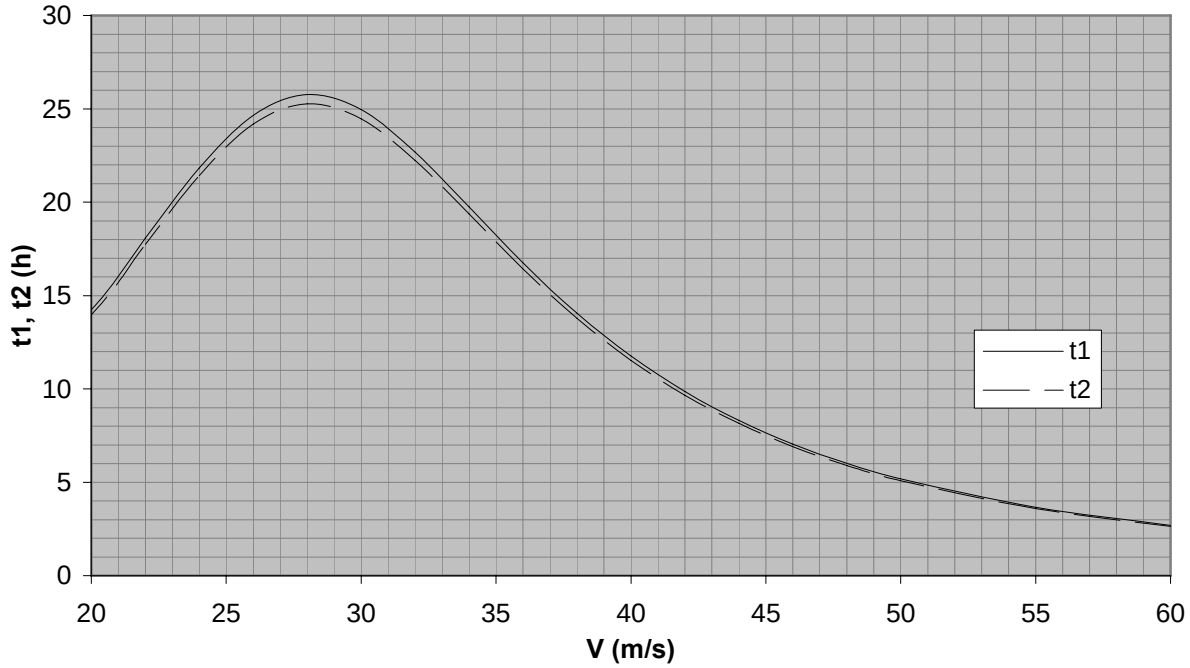

Figure 5.6 Endurance versus Speed

The numerically gained maximum endurance values t_1 and t_2 are:

- t_1 **= 25.8 h at a speed of** V **= 28.1 m/s** (54.6 kn)
- t_2 **= 25.3 h at a speed of** V **= 28.1 m/s** (54.6 kn)

For cruise flight at a speed of 50 m/s the values of t_1 and t_2 result as:

- t_1 **= 5.2 h at a speed of** V **= 50 m/s** (97.2 kn)
- t_2 **= 5.1 h at a speed of** V **= 50 m/s** (97.2 kn).

Again, the cruise flight values are of a realistic order of magnitude and the maximum values are calculated as about a factor of two too large, compared to data given in **Jackson 2005**. For a first attempt of explanation of these values see end of section 5.2.3.

5.2.5 Rate of Climb, Maximum Level Speed and Absolute Ceiling

At each altitude and speed only a certain maximum amount of thrust power is available. With increasing altitude, the air density and the internal combustion engine's maximum power output drop. As stated in section "Terms and Definitions", this power drop can be expressed by the equation

$$\frac{P_S}{P_{S,0}} = \sigma - \frac{1-\sigma}{7.55} \quad , \tag{5.18}$$

which is given in **Raymer 1999** and was published by Gagg and Farrar in 1934 (**Gagg 1934**).

For each speed, a fraction of the delivered shaft power is needed to equal the resulting drag power of this speed at this altitude. In the case of *Maximum Level Speed*, $V_{\max}$, these two values are identical, and as altitude stays constant, the lift exactly equals the weight.

$$\frac{T}{W}V = \frac{D}{L}V \tag{5.19}$$

In other cases, where a greater amount of thrust power may be produced than is needed to keep up altitude and speed, the surplus may be converted into an increase of altitude and/or speed. The vertical speed, V_z , is also called the *Rate of Climb* (ROC).

$$\begin{aligned} TV &= DV + WV_z \\ \mathrm{ROC} = V_z &= \frac{T}{W}V - \frac{D}{W}V \end{aligned} \tag{5.20}$$

The altitude, in which the maximum available thrust power is just sufficient to keep up unaccelerated level flight, i.e. ROC = 0 , is called the *Absolute Ceiling*, h_{abs}. The only flyable speed at absolute ceiling is (ideally) the minimum power speed. (In this case, this speed is also the stall speed and maximum level speed, too.)

When dealing with airspeeds at different altitudes, it is convenient to use the *Equivalent Airspeed* (EAS). Plotting drag power against the true airspeed (TAS) in figure 5.7 would result in one line of drag power for *each* altitude. By plotting against the equivalent airspeed, these lines are reduced to one. As stated in section “Terms and Definitions”, the TAS can be regained from the EAS by:

$$V = \frac{V_E}{\sqrt{\sigma}} = \sqrt{\frac{\rho_0}{\rho}}\, V_E \tag{5.21}$$

In figure 5.7 the maximum rate of climb and the maximum (equivalent) level speed at different altitudes are determined versus altitude. The available thrust is calculated for maximum continuous power ($P_{S,cont}$ = 58 kW at MSL).

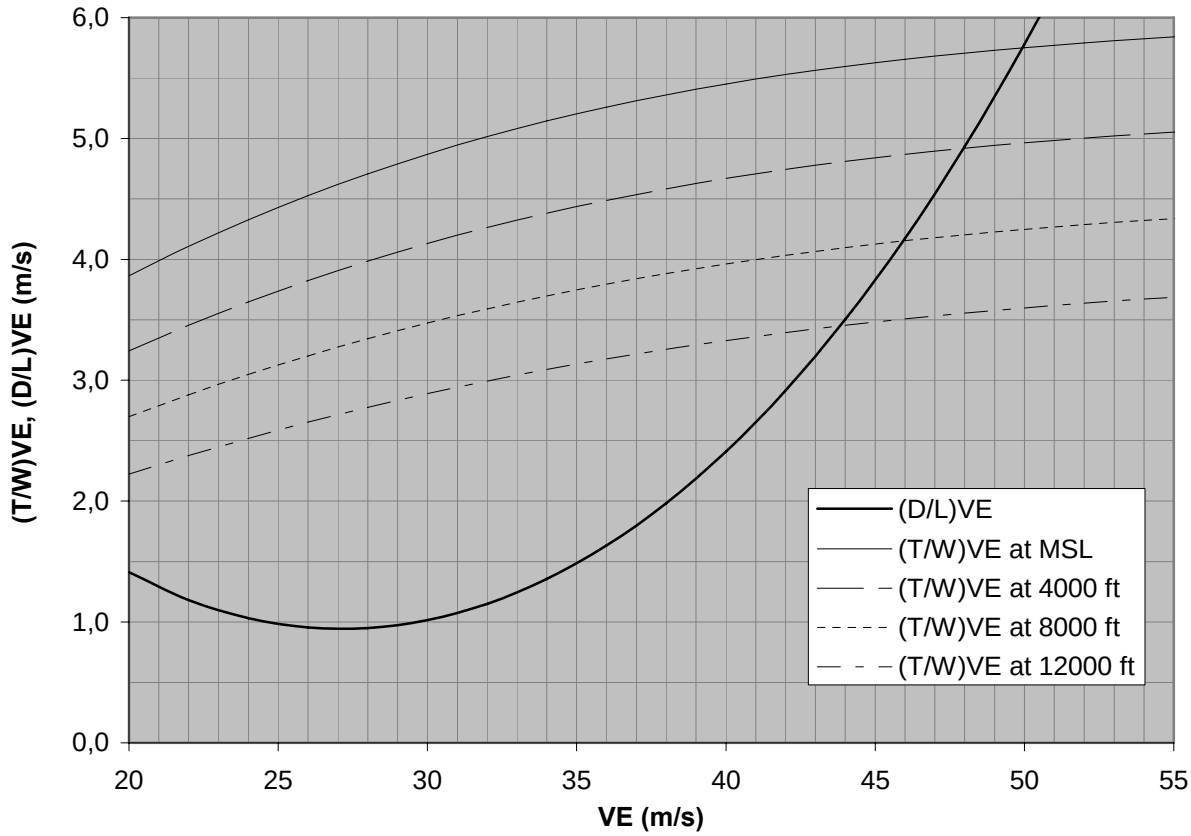

Figure 5.7 Rate of Climb versus Equivalent Airspeed

Table 5.3 Results for Maximum Rate of Climb, Maximum Level Speed and Absolute Ceiling

Item	Symbol	Value
Maximum ROC at MSL	ROC_0	**3.87 m/s** (762 ft/min) at 31.3 m/s (60.8 kn)
Maximum Level Speed at MSL	$V_{\max,0}$	**50 m/s**
Absolute Ceiling	h_{abs}	**8600 m** (28200 ft)

The most important results from figure 5.7 are listed in table 5.3. These values are of an expected and acceptable order of magnitude, but the maximum rate of climb is calculated as too good. In the flight manual (**Aeromot 2002** (p.5.3)), the maximum ROC is given as 2.6 m/s at a speed of 30.5 m/s (512 ft/min at 59 kn).

The low value of the maximum level speed of 50 m/s (180 km/h, 97 kn) at MSL can be explained by the higher drag coefficient of the drag polar equation (C_D = 0.0337) than the one separately determined for cruise (C_D = 0.0317). This increase of factor 1.063 directly leads to the fact that for a cruise speed of 50 m/s, a 1.063 times larger shaft power is needed. **Aeromot 2002** (p.5.3) gives for this speed an engine speed of 5000 RPM, which corresponds to a shaft power of 54.5 kW (**Rotax 2005**) and is of factor 1.063 less than the shaft power of 58 kW shown here.

6 Concept Design Study

Batteries, capable of storing enough electric energy to, at least partly, drive an aircraft, are heavy installations. So, the primary objective of this concept design study is to quantify the effects on the *AMT 200*'s mass, when changing its propulsion system to part-electric.

6.1 Note on Solar Cells as additional Power Source

Assuming equator solar radiation conditions of 1000 W/m² (**www.wikipedia.org 2006b**) and best efficient solar cells (figure 2.12), a maximum electric power of roughly 360 W/m² can be achieved. If 17 m² of the *AMT 200*'s wing, fuselage and horizontal stabilizer were covered with solar cells, this value would lead to a maximum amount of gained electric power of 6.1 kW. Note: this value is the **absolute maximum**, achieved under best conditions and newest, very expensive solar cells.

Assuming an efficiency of twenty percent and a solar radiation of 500 W/m² (condition of Berblinger prize 1996, see section 2.1.2), the gained electric power would be 1.7 kW.

So, compared to large power demands of the *AMT 200* (58 kW at 50 m/s (180 km/h, 97 kn)) or other reference aircraft, this value is not enough to justify their large extra costs, mass, aerodynamic disadvantages, etc. That is why solar cells are no element of this concept design study.

6.2 Collection of Input Masses

The AMT 200's maximum take-off mass is given in **Aeromot 2002** (p.2.3) as 850 kg, and its capacity of usable Avgas fuel is 88 l (p.2.2). So, as Avgas has a density of 0.72 kg/l (**Raymer 1999**, p.268), the fuel mass results as 63 kg. The remaining difference to the empty mass of 620 kg (**Jackson 2005**, p.19) is the payload of 167 kg.

To gain the mass of the 'naked' airframe, i.e. without any motor and energy storage device, the mass of the standard internal combustion (IC) engine of 57 kg (**Aeromot 2002**, p.6.5) and the average starter battery of 10 kg (**Aeromot 2002**, p.6.5) have to be subtracted. The outcome is the starting mass of this concept design study: the AMT 200's airframe mass of 553 kg. Table 6.1 lists up the named masses.

Table 6.1 Mass Breakdown

Mass	**Symbol**	**Value** [kg]
Maximum Take-off Mass	m_{MTO}	**850**
Fuel Mass	m_F	**63**
Payload	m_{PL}	**167**
Empty Mass	m_{empty}	**620**
Mass of standard Internal Combustion Engine	m_{ic}	**57**
Battery Mass	m_{Bat}	**10**
Airframe Mass	m_{AF}	**553**

6.3 Estimation of the Electric Motor Mass

The most important characteristic of an electric motor for this concept design study is its *power density*, i.e. its power output related to its mass. The ideal is a motor that delivers the requested amount of power for only a minimum mass penalty. That is why the most interesting electric motors are the ones that find their application in electric aircraft or, if not enough data should be available, other vehicles, e.g. cars.

Information was found on the three electric motors that are used in the *Antares*, *Icaré 2* and *AE-1 Silent*. For a **hypothetical** fourth one, data was found in an aircraft design study of an electric racing aircraft conducted by students, which is presented in **Jenkinson 2003**. As this motor does not really exist, it will only be used for a theoretical comparison between the results of this study and the work of others. Table 6.2 contains the data found on these motors.

Table 6.2 Mass and Power Data of Electric Motors

Aircraft	**Mass** m_{em}	**Maximum Shaft Power** $P_{S,e}$	**Reference**
Antares	28.5 kg	42 kW	**Marzinzik 2000**
Icaré 2	11.7 kg	14 kW	**Voit-Nitschmann 2005**
AE-1 Silent	8.5 kg	13 kW	**Air Energy 2005**
Student Project: Electric Racing Aircraft	26 kg	75 kW	**Jenkinson 2003**

As this data, so far, only delivers four points in a mass-over-power chart, a method to estimate the masses of hypothetical electric motors of different shaft power levels needs to be determined. This method is based on the *rubber motor*-method; i.e. no particular motor is chosen from a list, but a motor is sized by means of an equation for one's special power need. This means that the hypothetical motor is variable in size and in some way "formable like rubber".

For this purpose, a review was carried out, that discovered data on how the masses of electric motors of the same type-series differ with respect to their shaft power (**PML Flightlink 2005**). The gained data, based on the *PML Flightlink eWheel*-series, is collected in table 6.3. In addition, it is helpful that this series of electric motors was developed for application in electric vehicles, which makes the data comparable to the three aircraft electric motors. As terrestrial applications are less mass-sensitive than airborne ones, the elongated line described by equation (6.1) marks an upper boundary for the mass estimation in this concept design study.

Table 6.3 Mass and Shaft Power Collection of the *PML Flightlink eWheel*-Series (based on ***PML Flightlink 2005***)

Specification	**Mass** m_{em} [kg]	**Maximum Shaft Power** $P_{S,e}$ [kW]
EW 15/30	4	1.35
EW 15/60	6	1.8
EW 20/30	6	2.28
EW 20/60	9	4.2
EW 25/30	8.5	4.2
EW 25/60	13	8.5
EW 30/30	12	7.2
EW 30/60	18	14.4

The dependence between mass and shaft power for the *PML eWheel*-series can be expressed as a good approximation by the following equation; **the shaft power $P_{S,e}$ is in kW, the mass results in kg.**

$$m_{em} = 3.7218 \cdot P_{S,e}^{0.5926} \tag{6.1}$$

The masses of the three electric motors, which are used in the electric aircraft, will, in all probability, change in a quite similar order of magnitude, when their size is adapted to another power level. This means that for their particular equations of mass estimating, an exponent of 0.5926 will lead to acceptable results. The still absent factors in these equations are adjusted to match with the reference point of each specific motor.

The resulting equations for the different motors are:

- *Antares*-type: $m_{em} = 3.111 \cdot P_{S,e}^{0.5926}$ (6.2)
- *Icaré 2*-type: $m_{em} = 2.449 \cdot P_{S,e}^{0.5926}$ (6.3)
- *AE-1 Silent*-type: $m_{em} = 1.859 \cdot P_{S,e}^{0.5926}$. (6.4)

Again, all shaft powers are in kW, and all electric motor masses result in kg.

Figure 6.1 shows the reference points of the motors and the resulting lines from the mass estimation equations.

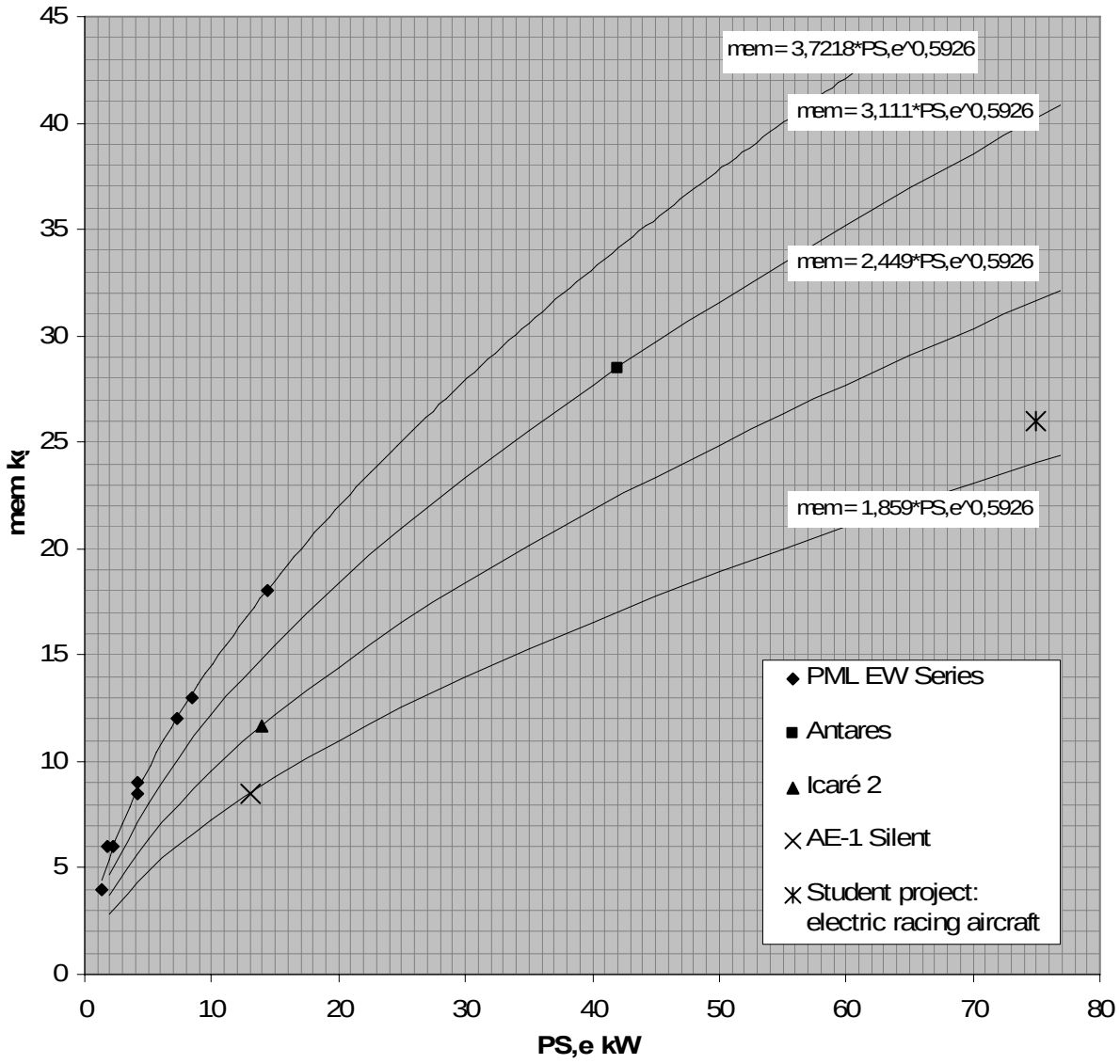

Figure 6.1 Dependency between Mass and Shaft Power of different electric Motor Types

As mentioned above, the hypothetical electric motor from the student project on the electric racing aircraft may be used as a comparison. This reference point is located in the vicinity of the *AE-1 Silent*'s line.

Using an equation that lies somewhat away from the upper boundary marked by the *eWheel*-line and the lower boundary marked by the *AE-1 Silent*-line, will lead to mass estimations in a realistic order of magnitude. Lighter motors than the estimated ones would certainly be possible but extremely expensive.

Additional equipment that is indispensable for the operation of an electric motor in an aircraft is a control device. What exactly is needed for a certain electric motor, depends on its

construction. Control devices are installations such as frequency generators, devices for speed regulation etc. Based on data from the *Icaré 2*, given in **Voit-Nitschmann 2005**, an equation was set up to represent this additional mass of the electric motor control device, m_{emc}. The data on the *Icaré 2* gives a value of 6.08 kg for frequency generator and control device; the mass of the electric motor is 11.7 kg.

As the mass of the control device is dependant on the motor size, there is a constant factor in this equation. In addition, a certain minimum mass will always have to be carried, when using an electric motor. These considerations led to the following equation for the mass of the electric motor control device.

$$\boldsymbol{m_{emc} = 3.5\,\mathrm{kg} + 0.22 m_{em}} \tag{6.5}$$

The total mass of electric motor **and** control device, m_e, results as

$$\boldsymbol{m_e = m_{em} + m_{emc} = 3.5\,\mathrm{kg} + 1.22\, m_{em}} \tag{6.6}$$

6.4 Estimation of the Internal Combustion Engine Mass

The second part of the hybrid engine in this concept design study is an internal combustion engine. Its mass, m_{ic}, will be estimated in a similar way to the electric motor by using a rubber engine-method.

The literature review led to a large number of IC engines which are applied in General Aviation aircraft (**Jackson 2005**, p.839-845). The masses and power outputs of a selection of these are listed in Appendix C.

In figure 6.2, these values are grouped, and each group of engines is described by an approximation equation to estimate the engine mass of a certain needed shaft power (of the IC engine). It is apparent that there are large differences in mass between different types of engines, although they have the same shaft power. Generally, one can say that engines types like *Hirth* and *Rotax* are of significantly less mass than engine types like *Teledyne Continental* or *Textron Lycoming*.

Also, Diesel engines are of a comparatively high mass. But it must be kept in mind that these engines have other advantages, especially in burning less expensive fuel (diesel or kerosene). This concept design study will concentrate on Otto engines, as the determined specific fuel consumption is only applicable for this type of IC engine. Nevertheless, an investigation of Diesel engines as the IC engine-part of the hybrid engine is a very promising possibility and may be performed in a very similar way as in this study.

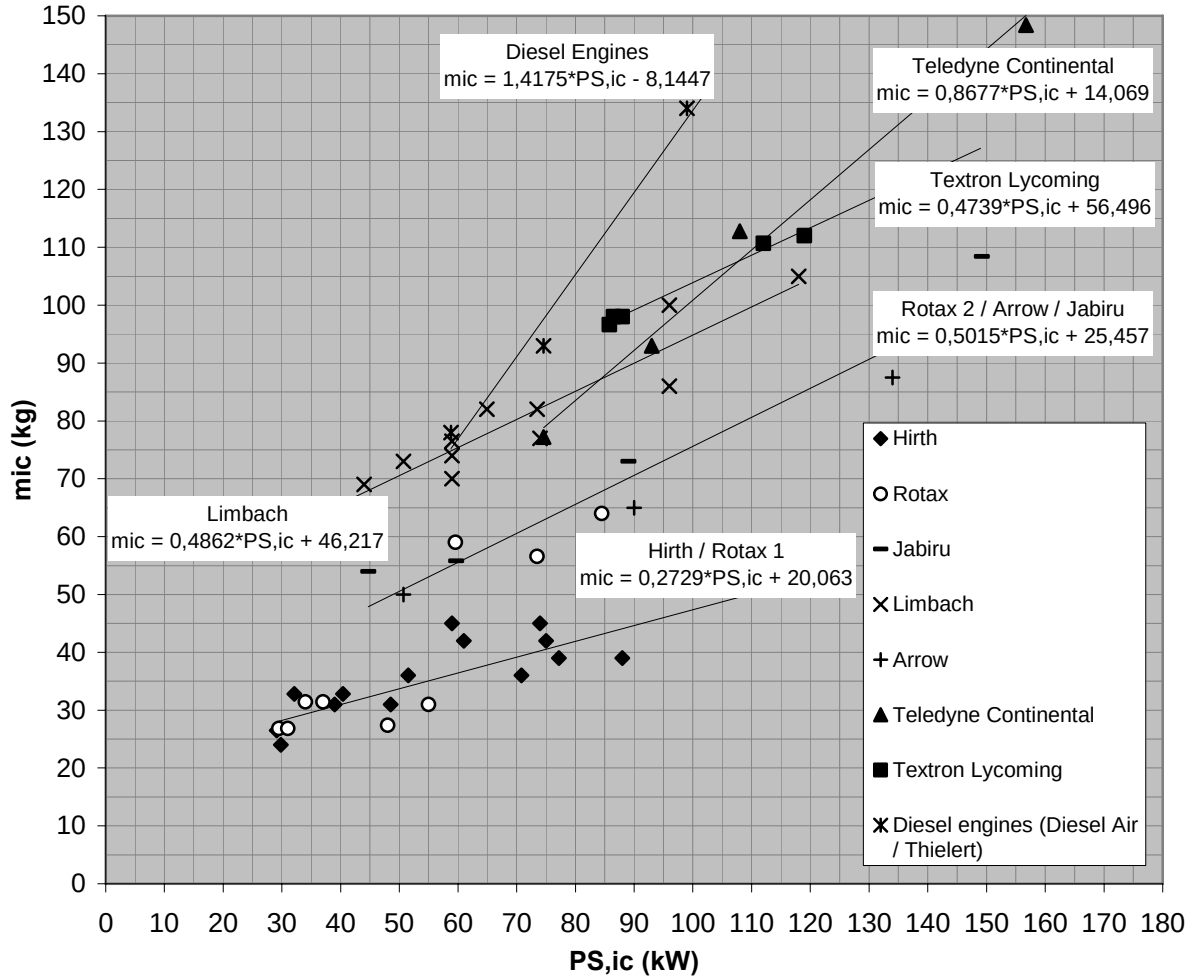

Figure 6.2 Internal Combustion Engine Data and Mass Estimation Equations (based on **Jackson 2005**)

Table 6.4 contains the mass estimation equations derived from figure 6.2. The shaft power of the internal combustion engine $\boldsymbol{P_{S,ic}}$ **has to be used in kW;** the internal combustion engine mass $\boldsymbol{m_{ic}}$ **results in kg.** The gained value of m_{ic} includes all installations needed for the use of each particular engine, except for the starter battery.

Table 6.4 Mass Estimation Equations depending on Internal Combustion Engine Type

IC Engine Type	Mass Estimation Equation
Hirth / Rotax1	$m_{ic} = 0.2729\ P_{S,ic} + 20.063$
Rotax 2 / Arrow / Jabiru	$m_{ic} = 0.5015\ P_{S,ic} + 25.457$
Limbach	$m_{ic} = 0.4862\ P_{S,ic} + 46.217$
Textron Lycoming	$m_{ic} = 0.4739\ P_{S,ic} + 56.496$
Teledyne Continental	$m_{ic} = 0.8677\ P_{S,ic} + 14.069$
Diesel Engine	$m_{ic} = 1.4175\ P_{S,ic} - 8.1447$

6.5 Determination of Energy Costs and CO_2-Emissions

In this section, two of the most important parameters for the assessment of an aircraft's engine modification to a hybrid engine are determined: the energy costs and the carbon dioxide-emissions. The CO_2-emissions are determined as a representative of an aircraft's air pollution. Of course, burning fossil fuel produces several other exhaust gases, such as nitrogen oxides (NO_x), as well, but their amounts are highly depending on the particular IC engine used and environmental circumstances. That is why their quantification is much more complicated, and CO_2 was chosen as the key indicator for an aircraft's air pollution.

6.5.1 Definition of a Reference Mission

Even though most aircraft offer a large maximum range and endurance, they are often used for so called pleasure flights of only short range. That is why the reference mission in this assessment is defined as a typical

- **cruise flight**
- **in 2500 ft**
- **over a time of 2.5 h**
- **at a speed of 50 m/s (180 km/h, 97 kn).**

6.5.2 Fuel Price, Electricity Price and Specific CO_2-Emissions

The fuel price used for the determination of the fuel costs is based on ExxonMobil data (**Zelch 2005**). It leads to an average fuel price for Avgas of 1.636 €/l in 2004 (see figure 6.3). Here, as fuel prices are generally rising, a value of 1.70 €/l is chosen, which, as Avgas has a density of ρ_F = 0.72 kg/l (**Raymer 1999**, p.268), accords with $\boldsymbol{p_F}$ **= 2.36 €/kg Avgas**.

According to **Bundesumweltministerium 2004**, Otto engines produce an average value of the specific CO_2-emission of 2.32 kg CO_2/l fuel, which accords with $\boldsymbol{e_F}$ **= 3.22 kg CO_2/kg Avgas**. The exact value of e_F depends on the particular engine and operational circumstances. For this general investigation, this average value is most suitable.

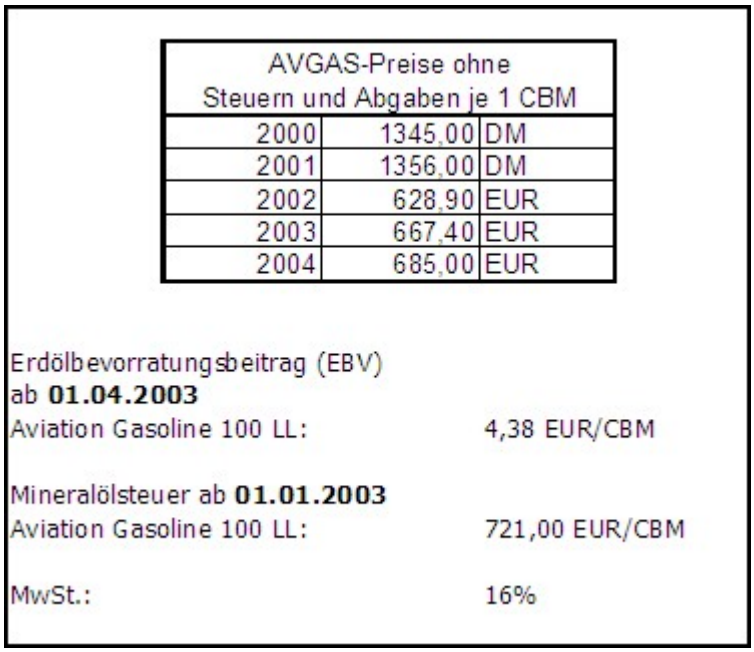

AVGAS-Preise ohne Steuern und Abgaben je 1 CBM		
2000	1345,00	DM
2001	1356,00	DM
2002	628,90	EUR
2003	667,40	EUR
2004	685,00	EUR

Erdölbevorratungsbeitrag (EBV)
ab **01.04.2003**
Aviation Gasoline 100 LL: 4,38 EUR/CBM

Mineralölsteuer ab **01.01.2003**
Aviation Gasoline 100 LL: 721,00 EUR/CBM

MwSt.: 16%

Figure 6.3 Development of the Avgas Price (**Zelch 2005)**

On the German electricity market, there are several suppliers of electric energy. The tariffs for private clients are currently lying between about 16 and 22 Ct/kWh (**verivox 2006**). For the determination of the electric energy costs, a value based on *Greenpeace Energy* of p_e **= 18.9 Ct/kWh** is used in this study. *Greenpeace Energy* was chosen to be the supplier of electric energy, because of its more environmentally friendly production compared to conventional produced electricity. *Greenpeace Energy* uses regenerative energies and natural gas power stations (**Haase 2006**). Figure 6.4 shows the composition of different energy sources and names a value of the specific CO_2-emisson of e_e **= 104 g CO_2/kWh**.

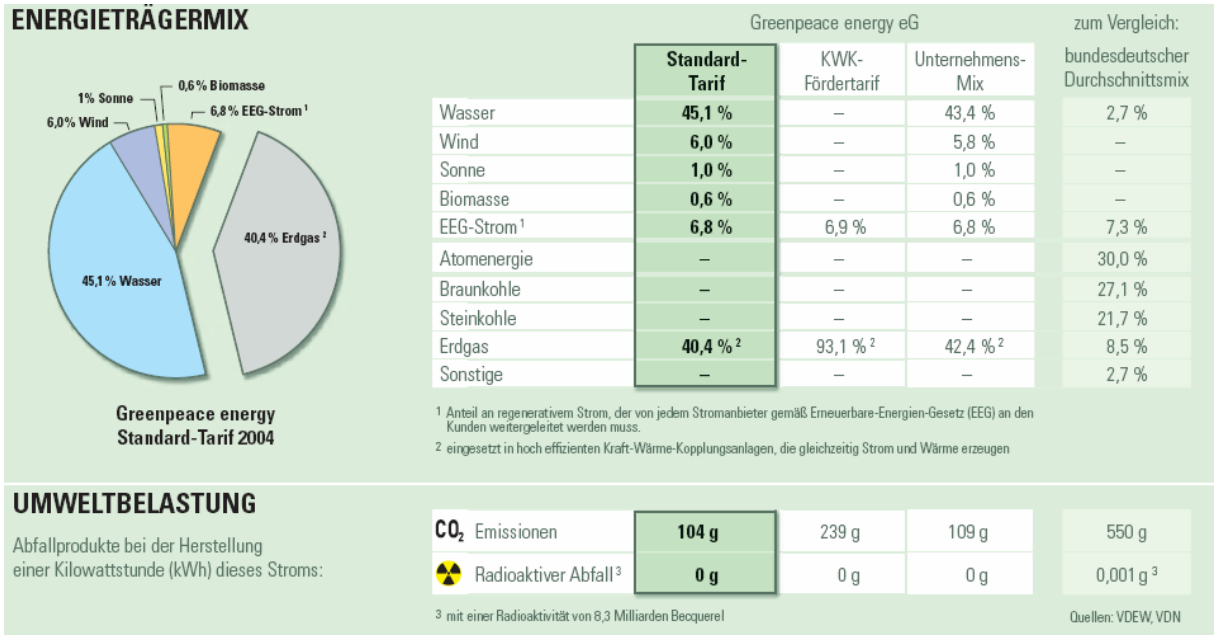

ENERGIETRÄGERMIX

Greenpeace energy Standard-Tarif 2004

	Greenpeace energy eG: Standard-Tarif	KWK-Fördertarif	Unternehmens-Mix	zum Vergleich: bundesdeutscher Durchschnittsmix
Wasser	**45,1 %**	–	43,4 %	2,7 %
Wind	**6,0 %**	–	5,8 %	–
Sonne	**1,0 %**	–	1,0 %	–
Biomasse	**0,6 %**	–	0,6 %	–
EEG-Strom 1	**6,8 %**	6,9 %	6,8 %	7,3 %
Atomenergie	–	–	–	30,0 %
Braunkohle	–	–	–	27,1 %
Steinkohle	–	–	–	21,7 %
Erdgas	**40,4 % 2**	93,1 % 2	42,4 % 2	8,5 %
Sonstige	–	–	–	2,7 %

1 Anteil an regenerativem Strom, der von jedem Stromanbieter gemäß Erneuerbare-Energien-Gesetz (EEG) an den Kunden weitergeleitet werden muss.
2 eingesetzt in hoch effizienten Kraft-Wärme-Kopplungsanlagen, die gleichzeitig Strom und Wärme erzeugen

UMWELTBELASTUNG

Abfallprodukte bei der Herstellung einer Kilowattstunde (kWh) dieses Stroms:

CO_2 Emissionen	**104 g**	239 g	109 g	550 g
Radioaktiver Abfall 3	**0 g**	0 g	0 g	0,001 g 3

3 mit einer Radioaktivität von 8,3 Milliarden Becquerel

Quellen: VDEW, VDN

Figure 6.4 Energy Sources and Specific CO_2-Emission per kWh of *Greenpeace Energy* (**Hasse 2005**)

6.5.3 Energy Costs and CO_2-Emissions of the Reference Aircraft

The amount of fuel that has to be carried, here, is regarded as exactly sufficient for this mission, so that the fuel tanks are empty after these 2.5 h. So, in the Breguet range equation, m_2 equals the maximum zero-fuel mass:

$$m_2 = m_{ZF} = m_{empty} + m_{PL} = 787 \text{ kg} \quad . \tag{6.7}$$

This mass leads to a needed lift coefficient *at the end of the mission with empty fuel tanks* of

$$C_{L,2} = \frac{2m_2 g}{\rho V^2 S} = \frac{2 \cdot 787 \text{ kg} \cdot 9.81 \frac{\text{m}}{\text{s}^2}}{1.225 \frac{\text{kg}}{\text{m}^3} \left(50 \frac{\text{m}}{\text{s}} \right)^2 \cdot 18.7 \text{ m}^2} = 0.29 \quad , \tag{6.8}$$

where the air density is reduced to (see section “Terms and Definitions”)

$$\rho = \rho_0 (1 - 6.8756 \cdot 10^{-6} \cdot 2500)^{4.25588} = 1.138 \frac{\text{kg}}{\text{m}^3} \quad . \tag{6.9}$$

By means of the drag polar equation (5.10)

$$C_D = 0.0251 + 0.0733 \left(C_L - 0.633 \right)^2 \tag{5.10}$$

the needed value of the drag coefficient *at the end of the mission with empty fuel tanks* can be determined as

$$C_{D,2} = 0.0337 \quad . \tag{6.10}$$

The resulting value of the drag power is

$$P_{D,2} = \frac{1}{2} \rho V^3 C_{D,2} S = 44.84 \text{ kW} \quad . \tag{6.11}$$

In **Bichlmeyr 2006**, all propeller efficiencies are given for Sea level. To adopt these values to different altitudes, the change in air density has to be accounted for, i.e. the equivalent airspeed has to be determined as

$$V_E = V\sqrt{\sigma} = V\sqrt{\frac{\rho}{\rho_0}} = 48.2\,\frac{\text{m}}{\text{s}} \quad . \tag{6.12}$$

Hence, the resulting propeller efficiency is

$$\eta_P = 3.48\cdot10^{-6}\,V_E^3 - 6.19\cdot10^{-4}\,V_E^2 + 3.88\cdot10^{-2}\,V_E - 7.12\cdot10^{-4} = 0.821 \quad , \tag{6.13}$$

and the needed shaft power *at the end of the mission with empty fuel tanks* results as

$$P_{S,2} = \frac{P_{D,2}}{\eta_P} = \frac{44.84\,\text{kW}}{0.821} = 54.62\,\text{kW} \quad . \tag{6.14}$$

Using the specific fuel consumption (SFC) as determined in chapter five of

$$c' = 6.18\cdot10^{-8}\,\frac{\text{kg}}{\text{Ws}} \tag{6.15}$$

and assuming a constant shaft power during the whole mission, lead to a needed fuel mass of

$$\boldsymbol{m_F = 30.4\,\text{kg}} \quad . \tag{6.16}$$

So, the mass at the beginning of the mission is in a good approximation

$$m_1 = m_2 + c'\cdot P_{S,2}\cdot t = 817\,\text{kg} \quad . \tag{6.17}$$

The determined value of $m_f = 30.4$ kg is slightly too high. Of course, the aircraft is heavier at the beginning of the reference mission, which means that for a given speed and altitude the lift coefficient must be higher. In this area of the drag polar, a higher lift coefficient means **less** drag (see figure 5.2).

A method to improve the determined mass at the beginning of the mission, is to determine the lift-to-drag ratio and to use this value in the equation

$$m_1 = m_2 \cdot e^{\frac{c'gR}{\eta_P \cdot E}} \quad . \tag{6.18}$$

Herein, "*e*" is not the Oswald efficiency factor but the *Euler number* (*e* = 2.71828), as equation (6.15) is nothing else but the Breguet range equation. As this equation is only applicable for flight schedules with a constant lift coefficient, an average value for the lift-to-drag ratio has to be determined for this reference mission with constant speed, constant altitude and *changing* lift coefficient. For this relatively short reference mission, the gained improvements from equation (6.18) are of a negligible order of magnitude (less than 0.5 kg). For other, longer, reference missions, it is advisable to use this improvement method. It is included in the created *Excel* spreadsheet (see appendix B).

The determined trip fuel mass of m_F = 30.4 kg leads to a mass of produced CO_2 of

$$\boldsymbol{m_{CO_2} = m_F \cdot e_F} = 30.4\ \text{kg} \cdot 3.22 \frac{\text{kg CO}_2}{\text{kg Avgas}} = \mathbf{98\ kg} \quad , \tag{6.19}$$

and fuel costs, which, as Avgas is the reference aircraft's sole energy source, are the total energy costs, of

$$\boldsymbol{C_E = C_F = m_F \cdot p_F} = 30.4\text{kg} \cdot 2.36 \frac{€}{\text{kg Avgas}} = \mathbf{71.78\ €} \quad . \tag{6.20}$$

6.5.4 Energy Costs and CO_2-Emissions of the Hybrid Aircraft

The energy costs and CO_2-emissions of the hybrid aircraft are determined in a similar, but more complex manner, as for the reference aircraft more individual masses of components have to be determined. This collection of determinations cannot be performed in one step. Hence, starting assumptions are made and further improved in (three) iteration steps.

Although the take-off performance is no issue of this assessment, it must be accounted for, as the required take-off distance determines the size (and mass) of the engine – here especially of the internal combustion engine. **Loftin 1980** (p.338-339) shows a correlation of an aircraft's take-off distance and a so called *Take-off parameter*, which is defined as

$$\text{Take-off parameter} = \frac{(W/S)(W/P)}{\sigma} \quad . \tag{6.21}$$

To achieve the same take-off distance as the reference aircraft, the take-off parameter must be kept the same for the hybrid aircraft. In this case, the take-off parameter is

$$\text{Take-off parameter} = \frac{(W/S)(W/P)}{\sigma} = \frac{\left(\frac{850}{18.7}\right)\left(\frac{850}{59600}\right)}{1} = 0.648 \quad . \tag{6.22}$$

Note: here, SI units are used, as the take-off parameter is only used for comparison between reference and hybrid aircraft. If one intends to work with the given figures in **Loftin 1980**, one has to use English units.

Two more values are needed to determine the individual component masses and the overall results of energy costs and CO_2-emission: the energy density of the batteries and the fraction of electrically produced shaft power of the total shaft power.

The highest energy density of batteries ρ_E in practice was found in **Air Energy 2005**. Here, a value of ρ_E of up to 190 Wh/kg is given. Furthermore, it is said that for installation (housing, brackets, etc.) an additional mass of ten to fifteen percent of the battery mass has to be accounted for.

For this investigation, a scaled down energy density of

$$\rho_E = 150 \frac{\text{Wh}}{\text{kg}} \tag{6.23}$$

is used.

For the fraction f of electrically produced shaft power $P_{S,e}$ of the total shaft power P_S during cruise flight, there are generally no restrictions. Each fraction is possible from fully electrical to fully powered by the IC engine. Here, a value of 0.5 is used.

$$f = 0.5 \tag{6.24}$$

As stated above, the component masses are determined in three iteration steps. The first one starts with the reference aircraft. Assuming the same aircraft mass and taking the fraction of electrically produced shaft power into account leads to a first estimation of needed electrically produced shaft power $P_{S,e}$ and, by multiplying it with the endurance of 2.5 h, to the needed amount of stored electric energy.

Equation (6.14) delivered a value of 54.62 kW of needed shaft power for the reference aircraft. Hence, the electrically produced shaft power results as

$$P_{S,e} = f \cdot P_{S,ref} = 27.31\,\text{kW} \tag{6.25}$$

and the needed electric energy as

$$E_e = 68.27\,\text{kWh} \quad . \tag{6.26}$$

Using the energy density of the batteries of 150 Wh/kg and an average "installation factor" of 0.12, give values of the *battery* mass of

$$m_B = 455.1\,\text{kg} \quad , \tag{6.27}$$

the *battery installation* mass of

$$m_{B,inst} = 54.6\,\text{kg} \tag{6.28}$$

and an *overall battery* mass of

$$m_{Bat} = 509.8\,\text{kg} \quad . \tag{6.29}$$

For the estimation of the electric motor mass (see section 6.2), an average factor of 2.7 is used (see figure 6.1 and appendix B, p.119. This leads, using equation (6.6), to an electric motor mass of

$$m_e = 1.22 \cdot 2.7 \cdot 27.31^{0.5926} + 3.5 = 26.9\,\text{kg} \quad . \tag{6.30}$$

In this investigation, the internal combustion engine is assumed to be of the "Rotax 2 / Arrow / Jabiru"-type (see figure 6.2), which means that a factor of 0.5015 and a summand of 25.457 have to be used in the estimation equation. At this stage of the iteration process, the value, or not even the order of magnitude, of the really needed shaft power of the IC engine is not available yet, since the resulting aircraft mass from the battery has not yet been determined. That is why in this first iteration step, for the needed shaft power the maximum continuous shaft power of the reference aircraft is taken. This is very imprecisely but does not matter, as the main driving mass in this iteration step is the battery mass m_{Bat}. So,

$$m_{ic} = 25.457 + 0.5015 \cdot P_{S,cont,ref} = 54.5 \text{ kg} \quad . \tag{6.31}$$

A summation of all here determined masses, the airframe mass and the payload give a **first** value of the aircraft mass at the end of the reference mission:

$$m_2 = m_{AF} + m_{PL} + m_{Bat} + m_{ic} = 1311 \text{ kg} \quad . \tag{6.32}$$

This value still is very inaccurate but already defines the **order of magnitude**, in which the aircraft mass of the hybrid aircraft will lie. So, as a **first** improvement, a better shaft power and mass of the internal combustion engine may be determined using the take-off parameter:

$$P_{S,ic} = \frac{m_2}{\text{T-O Parameter} \cdot S} = \frac{1311^2}{0.648 \cdot 18.7} = 141.8 \text{ kW} \quad . \tag{6.33}$$

Note: Of course, m_2 is not the take-off mass, but here, the **order of magnitude** of the IC engine mass is determined iteratively. The gained value will be improved later on.

This value of $P_{S,ic}$ causes a mass of the IC engine of

$$m_{ic} = 25.457 + 0.5015 \cdot P_{S,ic} = 96.5 \text{ kg} \tag{6.34}$$

and a new value of the aircraft mass at the end of the reference mission of

$$m_2 = m_{AF} + m_{PL} + m_{Bat} + m_{ic} = 1353 \text{ kg} \quad . \tag{6.35}$$

This value is used to determine the corresponding lift and drag coefficient, drag power and shaft power (as done in eqns. (6.8), (5.10), (6.11), (6.14)). The shaft power value is split into electrically and by the IC engine produced (equal) shares. They result as

$$P_{S,e} = P_{S,ic} = 21.4 \text{ kW} \quad . \tag{6.36}$$

The intermediate results for C_L, C_D, P_D and P_S can be found in the *Excel* spreadsheet (Appendices B and D). Note: even though a value for $P_{S,ic}$ of 21.4 kW is determined here, the IC engine is not sized by this value, as it only represents the cruise flight and not the very power demanding take-off.

The value of $P_{S,e}$ = 21.4 kW leads to an amount of stored (and consumed) electric energy of

$$E_e = P_{S,e} \cdot 2.5\ \text{h} = 53.5\ \text{kWh} \quad , \tag{6.37}$$

which corresponds to a value of the overall battery mass of

$$m_{Bat} = 1.12 \cdot \frac{E_e}{\rho_e} = 399.5\ \text{kg} \quad . \tag{6.38}$$

Here starts the next iteration step, which is similar to described first one. In this investigation and in the *Excel* spreadsheet, three improving iteration steps follow. More would, of course, be possible, but lead to no more significant improvements.

The results of the **last iteration step** are listed in table 6.5.

Table 6.5 Results of the Mass and Shaft Power Estimation Iteration Process

Item	Symbol	Value
Stored Electric Energy	E_e	55.24 kWh
Overall Battery Mass	m_{Bat}	412.4 kg
Electric Motor Mass	m_e	24.1kg
Internal Combustion Engine Mass	m_{ic}	89.7 kg
Aircraft Mass at the End of Reference Mission	m_2	1246 kg
Lift Coefficient at the End of Ref. Mission	$C_{L,2}$	0.4595
Drag Coefficient at the End of Ref. Mission	$C_{D,2}$	0.0273
Lift-to-Drag Ratio at the End of Ref. Mission	E_2	16.83
Drag Power at the End of Ref. Mission	$P_{D,2}$	36.3 kW
Shaft Power at the End of Ref. Mission	$P_{S,2}$	44.2 kW

To achieve a value of the aircraft mass at the beginning of the reference mission m_1, the fuel mass m_F is determined in a similar way as for the reference aircraft in section 6.4.3. Again, a specific fuel consumption (SFC, c') of $6.18 \cdot 10^{-8}$ kg/(Ws) is used. But this time, only a by the factor $(1 - f)$ reduced share of the whole shaft power has to be produced by the internal combustion engine; so:

$$m_F \approx P_{S,2} \cdot (1 - f) \cdot c' \cdot 2.5\,\text{h} = 12.3\,\text{kg} \quad . \tag{6.39}$$

Here, again the fuel mass is slightly too high, as the drag and drag power reduce with rising lift coefficient in this region of the drag polar, but of a negligible order of magnitude and "on the safe side".

This value of m_F corresponds to a fuel flow of

$$Q = P_{S,2} \cdot (1 - f) \cdot c' = 4,92\,\frac{\text{kg}}{\text{h}} = 6.83\,\frac{\text{l}}{\text{h}} \tag{6.40}$$

and leads to a first value of the aircraft mass at the beginning of the reference mission of

$$m_1 = m_2 + m_F = 1258\,\text{kg} \quad , \tag{6.41}$$

which again is used for one **last improvement** of the IC engine and aircraft mass at the beginning of the reference mission:

$$P_{ic} = \frac{m_1^2}{0.648 \cdot S \cdot 1000} = 130.8\,\text{kW} \quad , \tag{6.42}$$

$$m_{ic} = \frac{m_1^2}{0.648 \cdot S \cdot 1000} \cdot 0.5015 + 25.457 = 91\,\text{kg} \quad , \tag{6.43}$$

$$m_1 = 1246\,\text{kg} - 89.7\,\text{kg} + 91\,\text{kg} + 12.3\,\text{kg} = 1260\,\text{kg} \quad . \tag{6.44}$$

As for the reference aircraft, one could improve the value of m_1 again by using the rearranged Breguet range equation (eqn. (6.18)). This is done in the *Excel* spreadsheet but not presented here, as the difference is of only 0.1 kg.

Table 6.6 lists up all **final** results of the described mass and shaft power determination process.

Table 6.6 Final Aircraft Data after three Itaration Steps

Item	Symbol	Value
Electric Energy Consumption	E_e	55.24 kWh
Overall Battery Mass	m_{Bat}	412.4 kg
Electric Motor Mass	m_e	24.1 kg
Internal Combustion Engine Mass	m_{ic}	91 kg
Aircraft Mass at the End of Reference Mission	m_2	1247 kg
Aircraft Mass at the Beginning of Ref. Mission	m_1	1259 kg
Fuel Mass needed for Ref. Mission	m_F	12.3 kg (17.1 l)
Shaft Power of internal Combustion Engine	$P_{S,ic}$	130.8 kW
Shaft Power of Electric Motor	$P_{S,e}$	22 kW

The main results are the electric energy Consumption E_e and the needed fuel mass m_F. Using the values for fuel price p_F, electricity tariff p_e and the specific CO_2-emissions e_F and e_e, as stated in section 6.4.2, lead to the following costs and emissions:

$$C_E = C_F + C_e = m_F \cdot p_F + E_e \cdot p_e \tag{6.45}$$

$$m_{CO_2} = m_{CO_2,F} + m_{CO_2,e} = m_F \cdot e_F + E_e \cdot e_e \tag{6.46}$$

Table 6.7 Energy Costs of Hybrid Aircraft for Reference Mission

Costs			
Fuel Mass m_F	**Fuel Price** p_F	**Fuel Costs** C_F	**29.00 €**
12.3 kg	2.36 €/kg Avgas		
Electric Energy E_e	**Electricity Tariff** p_e	**Electricity Costs** C_e	**10.44 €**
55.24 kWh	18.9 Ct/kWh		
		Total Energy Costs C_E	**39.44 €**

Table 6.8 CO_2-Emissions of Hybrid Aircraft for Reference Mission

CO2-Emissions			
Fuel Mass m_F	**Specific CO_2-Emission** e_F	**CO_2-Emission** $m_{CO_2,F}$	**39.61 kg**
12.3 kg	3.22 kg CO_2/kg Avgas		
Electric Energy E_e	**Specific CO_2-Emission** e_e	**CO_2-Emission** $m_{CO_2,e}$	**5.74 kg**
55.24 kWh	104 g CO_2/kWh		
		Total CO_2-Emission m_{CO_2}	**45.35 kg**

As a comparison: the energy costs and CO_2-emissions of the reference aircraft were determined as:

- $m_{CO_2,ref} = 98\ \text{kg}$
- $C_{E,ref} = 71.78\ €$

Hence, the determined values of the hybrid aircraft for total energy costs and total CO_2-emission are roughly fifty percent less that the ones of the reference *AMT 200 Super Ximango*. This significant reductions (energy costs: 45 percent, CO_2-emission: 53 percent) indicate that a change to a hybrid engine is economically and ecologically reasonable **from a flight mechanical point of view**. For a final judgement, several more aspects, such as structural issues, certification, operation, acquisition costs, etc., will have to be investigated.

7 Description of the *Excel* Spreadsheet

The created *Microsoft Excel* spreadsheet consists of eight sheets. It can be used as a tool to determine a reference aircraft's performance characteristics and to investigate a change in its propulsion system from an internal combustion engine to a hybrid engine, consisting of an IC engine and an electric motor. The spreadsheet attached to this report uses the data of the reference aircraft *Aeromot AMT 200 Super Ximango*, but it may be adapted to other General Aviation aircraft for investigation.

In the vicinity of calculated results, the used equation is presented in a textbox. The user has to enter the requested values in the yellow marked cells; green marked cells indicate important results. Print-outs of all eight sheet s are attached to this report in Appendix B; the spreadsheet itself can be found on the enclosed CD-ROM (Appendix D)

The experiences during this study led to the fact, that all performance characteristics are *not* determined using the idealised parabolic drag polar but a more accurate drag polar equation having the form

$$C_D = C_{D,\min} + k\left(C_L - C_L\left(C_{D,\min}\right)\right)^2 \quad . \tag{7.1}$$

This leads to the fact that, in some parts of the spreadsheet, the *Excel* Ad-In *Solve*r has to be used, to find results in a **numerical** way. Each time, *Solver* has to be used, a textbox tells the user, what has to be filled in the *Solver*-dialog box.

Sheet 1: Polar (p.111-112)
In this sheet, the main reference aircraft data is collected for later calculations. Main data means: geometrical data (wing span and wing area), masses of the whole aircraft and some components and engine data (maximum and max. continuous shaft power). Furthermore, values for the variables used in the drag polar equation (7.1) and the propeller efficiency equation (7.2) have to be inserted. For a comparison between drag polar equation and the real aircraft, flight polar data, taken from the aircraft's flight manual, may be filled in. This comparison is presented in form of a chart and table.

In the current form, the propeller efficiency is calculated as speed-dependent. It has the form

$$\eta_P = k_1 V^3 + k_2 V^2 + k_3 V + k_4 \quad . \tag{7.2}$$

The resulting development of the propeller efficiency versus speed is also presented in form of a chart. Due to the received input data from the propeller manufacturer, *Hoffmann*

Propeller (**Bichlmeyr 2006**), the propeller efficiency is calculated and displayed up to a speed of 60 m/s.

Sheet 2: Range + Endurance (p.113-114)
In this sheet, the reference aircraft's specific fuel consumption (SFC) is calculated from input data. In the current form, this data was taken from the flight manual of the *AMT 200* and data gained from the propeller manufacturer.

The SFC and drag polar data is used to calculate maximum range and endurances for default speeds up to 60 m/s and presented as a chart and table. Maximum values for range and endurances are highlighted in green. Range and endurance values are calculated for the flight schedules one and two (both with constant lift coefficient during cruise flight). As absolute maximum values for range and endurance will most often lie between two default speeds, a section is included to search numerically for maximum values of range or endurance. This search has to be performed by the user, using the *Excel* Ad-In *Solver*. All work steps for this search are explained in a textbox next to this section.

Sheet 3: Drag + Power (p.115)
In this sheet, the drag, drag power and shaft power are calculated for default speeds up to 60 m/s and presented in a table. Minimum values are highlighted in green, and all used equations are given right of the table.

Solver can be used by the user of this spreadsheet to find the absolute values of minimum drag, minimum drag power and minimum shaft power and each correlated speed. Again, all settings in the *Solver*-dialog box are given in textboxes next to the input and result cells. It is recommended, to perform this search using *Solver*. At least, the corresponding default speeds of the minimum values of drag, drag power and shaft power have to be filled in the yellow highlighted cells, as some of these values are used in following calculations.

The developments of drag, drag power and shaft power versus speed are presented in a chart. In this chart, the drag is correlated to the left vertical axis; drag power and shaft power are correlated to the right vertical axis.

Sheet 4: Climb + Ceiling (p.116-117)
In this sheet, the maximum climb speed (Rate of Climb, ROC) and the maximum level speed are calculated numerically for Sea level. Furthermore, the theoretical absolute ceiling of the reference aircraft is determined numerically. So, for these results, again, *Solver* has to be used.

The developments of climb speed versus airspeed and available versus needed shaft power versus altitude are presented in charts. For a visual comparison of theoretical versus real climb speed at Sea level, the user may insert data from the flight manual, if available.

Sheet 5: Thrust vs Drag (p.118)
In this sheet, the development of drag power and available thrust power at Sea level and seven more altitudes of choice are calculated and displayed in a table. All values are calculated versus equivalent airspeed (EAS). The results of drag power versus EAS, thrust power versus EAS and thrust power in three of the seven different altitudes versus EAS are displayed in a chart.

Sheet 6: E-Motor (p.119)
In this sheet, the equation to estimate the mass of the electric motor, depending on its needed shaft power, is determined. Four curves are presented in a chart. Each curve is the result of an equation having the form

$$m_e = k \cdot P_{S,e}^{\ 0.5926} \quad , \tag{7.3}$$

in which the electric motor shaft power $P_{S,e}$ is in kW, and the electric motor mass m_e results in kg.

The highest curve describes the development of the electric motor mass with rising shaft power and delivers the exponent 0.5926 (derived from the *PML eWheel*-series (**PML Flightlink 2005**)). The other three curves also use this exponent, but their factors are adapted to match with given mass-power relationships of the three reference motors (*Antares, Icaré 2, AE-1 Silent*).

The user, here, has to define the factor and exponent for the electric motor mass estimation equation that will be used in following steps. In addition, the user may perform separate estimations by filling in a hypothetical needed shaft power value and see the resulting electric motor mass derived from this value. As in later steps, the shaft power value for the hybrid aircraft is determined automatically, only the chosen **values of the factor and the exponent** are of influence on later steps.

Sheet 7: IC Engine (p.120)
This sheet is in its use very similar to sheet 6: E-Motor. Here, the mass of the used internal combustion (IC) engine is estimated depending on its construction. For this purpose, several reference engines' mass versus shaft power data are displayed in a chart and grouped. For each group, an average describing equation is given. All equations are of the form

$$m_{ic} = k_1 \cdot P_{S,ic} + k_2 \quad . \tag{7.4}$$

The units used for internal combustion engine mass m_{ic} and internal combustion engine shaft power, again, are kg and kW.

For the following step, here, the user has to decide, which group's equation shall be used. Like in sheet 6, the user may perform a separate mass estimation of no influence on the following step by inserting a group's mass estimation equation and a hypothetical needed shaft power of choice in the particular cells.

Sheet 8: Mission (p.121)
In this sheet, the reference aircraft is compared to the same reference aircraft with a hybrid propulsion system consisting of an IC engine and an electric motor. For this purpose, first of all, a reference mission is defined, consisting of altitude, cruise speed and either endurance or distance.

Afterwards, data on the fuel and electricity used have to be filled in: fuel price, electricity tariff and specific CO_2-emission of the electricity used. Together with an energy density of the batteries used and the fraction of electrically produced shaft power of the whole shaft power during cruise, following data is calculated:

- needed shaft power for cruise flight,
- aircraft mass at the beginning and end of the reference mission, (empty tanks at the end of reference mission)
- fuel flow in kg/h and l/h,
- total consumption of fuel and electricity for reference mission,
- total energy costs and
- mass of produced CO_2 for reference mission.

In addition, a value for the needed IC engine shaft power of the hybrid aircraft to keep up the same take-off performance as the reference aircraft is calculated.

Discussion

As mentioned in this report, this study may be regarded as a first step in investigating and assessing a change of a reference aircraft to a hybrid aircraft. Here, the new aircraft is investigated from a flight mechanical point of view. Other aspects, e.g. structural and installation issues, certification, operation, maintenance, acquisition costs, etc., will have to be examined as well, before one can achieve a final result. It is apparent that a change in an aircraft's powerplant to a combination of an IC engine and an electric motor will have large influences on the aircraft's structure, especially because of the large additional battery mass.

This study uses a "minimum change solution", i.e. the powerplant is the only component of the reference aircraft that is regarded as modified. In addition, the new hybrid engine mass was gained by adding together the masses of the *rubber* IC engine and the *rubber* electric motor. A real hybrid engine will need a transmission to integrate an IC engine and an electric motor. The installation of IC engine, electric motor, transmission and accessory installations in a reference aircraft will require more installation volume than the original IC engine alone. This leads inevitably to e.g. a longer nosecone and/or a larger fuselage diameter, which causes aerodynamic changes.

In this thesis' concept design study, Diesel engines were not taken into account. For future investigations, it is advisable to investigate Diesel engines as the IC engine part of the hybrid engine, because under certain circumstances, modern Diesel engines are economically and thermodynamically more efficient than Otto engines. For instance, Diesel engines burn less expensive fuel (diesel or kerosene) and have relatively low fuel consumptions.

Conclusions

The following main conclusions are drawn from this study:

1. The simple parabolic drag polar, having the form

$$C_D = C_{D,0} + \frac{C_L^2}{\pi A e} \quad ,$$

delivers only poor results for this type of reference aircraft at low lift coefficients. As for cruise flight reference missions relatively high speeds are used and consequently low lift coefficients are needed, another drag polar equation must be used. This equation has the form

$$C_D = C_{D,\min} + k\left(C_L - C_L\left(C_{D,\min}\right)\right)^2 \quad .$$

2. A *Microsoft Excel* spreadsheet has been created as a tool to compare and assess the reference aircraft and the new hybrid aircraft regarding their aircraft masses, energy consumptions, energy costs and carbon dioxide-emissions. This tool uses a flight mechanical point of view. The structure of this spreadsheet allows future users to enlarge and improve the assessment process.

3. A large fraction of electrically produced shaft power causes a large aircraft mass penalty. This thesis' reference mission of 2.5 h flight in 2,500 ft at a speed of 50 m/s (180 km/h, 97 kn) results in a more than 50 percent greater aircraft mass of the hybrid aircraft compared to the reference aircraft.

4. Despite larger aircraft mass, the hybrid aircraft produces less energy costs and CO2-emissions. For the applied reference mission, the savings in energy costs and CO_2-emissons are of an order of magnitude of 50 percent. For these values, a fuel price (Avgas) of 1.70 €/l was assumed. For electricity, tariff and specific CO_2-emission were taken as values of Greenpeace energy.

5. Due to the large economisations in costs and CO_2-emission when using electric energy, a third construction type of hybrid engines appears to be favourable for General Aviation aircraft: an electric motor for cruise flight, which is assisted during take-off and climb by an internal combustion engine.

6. A change of a General Aviation aircraft's engine to a hybrid engine causes major modifications of the whole aircraft. These modifications lead to changes in an aircraft's structure, aerodynamic, certification, operation, maintenance, etc. Hence, a change of a

reference aircraft to a hybrid aircraft will rather be a new development than a modification – especially regarding certification.

Acknowledgements

First of all, it is time to thank my girlfriend and parents for all their support during my studies and especially during this thesis in a lot more than just a financial way. Without your appreciation and assistance, I could never have done this work in Ireland.

Then, I would like to thank my supervisors in Ireland and Germany, Dr. Trevor Young and Prof. Dr. Scholz, who always answered my questions very helpfully. Furthermore, I am fully aware that writing my thesis at the University of Limerick only was possible because of your personal involvement.

And last but definitely not least, there are Andrea and André, who very often reminded me of more reasons for being in Ireland than just writing my thesis. You really became dear friends of mine.

References

Aeromot 2002
AEROMOT INDÚSTRIA MECÂNICO METALÚRGICA LTDA: *Super Ximango AMT 200 Flight Manual 200-07*. Company Location: Aeromot Indústria Mecânico Metalúrgica LTDA, Av. das Indústrias, 1210, 90200-290, Porto Alegre, RS, Brasil, 2002. – Corporate Publication, Rev. 05

Aeromot 2006
AEROMOT INDÚSTRIA MECÂNICO METALÚRGICA LTDA –
URL: http://www.ximango.com.br/ingles/images/galeria14.jpg (accessed 2006-02-21)

AeroVironment 2005
AEROVIRONMENT INC.: *AeroVironment Flies World's First Liquid Hydrogen Powered UAV*. -
URL: http://www.aerovironment.com/news_detail.php?id=10 (accessed 2006-02-20)

Air Energy 2005
AIR ENERGY ENTWICKLUNGSGESELLSCHAFT MBH & CO KG: *AE-1 Silent.* –
URL: http://www.airenergy.de/html/ae-1_silent.html (accessed 2005-09-30)

airliners.net 2006a
LUNDGREN AEROSPACE INTERNATIONAL –
URL: http://www.airliners.net/search/photo.search?front=yes&maxres=500&keywords=falke+scheibe (accessed 2006-02-21)

airliners.net 2006b
LUNDGREN AEROSPACE INTERNATIONAL –
URL: http://ww.airliners.net/search/photo.search?front=yes&maxres=500&keywords=stemme+s10 (accessed 2006-02-21)

AMS 2006
AMS-FLIGHT, D.O.O: *Carat Photos* –
URL: http://www.ams-flight.si/picView.php?lng=eng&pic=Carat/Photos/Carat04_04_D_resize.jpg (accessed 2006-02-21)

Anderson 2005
ANDERSON, John D., Jr.: *Introduction to Flight*, 5th Ed. New York : McGraw-Hill, 2005

Bert 1999
BERT, Charles W.: *Range and endurance of turboprop, turbofan or piston-propeller aircraft having wings with or without camber*. Norman, University of Oklahoma, USA, School of Aerospace and Mechanical Engineering, Research article, 1999

Berton 2003
BERTON, Jeffrey J., FREEH, Joshua E., WICKENHEISER, Timothy J.: *An Analytical Performance Assessment of a Fuel Cell-Powered, Small Electric Airplane.* NASA Glenn Research Center, 2003. – NASA/TM–2003-212393; URL: http://www-psao.grc.nasa.gov/Library/Abstracts/TM-2003-212393.pdf (accessed 2005-10-05)

Bichlmeyr 2006
BICHLMEYR, Stefan: *Diplomarbeit* : email to Kolja Seeckt (k.seeckt@gmx.net). Hoffmann Propeller GmbH & Co KG, Rosenheim, Germany, 2006-01-09

Boeing 2003
JENKINS, Maureen: Cool Fuel. In: *Boeing Frontiers online*, vol. 02 (2003), issue 04 – URL: http://www.boeing.com/news/frontiers/archive/2003/august/i_atw.html (accessed 2005-11-13)

Bundesumweltministerium 2004
GERMANY, BUNDESMINISTERIUM FÜR UMWELT, NATURSCHUTZ UND REAKTORSICHERHEIT: *CO_2-Ausstoss im Haushalt*, 2004. –
URL: http://www.bmu.de/files/klimaschutz/bildungsservice/application/pdf/verursacher_haushalt.pdf (accessed 2005-11-20)

Bundesumweltministerium 2005
GERMANY, BUNDESMINISTERIUM FÜR UMWELT, NATURSCHUTZ UND REAKTORSICHERHEIT: *General Information – Climate Protection*, 2004. –
URL: http://www.bmu.de/english/climate/general_information/doc/4311.php (accessed: 2006-02-14)

Diamond 2006
DIAMOND AIRCRAFT INDUSTRIES: *HK36 Super Dimona* –
URL: http://www.diamond-air.at/de/products/HK36/index.htm (accessed 2006-02-21)

Farschtschi 2001
FARSCHTSCHI, ALI: *Elektromaschinen in Theorie und Praxis*. Berlin : VDI Verlag, 2001

Fraunhofer ISE 2002
FRAUNHOFER INSTITUT SOLARE ENERGIESYSTEME: *Meilensteine*, 2002. –
URL: http://www.ise.fhg.de/german/profile/history/index.html (accessed 2006-02-23)

Gagg 1934
GAGG, R. F.; FARRAR, E.V.: Altitude Performance of Aircraft Engines Equipped with Gear Driven Superchargers. In: *SAE Journal*, vol. 34 (1934), no. 6, p.217-225

Haase 2006
HAASE, Jan: Antwort: *Anfrage zum Schadstoffausstoß pro kWh Preises* : email to Kolja Seeckt (k.seeckt@gmx.net). Greenpeace Energy eG, Germany, 2006-01-03

Honda 2005
URL: http://www.insightcentral.net (accessed 2005-10-08)

Honda 2006a
URL: http://world.honda.com/FuelCell/FCX/ultracapacitor/charging/ (accessed 2006-02-20)

Honda 2006b
URL: http://world.honda.com/FuelCell/FCX/fuelcell/generation/ (accessed 2006-02-21)

Howe 2000
HOWE, Denis: *Aircraft Conceptual Design Synthesis.* London : Professional Engineering Publishing, 2000

Jackson 2005
JACKSON, Peter (Ed.): *Jane's all the World's Aircraft* 2005/2006. Coulsdon, Surrey, UK : Jane's Information Group, 2005

Jenkinson 2003
JENKINSON, Lloyd R.; MARCHMAN, James F.: *Aircraft Design Projects : For Engineering Students*. Oxford : Butterworth-Heinemann, 2003

Lange Flugzeugbau 2005
LANGE FLUGZEUGBAU GMBH: *Antares – The Electric Motorglider.* –
URL: http://www.lange-flugzeugbau.de/english/menu/menu-akt.htm (accessed 2005-12-08)

Loftin 1980
LOFTIN, L.K., Jr.: *Subsonic Aircraft: Evolution and the Matching of Size to Performance*, NASA Reference Publication 1060, 1980

Marzinzik 2000
MARZINZIK, Gerhard: Nach den Sternen gegriffen. In: *aerokurier* (2000), No. 1, p.44-49

NASA 2005a
NASA Dryden Flight Research Center: *Pathfinder Solar Powered Aircraft*, 2005. –
URL: http://www.nasa.gov/centers/dryden/news/FactSheets/FS-034-DFRC.html (accessed 2005-10-18)

NASA 2005b
NASA Dryden Flight Research Center: *Centurion*, 2005. –
URL: http://www.nasa.gov/centers/dryden/news/FactSheets/FS-056-DFRC.html (accessed 2005-10-18)

NASA 2005c
NASA Dryden Flight Research Center: *Helios Prototype: The forerunner of 21st century solar-powered "atmospheric satellites"*, 2005. –
URL: http://www.nasa.gov/centers/dryden/news/FactSheets/FS-068-DFRC.html (accessed 2005-10-18)

NASA 2005d
NASA: *Helios Crash Probed*, 2004. –
URL: http://www.nasa.gov/missions/research/helios.html (accessed 2005-10-18)

NREL 2006
NATIONAL RENEWABLE ENERGY LABORATORY: *Best Research-Cell Efficiencies*; 2004. –
URL: http://www.nrel.gov/ncpv/thin_film/docs/kaz_best_research_cells.ppt (accessed 2006-02-23)

Oswald 1933
OSWALD, W. Bailey: *General Formulas and Charts for the Calculation of Airplane Performance*, NACA Report 408, 1933

Pehnt 2001
PEHNT, MARTIN; NITSCH, JOACHIM; Deutsches Zentrum für Luft- und Raumfahrt: Bedeutung alternativer Antriebe und Kraftstoffe für den Ressourcen- und Klimaschutz. Stuttgart : Deutsches Zentrum für Luft- und Raumfahrt, 2001.
URL: http://www.dlr.de/tt/institut/abteilungen/system/publications/ET-Artikel_nitsch_pehnt.pdf (accessed 2005-11-10)

PML Flightlink 2005
PML FLIGHTLINK LTD: *EW Series Wheel Motor.* –
URL: http://www.pmlflightlink.com/pdfs/eWheel.pdf (accessed 2005-11-13)

Raymer 1999
RAYMER, Daniel P.: *Aircraft Design: A Conceptual Approach.* 3rd Ed. Washington D.C. : AIAA, 1999

RMI 2006
ROCKY MOUNTAIN INSTITUTE: *Ultracapacitors*. –
URL: http://www.rmi.org/sitepages/pid461.php (accessed 2006-02-20)

Roskam 1997
ROSKAM, Jan: *Airplane Design.* Part 1 : Preliminary Sizing of Airplanes, Ottawa, Kansas : Analysis and Research Corporation, 1997 – Although 1985 is given as the book's first date of printing, some differences exist to older versions of this book, and some cited figures are not included in older versions.

Rotax 2005
ROTAX GMBH: *ROTAX® AIRCRAFT engine type 912 A (series)*. –
URL: http://www.rotax-aircraft-engines.com/aircraft/aircraft.nsf/eng_912A?OpenPage

Skeleton Technologies 2003
SKELETON TECHNOLOGIES: *Breakthrough in Supercapacitors*. Baar, Switzerland -
URL: http://www.skeleton-technologies.com/docs/pdf/SuPCaP_web.pdf (accessed 2005-10-20)

Solair 2005
URL: http://www.solair.de/frame.htm (accessed 2005-09-29)

solarmobil.net 2005
URL: http://www.solarmobil.net/download/2005-03-23-fortu.pdf (accessed 2005-10-20)

Stemme 2006
STEMME AG: *S8* –
URL: http://www.stemme.de/daten/d/produkte/s8/phils8.htm (accessed 2006-02-21)

Stinton 1983
STINTON, Darrol: *The Design of the Aeroplane.* Oxford : Marston Book Services, 1983

Toyota 2005
URL: http://www.hybridsynergydrive.com/en/ev_drive_mode.html (accessed 2005-09-27)

Universität Stuttgart 2005a
UNIVERSITÄT STUTTGART, Institut für Flugzeugbau: *icaré II.* –
URL: http://www.ifb.uni-stuttgart.de/icare/icare.html (accessed 2005-09-27)

Universität Stuttgart 2005b
UNIVERSITÄT STUTTGART, Institut für Flugzeugbau: *icaré II – Zusammenfassung der Flugzeugdaten und Flugleistungen.* – URL: http://www.ifb.uni-stuttgart.de/icare/techdat.htm (accessed 2005-09-27)

Universität Stuttgart 2005c
UNIVERSITÄT STUTTGART, Institut für Flugzeugbau: *icaré II.* –
URL: http://www.ifb.uni-stuttgart.de/icare/galerie.htm (accessed 2005-09-27)

VDI 2000
VDI-GESELLSCHAFT FAHRZEUG- UND VERKEHRSTECHNIK, VDI-GESELLSCHAFT ENERGIETECHNIK: *Innovative Fahrzeugantriebe – Innovative Power Train Systems (Dresden 2000)*. Düsseldorf : VDI Verlag, 2000 – VDI Bericht 1565, ISBN 3-18-091565-X

verivox 2006
URL: http://www.verivox.de/power/ (accessed 2006-02-06)

Voit-Nitschmann 2001
VOIT-NITSCHMANN, Rudolf: *Solar- und Elektroflugzeuge – Geschichte und Zukunft.* Stuttgart, Universität Stuttgart, Institut für Flugzeugbau, 2001. –
URL: http://www.uni-stuttgart.de/wechselwirkungen/ww2001/nitschmann.pdf (accessed 2005-11-14)

Voit-Nitschmann 2005
VOIT-NITSCHMANN, Rudolf: *Re: Recherche zu elektrischen Antrieben* : email to Kolja Seeckt (k.seeckt@gmx.net). Universität Stuttgart, Institut für Flugzeugbau, Germany, 2005-11-14

Wickenheiser 2003
WICKENHEISER, Timothy J.; SEHRA, Arun K.; SENG, Gary T.; et al.: Emissionless Aircraft: Reqirements and Challenges. In: *AIAA/ICAS International Air and Space Symposium and Exposition: The Next 100 Y* (*Dayton, Ohio 2003*). – AIAA Report 2003-2810;
URL: http://www-psao.grc.nasa.gov/Library/Abstracts/EmissionlessAircraft.pdf (accessed 2005-10-05)

www.hybridsynergydrive.com 2006
URL: http://www.hybridsynergydrive.com/en/top.html (accessed 2006-02-20)

www.wikipedia.org 2005
URL: http://en.wikipedia.org/wiki/Fuel_cell (accessed 2005-09-18)

www.wikipedia.org 2006a
URL: http://en.wikipedia.org/wiki/Hybrid_vehicle (accessed 2006-02-20)

www.wikipedia.org 2006b
URL: http://en.wikipedia.org/wiki/Solar_cell (accessed 2006-02-23)

www.batteryuniversity.com 2005
URL: http://www.batteryuniversity.com (accessed 2005-10-05)

www.fuelcells.org 2005
URL: http://www.fuelcells.org (accessed 2005-09-26)

www.fuelcelltoday.com 2005a
URL: http://www.fuelcelltoday.com (accessed 2005-09-24)

www.fuelcelltoday.com 2005b
URL: http://www.fuelcelltoday.com/FuelCellToday/EducationCentre/EducationCentreExternal/EduCentreDisplay/0,1741,FCImages,00.html?id=6&start=12# (accessed 2005-12-21)

www.fuelcellworld.org 2005
URL: http://www.fuelcellworld.org (accessed 2005-09-24)

Young 2005
YOUNG, Trevor M.: *Flight Mechanics*. Limerick, University of Limerick, Department of Mechanical and Aeronautical Engineering, lecture notes, 2005

Zelch 2005
ZELCH, Markus: *Entwicklung des Avgas-Preises* : email to Kolja Seeckt (k.seeckt@gmx.net). ExxonMobil Central Europe Holding GmbH, Germany, 2005-12-05

Appendix A

AMT 200 Flight Manual Data

This appendix contains the most important pages of the *Aeromot AMT 200 Super Ximango*'s flight manual (**Aeromot 2002**).

1.4 Drawing of Motorglider in Three View

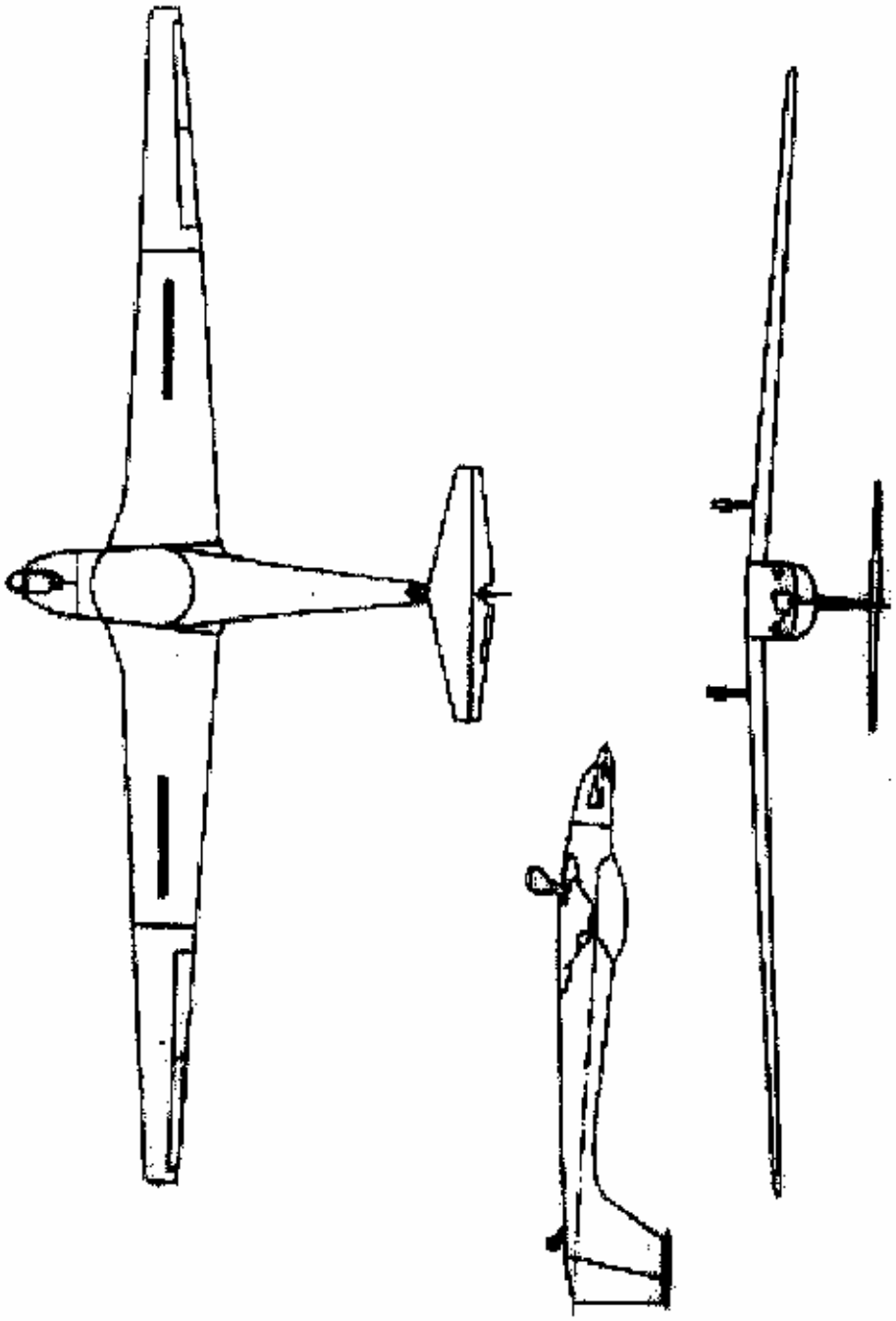

2.4 Power plant, fuel, and oil limitations

Engine:

- Manufacturer:	BOMBARDIER - ROTAX
- Part Number:	ROTAX 912 A2 (engines S/N 4.380.600 and on are equipped with a new propeller shaft and must be used with Propeller Assy P/N HO-V62R-1/170FA)
- Maximum Take Off RPM:	5800 RPM - 81 HP (59.6 KW) for 5 min
- Maximum Continuos RPM:	5500 RPM - 79 HP (58 KW)

Caution: Starter must be operated no more then 20s; An interruption of 1 min is necessary for starter cooling between consecutive starts.
If Starter Engaged light stays "ON" after engine start, Master Switch and Magnetos Switches must be turned-off (motorgliders S/N 200.046 and on) and troubleshooting must be done prior to attempt new start; the Starter Engaged light will remain "ON" until the starter relay is replaced.

Propeller:

- Manufacturer:	HOFFMANN
- Part Number:	HO-V62R/170FA (installed on motorgliders S/N 200.040, 200.045, 200.048 and 200.050) HO-V62R-1/170FA (installed on motorgliders S/N 200.046, 200.047, 200.049 and on).
- Maximum engine RPM pre take off check at sea level:	5100 RPM ± 100 RPM

Fuel:

- Fuel AVGAS:	100/130 or 100 LL octanes
- Fuel tank capacity:	2 x 11.89 U.S. Gallons (45 litres)
- Usable capacity	2 x 11.62 U.S. Gallons (44 litres)
- Unusable fuel	2 x 0.26 U.S. Gallons (1 litres)

Coolant:

-100% ethilene glycol	0°F (-18°C)
-80% ethilene glycol/water	-36°F (-38°C)

Lubricating Oil:
Automotive Mineral Oil Selected by the table below (API Classification SF or SG)

NOTE: Do not use General Aviation Engine Oil (detergent or not).

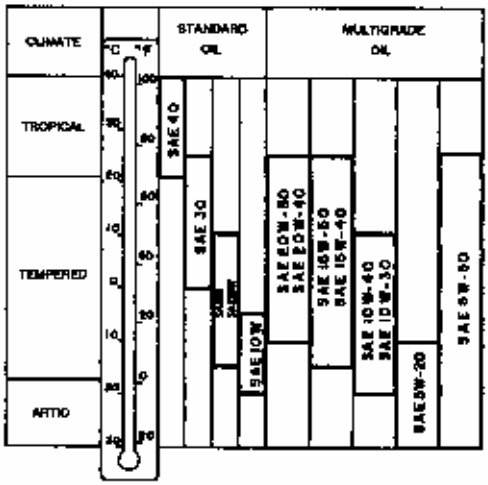

NOTE: The ambient ground air temperatures listed in the chart shown in the previous page are meant only as a guide specified by the engine manufacturer and an indication that higher viscosity oil should be considered when the oil inlet temperature approaches the maximum allowable during operation.

2.5 Power plant Instrument Markings

INSTRUMENT	RED LINE	GREEN ARC (Normal operation)	YELLOW ARC (Caution)
Tachometer	maximum 5800 RPM (5 min)	1500 - 5500 RPM	0 - 1500 5500 - 5800 RPM
Oil temperature	maximum 284°F (140°C)	122 - 284°F (50° - 140°C)	—
Oil pressure	minimum 21.8 PSI maximum 72.5 PSI	21.8 - 72.5 PSI	—
Ammeter	---	0 to +20 A	0 to -20 A
Fuel quantity	unusable fuel	—	—
Cylinder head temperature	Maximum 302°F (150°C)	122 - 302°F (50 - 150°C)	—

WARNING: The fuel quantity when the red line is reached permits approximately 5 min. of flight at maximum continuous power.

2.6 Weights Limitations:

- Maximum weight: 1874 lb (850 kg)
- Maximum Baggage weight: 11 lb (5 kg) - solo
  22 lb (10 kg) - 2 pilots

5.3 Additional information

5.3.1 Soaring performance

Motorglider with 1874 lb (850 kg) - maximum
- Speed at minimum sink rate:
  188.93 ft/min. (0.96m/s) at VI = 52 knots (97km/h)
- Maximum glide ratio:
  30 at VI = 58 knots (107 km/h)

- Glide ratio in landing configuration/spoilers extended:
  5.35 at VI = 59 knots (110 km/h)

5.3.2 Cruise Flight - cruise fuel consumption

Fuel Consumption:
4.49 gallon/hour (17 liter/hour) at 97 knots (180 km/h) engine at 5000 RPM
Altitude: Sea level

5.3.3 Climb

Weight - 1874 lb (850 kg)
Altitude - Sea level
Ambient temperature - 59°F (15°C)
- Vertical speed - 512 ft/min (2.6 m/s)
- Airspeed - 59 knots (110 km/h)

5.3.4 Crosswind landing

Maximum demonstrated crosswind - 15 knots (28 km/h)

5.3.5 Spoiler operation near VNE

Apply spoiler gradually. Spoilers are very effective at high speed.

5.3.6 Flight polar

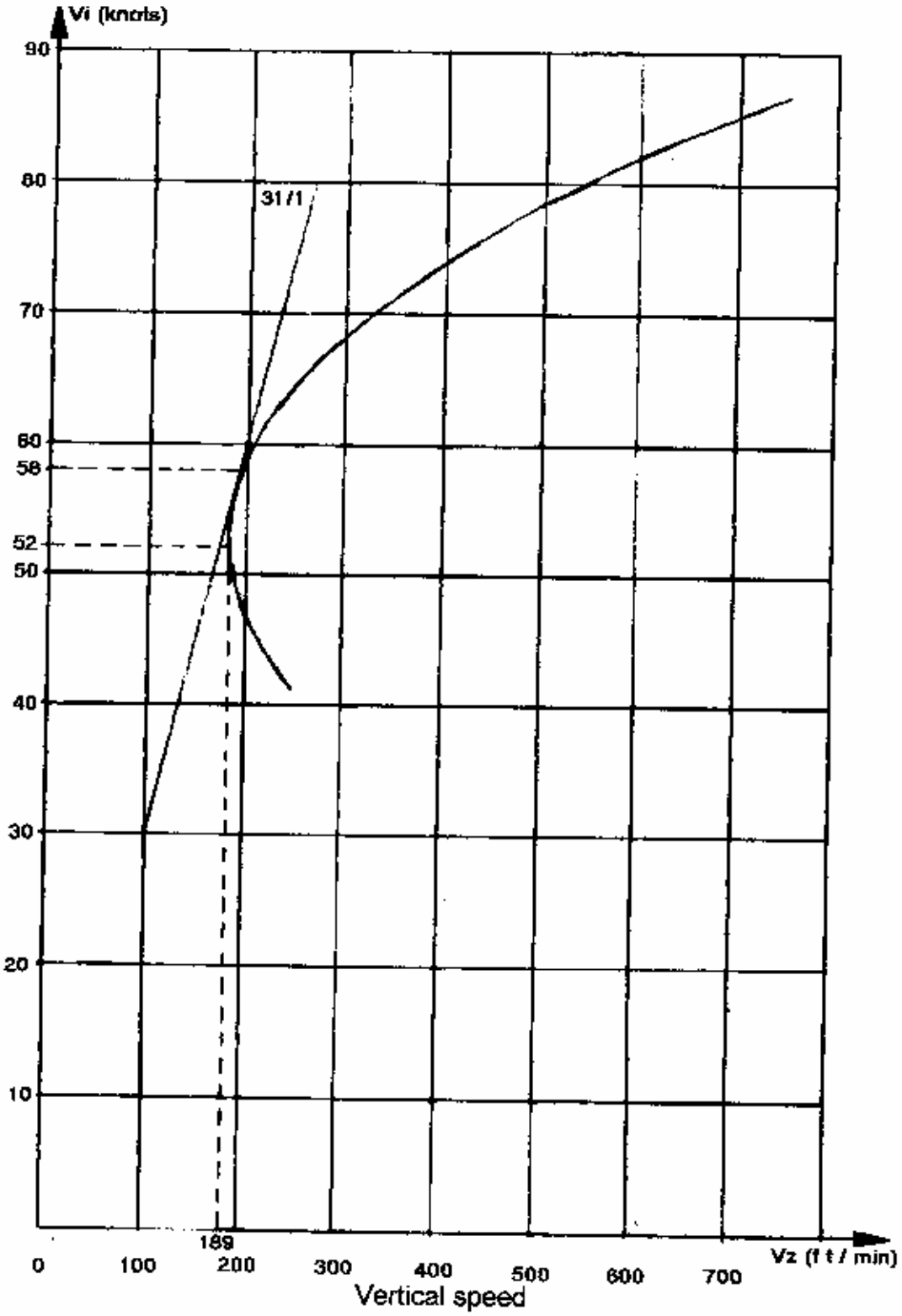

6.4 List of approved equipment

EQUIPMENT	MANUFACTURER	REFERENCE	WEIGHT (lb)	ARM (ft)
AIRSPEED	UNITED	8025-B541	0.463	+ 1.745
VERTICAL SPEED	UNITED	7000-C62	0.564	+ 1.772
COMPASS	AIRPATH	C2400 L4P-B	0.670	+ 1.782
ALTIMETER	UNITED	5934M-1 5934P-1	0.752	+ 1.729
SLIP-SKID	AIRCRAFT SPRUCE	1X4 3 1/2	0.099	+ 1.890
TACHOMETER/HOURMETER	AVIOSPORT	966073	0.716	+ 1.801
TACHOMETER	MOTOMETER	6010809997	0.716	+ 1.801
BATTERY	GILL VARTA-BAROCLEN SONNENSCHEIN	G35 528.16 530.30	25.600 19.069 19.731	+ 0.390 + 0.295 + 0.295
FUEL LEVEL IND.	WESTACH CRONOMAC	G4010 MNG 16	1 x 0.243 2 x 0.243	+ 1.847 + 1.847
FUEL FILTER	ACFT SPRUCE	10.560	1.005	+ 0.148
ELETRICAL FUEL PUMP	HARDI	170.093.010	1.982	+ 0.115
ENGINE	ROTAX	912 A2	125.661	- 1.585
PROPELLER	HOFFMANN	HO-V62R/170FA HO-V62R-1/170FA	22.045 23.050	- 2.690 - 2.690
FUEL SELEC. VALVE	OLDI	DI-1222-21-0L	1.045	+ 0.043
SOLENOID	IKRO	IK 171	3 X 0.703	- 2.109
FIRST AID KIT	PLANAVE	PLA 007	4.067	+ 6.496
AMMETER/CHT	CFAX	2DA8-18	0.500	+ 1.772
OIL PRESSURE/ OIL TEMP. INDICATOR	CFAX	2DA3-80	0.500	+ 1.772
OIL PRES. INDICATOR	CRONOMAC	M6KM	0.236	+ 1.772
OIL TEMP. INDICATOR	CRONOMAC	TO150E	0.236	+ 1.772
FUSE BOX	AEROMOT	AI 61489	0.716	+ 1.788
CYLINDER TEMPERATURE INDICATOR	SIMPSON	29-2006-2	0.500	+ 1.772
AMMETER	CRONOMAC	A40	0.166	+ 1.788
SOLENOID	STANCOR	70-902	3 X 0.650	- 2.109

SECTION 7 - DESCRIPTION

7.1 Introduction

This section provides the description and the operation of the motorglider and its systems.

7.2 Basic dimensions

Wing span	57.32 ft (17.47 m)
Wing span (wings folded)	33.30 ft (10.15 m)
Length	26.41 ft (8.05 m)
Maximum height	6.33 ft (1.93 m)

7.2.1 Wings

Wing surface (area)	61.35 ft² (18.70 m²)
Dihedral	2° 30'
Profile	Naca 64_3618
Angle of wing incidence	2°
Wing torsion	-2°

7.2.2 Ailerons

Relative width	30%
Aileron span	10.24 ft (3.12 m)
Aileron surface (area)	2.23 Sqft (0.68 m²)

7.2.3 Spoilers

Position:	at 45% of wing chord
Spoiler span	4.76 ft (1.45 m)
Type: face	Schempp hirth on wing upper

7.2.4 Horizontal Stabilizer

Horiz. stabilizer span	12.07 ft (3.68 m)
Horiz. stabilizer surface (area)	9.51 Sqft (2.90 m²)
Elevator surface	3.12 Sqft (0.95 m²)
Horiz. stabilizer - angle of incidence	-1°

Appendix B

Excel Spreadsheet

This appendix includes print-outs of the created *Microsoft Excel* spreadsheet. A description of these pages is given in chapter seven.

Performance Assessment of part-electric General Aviation Aircraft

Description of Reference Aircraft

Using this Spreadsheet:
Only yellow marked cells are to be filled out by the operator.
Green marked cells indicate important calculated results.

Item	Symbol	Unit	Value
Aircraft data			
Wing area	S	m²	18,7
Wing span	b	m	17,47
Aircraft mass	m	kg	850
Maximum fuel *volume*	/	l	88
Maximum fuel mass	mF,max	kg	63,4
Maximum zero fuel mass	m2	kg	787
Standard payload	mPL	kg	167
Aircraft empty mass	mempty	kg	620
Mass of standard internal combustion engine	mic	kg	57
Battery mass	mBat	kg	10
Airframe mass	mAF	kg	553
Engine power output			
Maximum continuous shaft power	PS,cont	kW	58,0
Maximum shaft power	PS,max	kW	59,6
Parameters			
Aspect ratio	A	/	16,32
Take-off parameter at MSL	/	/	648,3
Drag Polar Equation			
Minimum drag coefficient	CDmin	/	0,0251
Correlation factor	k	/	0,0733
Lift coefficient of minimum drag coefficient	CL(CDmin)	/	0,633
Flight Manual Data			
Air density	ρ	kg/m³	1,225

$$A = \frac{b^2}{S}$$

$$\text{Take-Off Parameter} = \frac{(W/S)(W/P)}{\sigma}$$

at MSL: $\sigma = 1$

Drag Polar Equation:

$$C_D = C_{D,\min} + k\left(C_L - C_L\left(C_{D,\min}\right)\right)$$

V (m/s)	Vz (m/s)	V (kn)	Vz (ft/min)	Flight Path Angle, γ	CL	E	CD	CD (Drag Polar Equation)	Relative Error
21,09	1,27	41,00	250,0	3,45	1,633	16,58	0,0985	0,0985	4,27316E-09
24,05	1,02	46,75	200,0	2,42	1,258	23,65	0,0532	0,0537	2,67567E-07
25,72	0,97	50,00	191,0	2,16	1,100	26,49	0,0415	0,0411	2,03511E-07
26,75	0,96	52,00	189,0	2,06	1,017	27,84	0,0365	0,0359	3,87971E-07
29,84	0,96	58,00	189,6	1,85	0,817	30,97	0,0264	0,0276	1,43528E-06
30,71	1,02	59,70	200,0	1,90	0,771	30,21	0,0255	0,0265	9,43426E-07
35,24	1,52	68,50	300,0	2,48	0,586	23,10	0,0254	0,0253	8,01335E-09
37,94	2,03	73,75	400,0	3,07	0,505	18,64	0,0271	0,0263	6,18853E-07
40,38	2,54	78,50	500,0	3,61	0,446	15,87	0,0281	0,0277	1,60327E-07
42,18	3,05	82,00	600,0	4,14	0,408	13,80	0,0296	0,0288	5,62447E-07
43,73	3,56	85,00	700,0	4,66	0,379	12,26	0,0310	0,0298	1,32422E-06
Cruise flight									
50,00	/	97,20	0,0	0,00	0,291	9,19	0,0317	0,0337	3,85392E-06
									9,76981E-06

$$C_L = \frac{2mg\cos\gamma}{\rho V^2 S}$$

$$E = \frac{1}{\tan\gamma}$$

$$C_D = \frac{C_L}{E}$$

Propeller Efficiency Equation			
First correlation factor	k1 (*V³)	/	3,48E-06
Second correlation factor	k2 (*V²)	/	-6,19E-04
Third correlation factor	k3 (*V)	/	3,88E-02
Fourth correlation factor	k4	/	-7,12E-04

Note: Here, the propeller efficiency is only defined up to 60 m/s.

Propeller Efficiency Equation

$$\eta_P = k_1 \cdot V^3 + k_2 \cdot V^2 + k_3 \cdot V + k_4$$

$$E = \frac{C_L}{C_D}$$

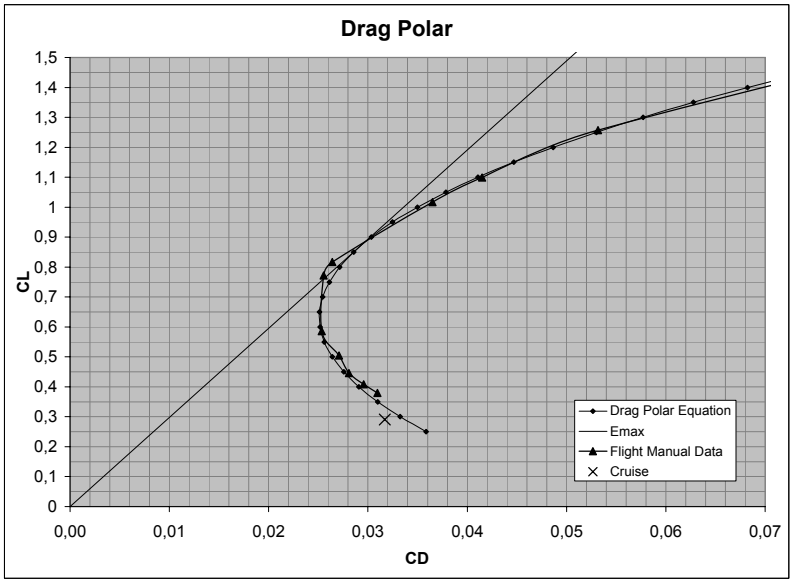

CL	CD	E
0,25	0,0359	6,97
0,3	0,0332	9,03
0,35	0,0310	11,30
0,4	0,0291	13,76
0,45	0,0276	16,33
0,5	0,0264	18,94
0,55	0,0256	21,48
0,6	0,0252	23,83
0,65	0,0251	25,87
0,7	0,0254	27,53
0,75	0,0261	28,73
0,8	0,0271	29,47
0,85	0,0286	29,77
0,9	0,0303	29,68
0,95	0,0325	29,26
1	0,0350	28,59
1,05	0,0378	27,74
1,1	0,0411	26,77
1,15	0,0447	25,73
1,2	0,0487	24,66
1,25	0,0530	23,58
1,3	0,0577	22,53
1,35	0,0628	21,50
1,4	0,0682	20,52
1,45	0,0740	19,59
1,5	0,0802	18,70
1,55	0,0867	17,87
1,6	0,0936	17,09

Emax Line	
0	0
0,5	14,88531806

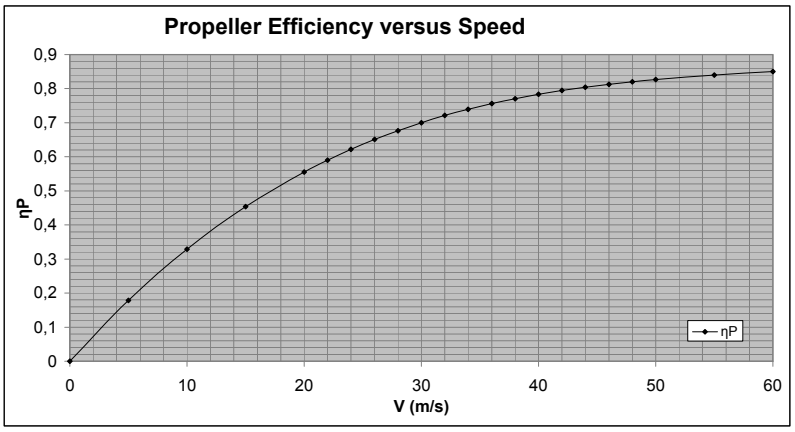

V (m/s)	ηP
0	0
5	0,178
10	0,329
15	0,454
20	0,556
22	0,590
24	0,622
26	0,651
28	0,677
30	0,700
32	0,721
34	0,740
36	0,756
38	0,771
40	0,784
42	0,795
44	0,805
46	0,813
48	0,820
50	0,827
55	0,840
60	0,851

Determination of Specific Fuel Consumption (SFC)

Item	Symbol	Unit	Value
Fuel flow related speed (TAS)	VQ	m/s	50
Fuel flow	Q	l/h	17
Shaft power	PS	kW	55
Fuel density Note: Density of Avgas 100LL is 0,72 kg/l	ρF	kg/l	0,72
Propeller Efficiency	ηP	/	0,827
Specific fuel consumption	c'	kg/Ws	6,18E-08

$$c' = \frac{Q \cdot \rho_F}{P_S}$$

Determination of Range and Endurances

V (m/s)	ηP	CL	CD	E	R1, R2 (km)	t1 (h)	t2 (h)
0	0	/	/	/	0	0	0
5	0,178	29,1206	59,5112	0,4893	11,1	0,6	0,6
10	0,329	7,2801	3,2638	2,2306	93,7	2,7	2,6
15	0,454	3,2356	0,5216	6,2032	359,6	6,8	6,7
20	0,556	1,8200	0,1284	14,1765	1006,0	14,2	14,0
22	0,590	1,5042	0,0807	18,6322	1405,1	18,1	17,7
24	0,622	1,2639	0,0543	23,2862	1850,3	21,8	21,4
26	0,651	1,0769	0,0395	27,2324	2263,9	24,7	24,2
28	0,677	0,9286	0,0315	29,4749	2548,2	25,8	25,3
30	0,700	0,8089	0,0274	29,5565	2643,4	25,0	24,5
32	0,721	0,7110	0,0255	27,8309	2563,5	22,7	22,3
34	0,740	0,6298	0,0251	25,0897	2370,7	19,7	19,4
36	0,756	0,5617	0,0255	22,0530	2130,3	16,8	16,4
38	0,771	0,5042	0,0263	19,1577	1886,3	14,1	13,8
40	0,784	0,4550	0,0274	16,5927	1660,9	11,8	11,5
42	0,795	0,4127	0,0287	14,4015	1462,1	9,9	9,7
44	0,805	0,3760	0,0299	12,5599	1290,8	8,3	8,1
46	0,813	0,3441	0,0312	11,0203	1144,5	7,0	6,9
48	0,820	0,3160	0,0325	9,7324	1019,9	6,0	5,9
50	0,827	0,2912	0,0337	8,6506	913,6	5,2	5,1
55	0,840	0,2407	0,0364	6,6148	709,6	3,7	3,6
60	0,851	0,2022	0,0387	5,2252	567,7	2,7	2,6

Note:
In this table, only the ranges and endurances of the default speeds are determined. The absolute maximum values can be found using the Excel Add-In "Solver" in the section below.

The Solver is located under Tools --> Solver (if not yet installed: Tools --> Ad-Ins; tick Solver).

Use: - Select G58, G62 or G67 as target cell
- Tick "Max"
- Select G49 as changing cell
- Click "Solve"

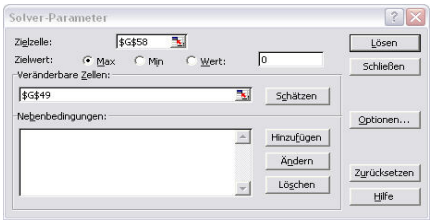

Ranges and endurances at MSL for any speed of interest

Item	Symbol	Unit	Value	knots
Speed	V	m/s	30,0	58,3
Lift Coefficient	CL		0,8091	
Drag Coefficient	CD		0,0274	
Lift-to-drag ratio	E (Emax)		29,6	
Drag	D (Dmin)	N	282	
Drag power = thrust power	PT	kW	8,5	
Propeller efficiency	ηP		0,700	
Shaft power	PS	kW	12,087	

Range for flight schedules 1 and 2 1: const. altitude & const. lift coefficient 2: const. airspeed & const. lift coefficient	R1 / R2	km	2643
Endurance for flight schedule 1	t1	h	25,0
Endurance for flight schedule 2	t2	h	24,5

$$R_1 = R_2 = \frac{\eta_P E}{c'g} \ln\left(\frac{m_1}{m_2}\right)$$

$$t_1 = \frac{2\eta_P E}{c'gV_1}\left[\sqrt{\frac{m_1}{m_2}} - 1\right]$$

where

V_1 is the TAS at the start of the cruise

$$t_2 = \frac{\eta_P E}{c'gV} \ln\left(\frac{m_1}{m_2}\right)$$

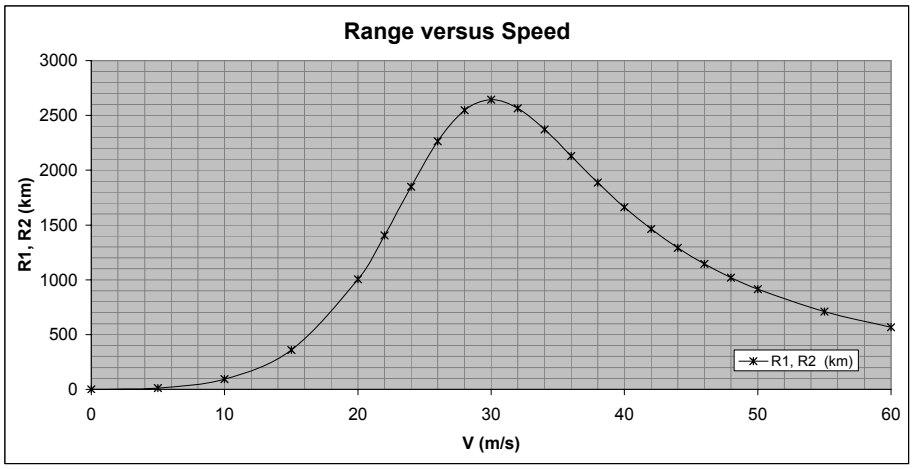
Range versus Speed
R1, R2 (km)
V (m/s)
R1, R2 (km)
0
500
1000
1500
2000
2500
3000
0
10
20
30
40
50
60

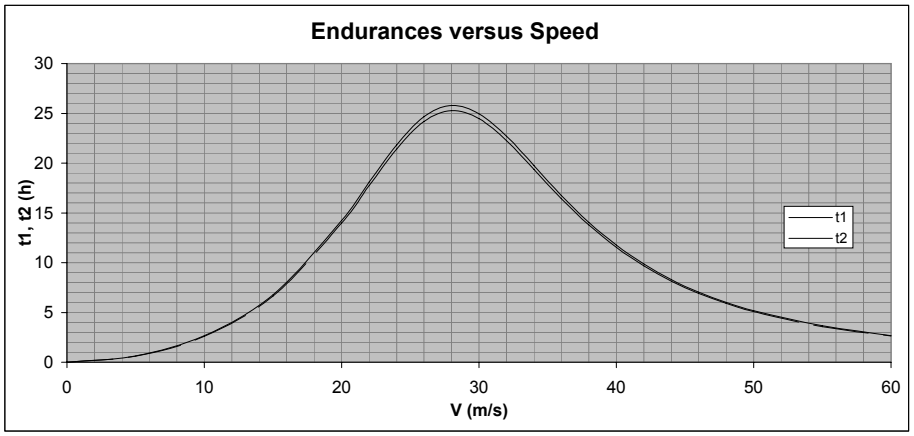
Endurances versus Speed
t1, t2 (h)
V (m/s)
t1
t2
0
5
10
15
20
25
30
0
10
20
30
40
50
60

Drag, Drag Power and Shaft Power vs. Speed (at MSL)

Item	Symbol	Unit	Value
Minimum Drag (Speed)			
Minimum drag speed	VDmin	m/s	29,06
Lift coefficient	CL	/	0,8620
Drag coefficient	CD	/	0,0289
Minimum drag	Dmin	N	280,0
Minimum Drag Power (Speed)			
Minimum power speed	VPmin	m/s	27,13
Lift coefficient	CL	/	0,9888
Drag coefficient	CD	/	0,0344
Minimum drag power	PDmin	kW	7,87
Minimum Shaft Power (Speed)			
Minimum shaft power speed	VPSmin	m/s	28,12
Lift coefficient	CL	/	0,9208
Drag coefficient	CD	/	0,0312
Propeller efficiency	ηP	/	0,6782
Minimum shaft power	PSmin	kW	11,70

Search for minimum using Solver:
- Target cell: G9
- Tick "Min"
- Changing cell: G6

Search for minimum using Solver:
- Target cell: G15
- Tick "Min"
- Changing cell: G12

Search for minimum using Solver:
- Target cell: G22
- Tick "Min"
- Changing cell: G18

V (m/s)	CL	CD	E	D	PD (kW)	ηP	PS (kW)
20	1,8200	0,1284	14,2	588	11,8	0,556	21,2
22	1,5042	0,0807	18,6	448	9,8	0,591	16,7
24	1,2639	0,0543	23,3	358	8,6	0,623	13,8
26	1,0769	0,0395	27,2	306	8,0	0,652	12,2
28	0,9286	0,0315	29,5	283	7,9	0,677	11,7
30	0,8089	0,0274	29,6	282	8,5	0,701	12,1
32	0,7110	0,0255	27,8	300	9,6	0,722	13,3
34	0,6298	0,0251	25,1	332	11,3	0,740	15,3
36	0,5617	0,0255	22,1	378	13,6	0,757	18,0
38	0,5042	0,0263	19,2	435	16,5	0,772	21,4
40	0,4550	0,0274	16,6	503	20,1	0,784	25,6
42	0,4127	0,0287	14,4	579	24,3	0,796	30,6
44	0,3760	0,0299	12,6	664	29,2	0,805	36,3
46	0,3441	0,0312	11,0	757	34,8	0,814	42,8
48	0,3160	0,0325	9,7	857	41,1	0,821	50,1
50	0,2912	0,0337	8,7	964	48,2	0,828	58,2
52	0,2692	0,0348	7,7	1078	56,0	0,833	67,3
54	0,2497	0,0359	7,0	1198	64,7	0,838	77,2
56	0,2321	0,0369	6,3	1325	74,2	0,843	88,0
58	0,2164	0,0378	5,7	1457	84,5	0,847	99,8
60	0,2022	0,0387	5,2	1596	95,7	0,851	112,5

$$D = \frac{1}{2}\rho V^2 C_D S$$

$$P_D = DV = \frac{1}{2}\rho V^3 C_D S$$

$$P_S = \frac{P_T}{\eta_P} = \frac{P_D}{\eta_P}$$

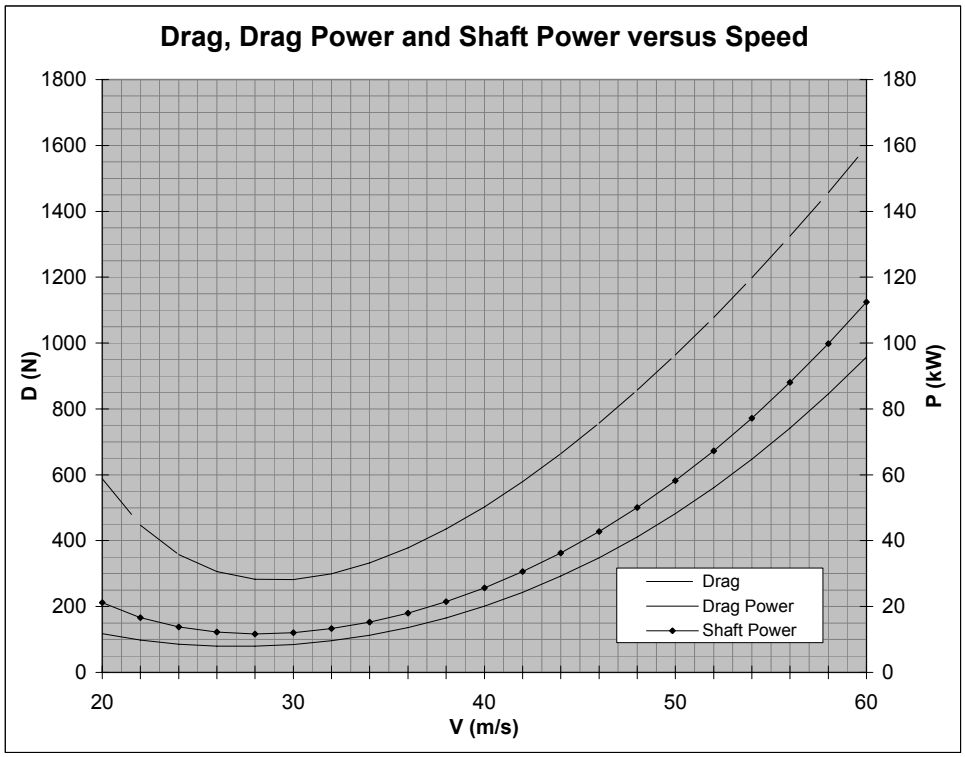

Determination of Climb Performance and Maximum Level Speed at MSL

Item	Symbol	Unit	Value
Flight Manual Data			
Maximum Rate of Climb	Vz,max	m/s	2,6
Best Climb Speed	Vy	m/s	30,5
Maximum Rate of Climb (ROC)			
Best climb speed	Vy	m/s	31,25
Maximum continuous shaft power	PScont	kW	58,0
Lift coefficient	CL	/	0,7456
Drag coefficient	CD	/	0,0260
Drag	D	N	291,1
Propeller efficiency	ηP	/	0,713
Aircraft mass	m	kg	850
Maximum Rate of Climb	Vz,max	m/s	3,87
Maximum Level Speed			
Maximum level speed	Vmax	m/s	49,93
Maximum continuous shaft power	PScont	kW	58,0
Lift coefficient	CL	/	0,2920
Drag coefficient	CD	/	0,0336
Drag	D	N	960,1
Propeller efficiency	ηP	/	0,827
Aircraft mass	m	kg	850
ROC (must be zero at maximum level speed)	Vz	m/s	0,00

$$V_z = \frac{\eta_P P_S \sqrt{\sigma}}{mg} - \frac{D}{mg} V$$

here: $\sqrt{\sigma} = 1$

Search for maximum using Solver:
- Target cell: G17
- Tick "Max"
- Changing cell: G10

Search for value "0" using Solver:
- Target cell: G27
- Tick "Value"
- Enter "0"
- Changing cell: G20

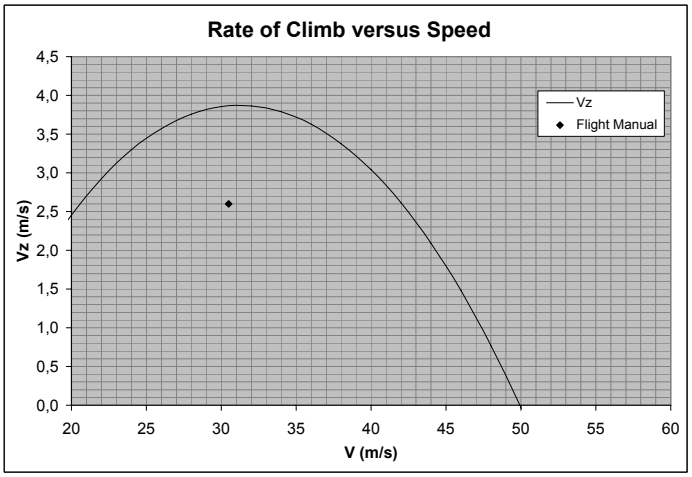

V (m/s)	CL	CD	PD (kW)	ηP	PT (kW)	(T/W)*V (m/s)	(D/L)*V (m/s)	Vz (m/s)
10	7,2801	3,2638	37,4	0,329	19,1	2,29	4,48	-2,20
12	5,0557	1,4588	28,9	0,382	22,1	2,66	3,46	-0,81
14	3,7144	0,7211	22,7	0,431	25,0	3,00	2,72	0,28
16	2,8438	0,3834	18,0	0,476	27,6	3,31	2,16	1,15
18	2,2470	0,2160	14,4	0,517	30,0	3,60	1,73	1,87
20	1,8200	0,1284	11,8	0,556	32,2	3,86	1,41	2,45
22	1,5042	0,0807	9,8	0,590	34,2	4,11	1,18	2,93
24	1,2639	0,0543	8,6	0,622	36,1	4,33	1,03	3,30
26	1,0769	0,0395	8,0	0,651	37,7	4,53	0,95	3,57
28	0,9286	0,0315	7,9	0,677	39,3	4,71	0,95	3,76
30	0,8089	0,0274	8,5	0,700	40,6	4,87	1,02	3,86
32	0,7110	0,0255	9,6	0,721	41,8	5,02	1,15	3,87
34	0,6298	0,0251	11,3	0,740	42,9	5,15	1,36	3,79
36	0,5617	0,0255	13,6	0,756	43,9	5,26	1,63	3,63
38	0,5042	0,0263	16,5	0,771	44,7	5,36	1,98	3,38
40	0,4550	0,0274	20,1	0,784	45,4	5,45	2,41	3,04
42	0,4127	0,0287	24,3	0,795	46,1	5,53	2,92	2,61
44	0,3760	0,0299	29,2	0,805	46,7	5,60	3,50	2,09
46	0,3441	0,0312	34,8	0,813	47,2	5,66	4,17	1,48
48	0,3160	0,0325	41,1	0,820	47,6	5,71	4,93	0,77
50	0,2912	0,0337	48,2	0,827	48,0	5,75	5,78	-0,03
52	0,2692	0,0348	56,0	0,832	48,3	5,79	6,72	-0,93
54	0,2497	0,0359	64,7	0,837	48,6	5,83	7,76	-1,93
56	0,2321	0,0369	74,2	0,842	48,8	5,86	8,90	-3,04
58	0,2164	0,0378	84,5	0,846	49,1	5,89	10,14	-4,25
60	0,2022	0,0387	95,7	0,851	49,3	5,92	11,48	-5,57

Determination of absolute ceiling

Item	Symbol	Unit	Value	
Minimum shaft power speed at MSL	VPSmin	m/s	28,12	
Lift coefficient	CL	/	0,9208	
Drag coefficient	CD	/	0,0312	
Propeller efficiency	ηP	/	0,678	
Maximum continuous shaft power	PScont	kW	58,00	m
Absolute ceiling	habs	ft	28240	8607
Relative density	σ	/	0,40	
True airspeed	V	m/s	44,51	
Drag power	PD	kW	12,57	
Needed shaft power	PS needed	kW	18,526	
Available shaft power	PS	kW	18,526	
Shaft power surplus	/	/	0,0000	

Search for value "0" using Solver:
- Target cell: G83
- Tick "Value"
- Enter "0"
- Changing cell: G77

$$\sigma = \frac{\rho}{\rho_0} = \left(1 - k_a \cdot H\right)^{4,25588}$$

with

$$k_a = 6,8756 \cdot 10^{-6} \left[\frac{1}{ft}\right]$$

$$P_S(h) = P_{S,0}\left(\sigma - \frac{1-\sigma}{7,55}\right)$$

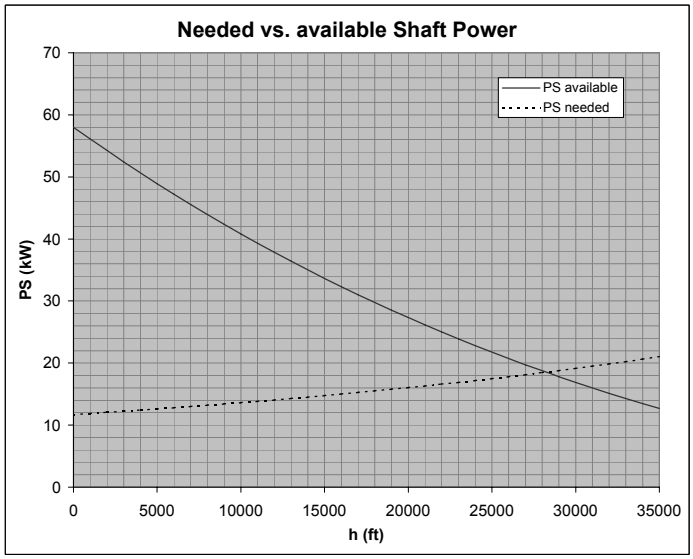

h (m)	h (ft)	σ	ρ (kg/m³)	PS (kW)	V (m/s)	PD (kW)	ηP	PS needed (kW)
0	0	1,000	1,225	58,0	28,1	7,9	0,678	11,7
304,8	1000	0,971	1,190	56,1	28,5	8,1	0,678	11,9
609,6	2000	0,943	1,155	54,2	29,0	8,2	0,678	12,1
914,4	3000	0,915	1,121	52,4	29,4	8,3	0,678	12,2
1219,2	4000	0,888	1,088	50,6	29,8	8,4	0,678	12,4
1524	5000	0,862	1,056	48,9	30,3	8,6	0,678	12,6
1828,8	6000	0,836	1,024	47,2	30,8	8,7	0,678	12,8
2133,6	7000	0,811	0,993	45,6	31,2	8,8	0,678	13,0
2438,4	8000	0,786	0,963	43,9	31,7	9,0	0,678	13,2
2743,2	9000	0,762	0,933	42,4	32,2	9,1	0,678	13,4
3048	10000	0,738	0,905	40,8	32,7	9,2	0,678	13,6
3352,8	11000	0,716	0,877	39,3	33,2	9,4	0,678	13,8
3657,6	12000	0,693	0,849	37,8	33,8	9,5	0,678	14,1
3962,4	13000	0,671	0,822	36,4	34,3	9,7	0,678	14,3
4267,2	14000	0,650	0,796	35,0	34,9	9,8	0,678	14,5
4572	15000	0,629	0,771	33,6	35,4	10,0	0,678	14,8
4876,8	16000	0,609	0,746	32,3	36,0	10,2	0,678	15,0
5181,6	17000	0,589	0,722	31,0	36,6	10,3	0,678	15,2
5486,4	18000	0,570	0,698	29,8	37,2	10,5	0,678	15,5
5791,2	19000	0,551	0,675	28,5	37,9	10,7	0,678	15,8
6096	20000	0,533	0,653	27,3	38,5	10,9	0,678	16,0
6400,8	21000	0,515	0,631	26,1	39,2	11,1	0,678	16,3
6705,6	22000	0,498	0,610	25,0	39,9	11,3	0,678	16,6
7010,4	23000	0,481	0,589	23,9	40,6	11,4	0,678	16,9
7315,2	24000	0,464	0,569	22,8	41,3	11,7	0,678	17,2
7620	25000	0,448	0,549	21,8	42,0	11,9	0,678	17,5
7924,8	26000	0,432	0,530	20,7	42,8	12,1	0,678	17,8
8229,6	27000	0,417	0,511	19,7	43,5	12,3	0,678	18,1
8534,4	28000	0,403	0,493	18,8	44,3	12,5	0,678	18,4
8839,2	29000	0,388	0,475	17,8	45,1	12,7	0,678	18,8
9144	30000	0,374	0,458	16,9	46,0	13,0	0,678	19,1
9448,8	31000	0,361	0,442	16,0	46,8	13,2	0,678	19,5
9753,6	32000	0,347	0,425	15,1	47,7	13,5	0,678	19,9
10058,4	33000	0,334	0,410	14,3	48,6	13,7	0,678	20,2
10363,2	34000	0,322	0,394	13,5	49,6	14,0	0,678	20,6
10668	35000	0,310	0,380	12,7	50,5	14,3	0,678	21,0

constant values for all altitudes	ka 1/ft	CL	CD
	6,87560E-06	0,9208	0,0312

Thrust Power vs. Drag Power at different Altitudes

VE (m/s)	alt	0	ft	ρ	1,225	kg/m³	alt	2000	ft	σ	0,943		alt	4000	ft	σ	0,888		alt	6000	ft	σ	0,836	
	CL	CD	ηP	PT (kW)	D (N)	PD (kW)	CL	CD	ηP	PT (kW)	D (N)	PD (kW)	CL	CD	ηP	PT (kW)	D (N)	PD (kW)	CL	CD	ηP	PT (kW)	D (N)	PD (kW)
20	1,8200	0,1284	0,56	3,86	588	1,41	1,9305	0,1485	0,54	3,54	641	1,54	2,0494	0,1722	0,53	3,24	700	1,68	2,1774	0,1999	0,52	2,96	766	1,84
22	1,5042	0,0807	0,59	4,11	448	1,18	1,5955	0,0930	0,58	3,77	486	1,28	1,6937	0,1076	0,57	3,45	530	1,40	1,7995	0,1248	0,56	3,16	579	1,53
24	1,2639	0,0543	0,62	4,33	358	1,03	1,3406	0,0618	0,61	3,98	384	1,11	1,4232	0,0709	0,60	3,65	415	1,20	1,5121	0,0817	0,59	3,34	451	1,30
26	1,0769	0,0395	0,65	4,53	306	0,95	1,1423	0,0441	0,64	4,17	322	1,00	1,2127	0,0497	0,63	3,82	342	1,07	1,2884	0,0566	0,62	3,50	366	1,14
28	0,9286	0,0315	0,68	4,71	283	0,95	0,9850	0,0342	0,67	4,34	289	0,97	1,0456	0,0376	0,66	3,98	300	1,01	1,1109	0,0418	0,65	3,65	314	1,05
30	0,8089	0,0274	0,70	4,87	282	1,02	0,8580	0,0288	0,69	4,49	280	1,01	0,9108	0,0308	0,68	4,13	282	1,01	0,9678	0,0333	0,67	3,79	287	1,03
32	0,7110	0,0255	0,72	5,02	300	1,15	0,7541	0,0262	0,71	4,63	289	1,11	0,8005	0,0272	0,70	4,26	283	1,09	0,8506	0,0286	0,69	3,92	280	1,07
34	0,6298	0,0251	0,74	5,15	332	1,36	0,6680	0,0252	0,73	4,75	314	1,28	0,7091	0,0255	0,72	4,38	300	1,22	0,7534	0,0262	0,71	4,03	290	1,18
36	0,5617	0,0255	0,76	5,26	378	1,63	0,5958	0,0252	0,75	4,86	353	1,52	0,6325	0,0251	0,74	4,49	331	1,43	0,6721	0,0252	0,73	4,13	313	1,35
38	0,5042	0,0263	0,77	5,36	435	1,98	0,5348	0,0258	0,76	4,96	402	1,83	0,5677	0,0254	0,75	4,58	373	1,70	0,6032	0,0252	0,75	4,22	348	1,59
40	0,4550	0,0274	0,78	5,45	503	2,41	0,4826	0,0268	0,78	5,05	462	2,22	0,5123	0,0262	0,77	4,67	426	2,04	0,5444	0,0257	0,76	4,31	393	1,89
42	0,4127	0,0287	0,79	5,53	579	2,92	0,4378	0,0279	0,79	5,13	531	2,68	0,4647	0,0272	0,78	4,74	488	2,46	0,4938	0,0265	0,77	4,38	448	2,26
44	0,3760	0,0299	0,80	5,60	664	3,50	0,3989	0,0291	0,80	5,19	609	3,21	0,4234	0,0283	0,79	4,81	558	2,94	0,4499	0,0276	0,78	4,45	511	2,70
46	0,3441	0,0312	0,81	5,66	757	4,17	0,3649	0,0304	0,81	5,25	694	3,83	0,3874	0,0295	0,80	4,87	635	3,51	0,4116	0,0287	0,80	4,50	581	3,21
48	0,3160	0,0325	0,82	5,71	857	4,93	0,3352	0,0316	0,82	5,30	786	4,53	0,3558	0,0307	0,81	4,92	720	4,15	0,3780	0,0299	0,80	4,55	659	3,79
50	0,2912	0,0337	0,83	5,75	964	5,78	0,3089	0,0328	0,82	5,35	885	5,31	0,3279	0,0319	0,82	4,96	812	4,87	0,3484	0,0310	0,81	4,60	743	4,45
52	0,2692	0,0348	0,83	5,79	1078	6,72	0,2856	0,0339	0,83	5,39	991	6,18	0,3032	0,0331	0,82	5,00	910	5,67	0,3221	0,0322	0,82	4,64	833	5,20

VE (m/s)	alt	8000	ft	σ	0,786		alt	10000	ft	σ	0,738		alt	12000	ft	σ	0,693		alt	14000	ft	σ	0,650	
	CL	CD	ηP	PT (kW)	D (N)	PD (kW)	CL	CD	ηP	PT (kW)	D (N)	PD (kW)	CL	CD	ηP	PT (kW)	D (N)	PD (kW)	CL	CD	ηP	PT (kW)	D (N)	PD (kW)
20	2,3155	0,2326	0,51	2,70	838	2,01	2,4646	0,2710	0,50	2,45	917	2,20	2,6257	0,3162	0,49	2,22	1004	2,41	2,8000	0,3693	0,48	2,01	1100	2,64
22	1,9137	0,1453	0,55	2,88	633	1,67	2,0368	0,1696	0,54	2,62	694	1,83	2,1700	0,1983	0,52	2,38	762	2,01	2,3140	0,2322	0,51	2,15	837	2,21
24	1,6080	0,0948	0,58	3,05	491	1,41	1,7115	0,1104	0,57	2,77	538	1,55	1,8234	0,1290	0,56	2,52	590	1,70	1,9444	0,1512	0,54	2,28	648	1,87
26	1,3701	0,0649	0,61	3,20	395	1,23	1,4583	0,0750	0,60	2,92	429	1,34	1,5536	0,0872	0,58	2,65	468	1,46	1,6568	0,1019	0,57	2,40	513	1,60
28	1,1814	0,0471	0,63	3,34	333	1,12	1,2574	0,0537	0,62	3,05	356	1,20	1,3396	0,0617	0,61	2,78	384	1,29	1,4285	0,0715	0,60	2,52	417	1,40
30	1,0291	0,0366	0,66	3,47	297	1,07	1,0954	0,0408	0,65	3,17	310	1,12	1,1670	0,0460	0,64	2,89	329	1,18	1,2444	0,0525	0,62	2,62	352	1,27
32	0,9045	0,0305	0,68	3,59	281	1,08	0,9627	0,0331	0,67	3,28	286	1,10	1,0256	0,0364	0,66	2,99	296	1,14	1,0937	0,0407	0,65	2,72	310	1,19
34	0,8012	0,0272	0,70	3,70	283	1,15	0,8528	0,0286	0,69	3,38	280	1,14	0,9085	0,0307	0,68	3,09	281	1,15	0,9688	0,0334	0,67	2,81	287	1,17
36	0,7147	0,0256	0,72	3,80	299	1,29	0,7607	0,0263	0,71	3,48	288	1,24	0,8104	0,0274	0,70	3,18	282	1,22	0,8642	0,0290	0,69	2,89	280	1,21
38	0,6414	0,0251	0,74	3,88	326	1,49	0,6827	0,0253	0,73	3,56	309	1,41	0,7273	0,0258	0,72	3,26	295	1,35	0,7756	0,0266	0,71	2,97	286	1,30
40	0,5789	0,0253	0,75	3,96	365	1,75	0,6161	0,0251	0,74	3,64	340	1,63	0,6564	0,0251	0,73	3,33	319	1,53	0,7000	0,0254	0,72	3,04	303	1,45
42	0,5251	0,0260	0,77	4,03	412	2,08	0,5589	0,0255	0,76	3,71	381	1,92	0,5954	0,0252	0,75	3,39	353	1,78	0,6349	0,0251	0,74	3,10	330	1,66
44	0,4784	0,0269	0,78	4,10	468	2,47	0,5092	0,0262	0,77	3,77	429	2,27	0,5425	0,0257	0,76	3,45	395	2,08	0,5785	0,0253	0,75	3,16	365	1,93
46	0,4377	0,0279	0,79	4,15	531	2,93	0,4659	0,0271	0,78	3,82	486	2,68	0,4963	0,0265	0,77	3,51	445	2,45	0,5293	0,0259	0,76	3,21	408	2,25
48	0,4020	0,0290	0,80	4,20	602	3,46	0,4279	0,0282	0,79	3,87	549	3,16	0,4558	0,0274	0,78	3,56	501	2,89	0,4861	0,0267	0,78	3,26	458	2,63
50	0,3705	0,0302	0,81	4,25	679	4,07	0,3943	0,0293	0,80	3,91	619	3,71	0,4201	0,0284	0,79	3,60	564	3,38	0,4480	0,0276	0,79	3,30	514	3,08
52	0,3425	0,0313	0,81	4,29	762	4,75	0,3646	0,0304	0,81	3,95	695	4,33	0,3884	0,0295	0,80	3,64	633	3,95	0,4142	0,0286	0,79	3,34	576	3,59

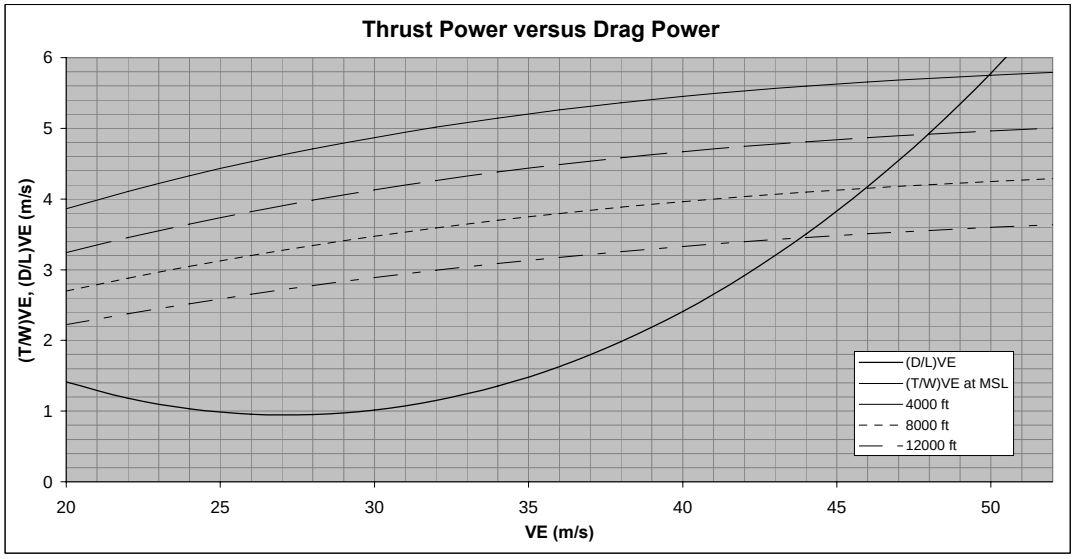

Estimation of e-motor characteristics

Item	Symbol	Unit	Value
E-motor shaft power	PS,e	kW	30,0

This value moves the vertical line in the chart below. It is of no influence on following calculations and can be changed freely for seperate estimations.

Choose a reference motor from the chart below and insert its function's factor and exponent.		Factor:	2,7000
		Exponent:	0,5926
E-motor mass acc. Rubber motor method	mem	kg	20,3
E-motor control device mass acc. Icaré 2 e.g. frequency generator	memc	kg	8,0
Mass of e-motor and control device	me	kg	28,2

First estimation acc. Icaré 2

$m_{emc} \approx 3,5kg + 0,22 \cdot m_{em}$

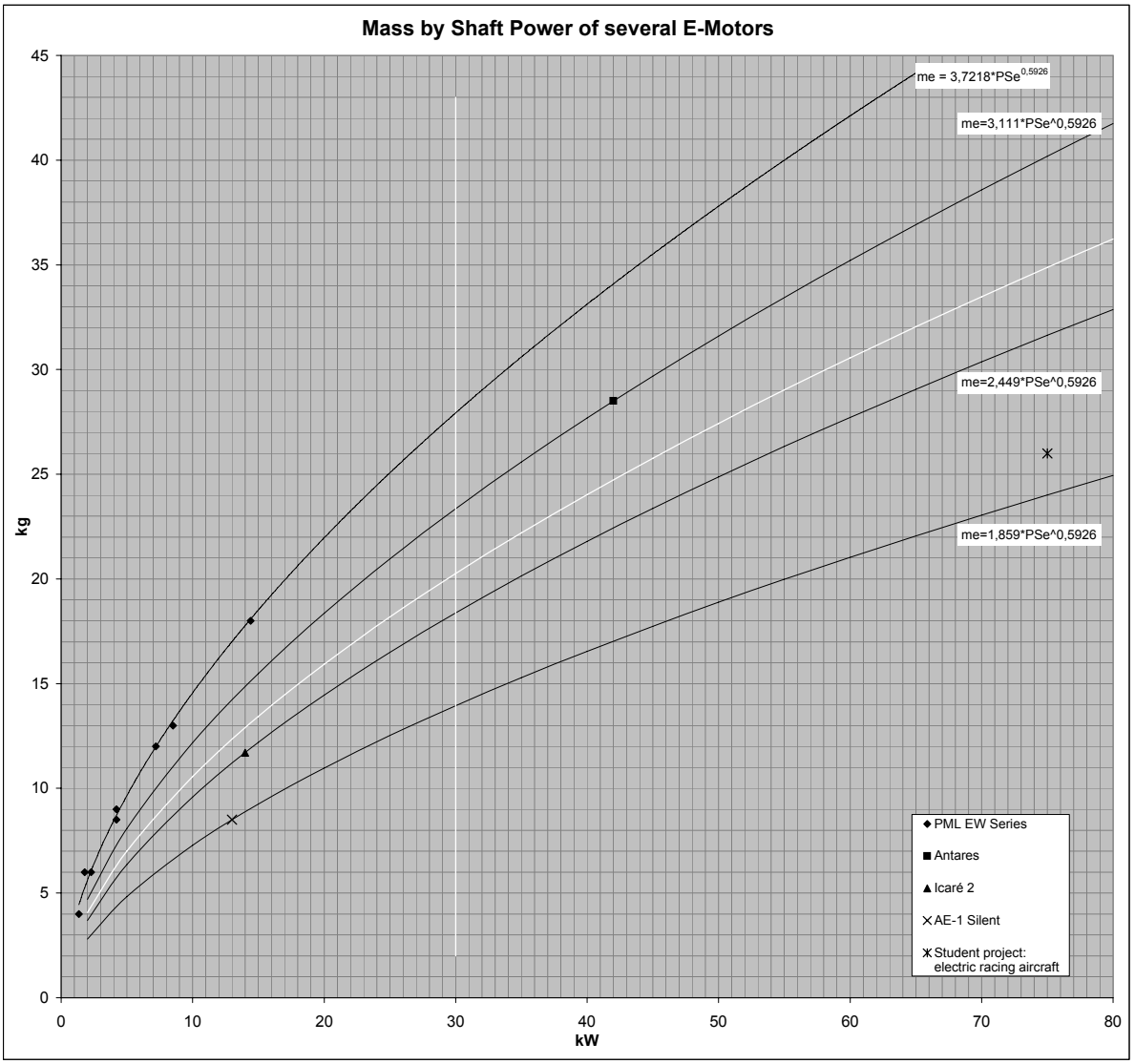

PSe kW	mem kg	PS,e kW	mem acc Icaré 2 kg	mem acc Silent kg	mem acc Antares kg
PML EW Series		2	3,69	2,80	4,69
1,35	4	5	6,36	4,82	8,07
1,8	6	10	9,58	7,28	12,18
2,28	6	15	12,19	9,25	15,48
4,2	9	20	14,45	10,97	18,36
4,2	8,5	25	16,50	12,52	20,96
8,5	13	30	18,38	13,95	23,35
7,2	12	35	20,14	15,29	25,58
14,4	18	40	21,80	16,54	27,69
Antares		45	23,37	17,74	29,69
42	28,5	50	24,88	18,88	31,60
Icaré 2		55	26,32	19,98	33,44
14	11,70	60	27,72	21,04	35,21
AE-1 Silent		65	29,06	22,06	36,92
13	8,5	70	30,37	23,05	38,57
Project: electric racing a/c		75	31,63	24,01	40,18
75	26	80	32,87	24,95	41,75
13	8,5		30,0	2	
75	26		30,0	43	

Estimation of new internal combustion engine characteristics

Item	Symbol	Unit	Value
IC engine shaft power	PS,i	kW	60,0
Choose a reference motor from the chart below and insert its function's factor and exponent.		Factor:	0,5015
		Summand:	25,4570
E-motor mass acc. Rubber motor method	mi	kg	55,5

This value moves the vertical line in the chart below. It is of no influence on following calculations and can be changed freely for seperate estimations.

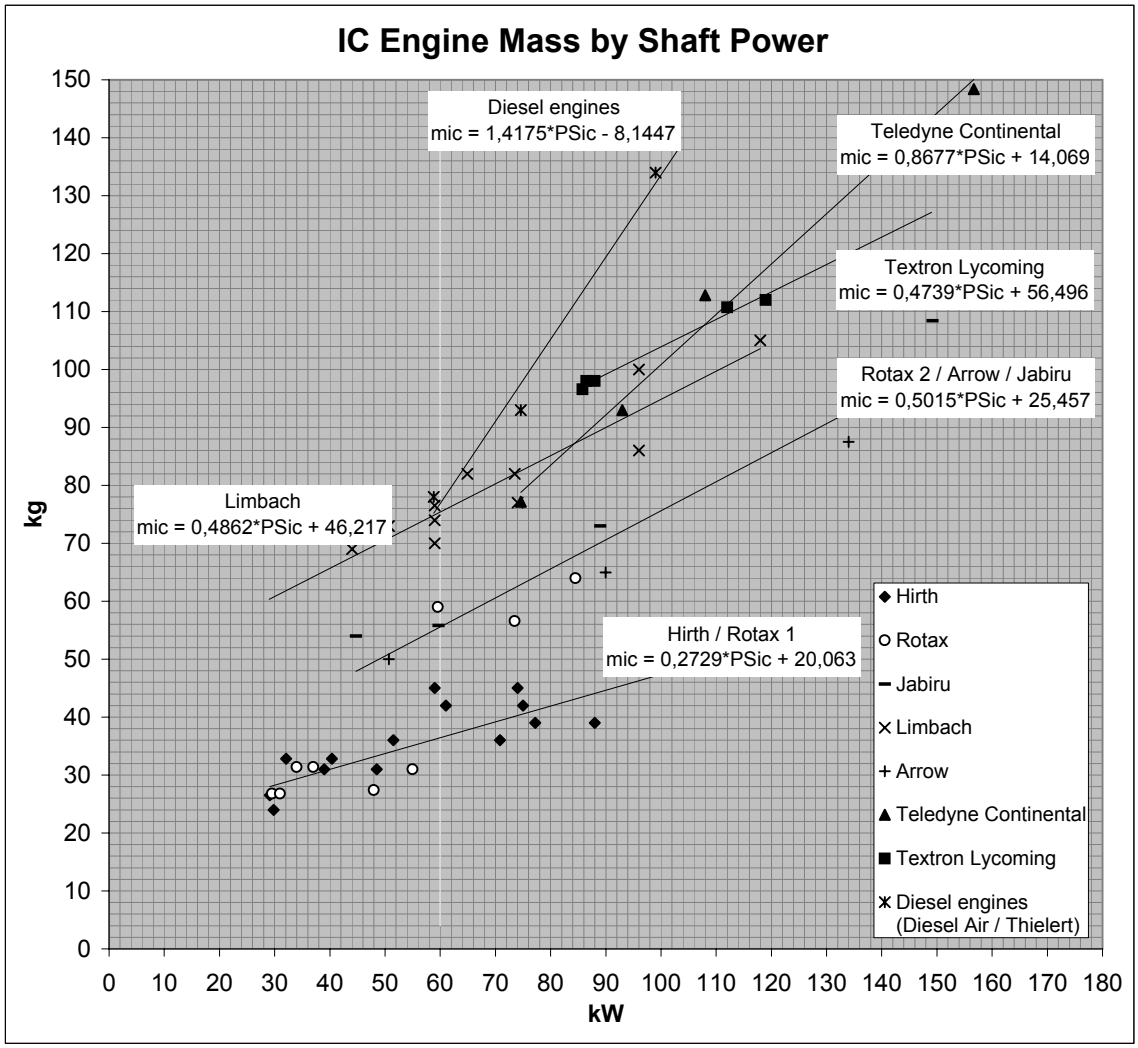

kg	kW
Hirth	
24	29,8
36	70,8
39	77,2
39	88
42	61
42	75
26,5	29,1
32,8	32,1
32,8	40,4
31	39
31	48,5
36	51,5
45	59
45	74
Arrow	
50	50,7
65	90
87,5	134
4	60,0
146	60,0

kg	kW
Diesel Air / Thielert	
78	58,8
93	74,6
134	99
Limbach	
73	50,7
69	44
70	59
74	59
76,5	59
82	64,9
82	73,5
77	74
100	96
86	96
105	118
Teledyne Continental	
77,2	74,6
93	93
112,8	108
148,4	156,7

kg	kW
Rotax	
26,8	29,5
26,8	31
31,4	34
31,4	37
27,4	48
31	55
59	59,6
56,6	73,5
64	84,5
Jabiru	
54	44,7
55,8	59,7
73	89
108,4	149,2
Textron Lycoming	
96,6	85,8
98	88
98	86,5
110,7	112
112	119

Investigation and comparison of level flight missions

Mission definition	Symbol	Value	Unit
Altitude	hcr	2500	ft
Cruise speed (TAS)	Vcr	50	m/s
Endurance	tcr	2,5	h
OR	↑ or ↓		
Distance	scr		km
Fuel price	pF	1,70	€/l
Electricity tariff	pe	0,189	€/kWh
Specific CO2-emission	ee	0,104	kg/kWh
Distance flown (still air)	scr	450	km
Time enroute	tcr	2,5	h

Definition of hybrid engine	Symbol	Value	Unit
Maximum continous shaft power of IC engine	PS,i,cont	130,8	kW
Energy density of batteries	ρE	150,0	Wh/kg
Fraction PSe / PS	f	0,500	

Mission results	Value ref a/c	Unit	Value hyb a/c
Shaft power needed (PS)	54,6	kW	44,0
Aircraft mass at beginning of cruise (m1)	817	kg	1259,4
Aircraft mass at end of cruise (max zero fuel mass, m2)	787	kg	1247,1
Fuel flow (Q)	16,7	l/h	6,82
	12,1	kg/h	4,91
Fuel needed (VF, mF)	41,8	l	17,1
	30,1	kg	12,28
Total comsumption of electricity (Ee)	/	kWh	55,16
Energy costs (CE = CF + Ce)	71,12	€	39,42
Produced CO2 (mCO2)	97,05	kg	45,31

Factor e-mot	2,7
Exp e-mot	0,5926
Factor ic	0,5015
Summand ic	25,457
T-O Param. (mMTO ref a/c)	648,3
ρ	1,138
S	18,7
PScont ref a/c	58,0
ηP	0,821
VE	48,2
c'	6,18E-08
ρF	0,72
m2 (ref a/c)	786,6
Fuel (ref a/c)	88
eF (kg/l)	2,32

ref a/c

CL2	0,2901	
CD2	0,0337	
E2	8,61	
D2	896,8	
PD2	44,84	
PS2	54,61	
Q2	12,15	kg/h
	16,88	l/h
mF ≈	30,4	
m1 ≈ Q*t+m2	817,0	kg
CL1	0,3013	
CD1	0,0332	
E1	9,09	
(E1+E2)/2	8,85	
m1	816,8	
D1	882,0	
PD1	44,10	
PS1	53,72	
Q1	11,95	kg/h
(Q1+Q2)/2	12,05	
	16,74	l/h
mF	30,12	kg
VF	41,834	l

hyb a/c

0. Iteration

PSe	27,3	kW
Ee	68,27	kWh
mB	455,1	kg
mBinst	54,6	kg
mBat	509,7	kg
mAF	552,6	kg
mpl	167,0	kg
me	26,9	kg
mic	54,5	kg
m2	1310,8	kg
mic	96,5	kg
m2	1352,8	kg
CL2	0,4990	
CD2	0,0264	
PD2	35,13	kW
PS2	42,79	kW
PSe	21,40	kW
PSi	21,40	kW

1. Iteration

Ee	53,49	kWh
mBat	399,4	kg
me	23,7	kg
m2	1239,3	kg
mic	89,0	kg
m2	1231,7	kg
CL2	0,4543	
CD2	0,0274	
PD2	36,49	kW
PS2	44,45	kW
PSe	22,22	kW
PSi	22,22	kW

2. Iteration

Ee	55,56	kWh
mBat	414,8	kg
me	24,2	kg
m2	1247,7	kg
mic	89,9	kg
m2	1248,5	kg
CL2	0,4605	
CD2	0,0273	
PD2	36,28	kW
PS2	44,19	kW
PSe	22,09	kW
PSi	22,09	kW

3. Iteration

Ee	55,24	kWh
mBat	412,4	kg
me	24,1	kg
m2	1246,1	kg
mic	89,7	kg
m2	1245,9	kg
CL2	0,4595	
CD2	0,0273	
E2	16,83	
PD2	36,31	kW
PS2	44,23	kW
Q2	4,92	kg/h
m1 ≈ Q2*t+m2	1258,2	kg
mic	90,9	kg
m1	1259,5	kg
m2	1247,1	kg
CL1	0,4645	
CD1	0,0272	
E1	17,09	
(E1+E2)/2	16,96	
c*	3,09E-08	kg/(Ws)
m1	1259,4	kg
PD1	36,15	kW
PS1	44,03	kW
PSe	22,01	kW
Q1	4,90	kg/h
(Q1+Q2)/2	4,91	kg/h
	6,82	l/h
mF	12,3	kg
	17,1	l

Estimation acc. Air Energy for housing, brackets, battery management, wiring and fuses:

$$m_{B,inst} = (0{,}10 \ldots 0{,}15) \cdot m_B$$

Appendix C

Collection of Internal Combustion Engine Data

This appendix includes the data on internal combustion engines used in chapter 6.3 for mass estimation of a new hypothetical *rubber* IC engine.

Table C.1 Masses and Power Outputs of Internal Combustion Engines (based on **Jackson 2005**)

Specification	**Mass** [kg]	**Shaft Power** [kW]
Arrow AE 530 AC	50	50.7
Arrow AE 1070 AC	65	90
Arrow GP 1500	87.5	134
Diesel Air D 280	78	58.8
Diesel Air Dair-100	93	74.6
Hirth F23A	24	29.8
Hirth F30	36	70.8
Hirth F30A	39	77.2
Hirth F30 A36	39	88
Hirth F30 E	42	61
Hirth F30 ES	42	75
Hirth F31	26.5	29.1
Hirth 2701	32.8	32.1
Hirth 2703	32.8	40.4
Hirth 2704	31	39
Hirth 2706	31	48.5
Hirth 3503 E	36	51.5
Hirth 3701	45	59
Hirth 3701 ES	45	74
Jabiru 1600	54	44.7
Jabiru 2200	55.8	59.7
Jabiru 3300	73	89
Jabiru 6000	108.4	149.2
Limbach SL 1700, L 1700EC	73	50.7
Limbach L 1700EA	69	44
Limbach L 2000	70	59

Limbach L 2000EO	74	59
Limbach L 2000EB	76.5	59
Limbach L 2400EB	82	64.9
Limbach L 2400EF	82	73.5
Limbach L 2400DFi, EFi	77	74
Limbach L 2400DWFIG	100	96
Limbach L 2400DT, ET	86	96
Limbach L 2400DT.X	105	118
Rotax 447 UL-1V	26.8	29.5
Rotax 447 UL-2V	26.8	31
Rotax 503 UL-1V	31.4	34
Rotax 503 UL-2V	31.4	37
Rotax 582 UL	27.4	48
Rotax 618 UL-2V	31	55
Rotax 912 UL, 912A, 912F	59	59.6
Rotax 912 UL DCDI, 912 ULS, 912S	56.6	73.5
Rotax 914 UL DCDI, 914F	64	84.5
Teledyne Continental O-200-A & B	77.2	74.6
Teledyne Continental IO-240-A & B	93	93
Teledyne Continental O-300-A, C & D	112.8	108
Teledyne Continental IO-300-CCB, et. al	148.4	156.7
Textron Lycoming O-235-C	96.6	85.8
Textron Lycoming O-235-I, M	98	88
Textron Lycoming O-235-N, P	98	86.5
Textron Lycoming O-320-A, E	110.7	112
Textron Lycoming (H)O-320-B2C	112	119
Thielert TAE Centurion 1.7	134	99

Appendix D

CD-ROM

This CD-ROM includes this report in PDF-format and the created *Excel* spreadsheet-tool.